



**Development of Manufacturing Techniques for
Graphene-based transducers with potential
application in biosensor technology**

Abdullah Abdu Faqihi

A thesis submitted in fulfilment of the requirement for
the Degree of Doctor of Philosophy

School of Engineering

Newcastle University

United Kingdom

March 2022

Abstract

Biosensors play a significant role in the healthcare sectors and in scientific and technological progress in general. Good diagnostic and biosensing interactions are mainly advantaged by the manufacture of electrodes that can efficiently deliver better electrochemical performance. Biosensors have been extensively implemented for various analytical tasks in areas such as medical diagnostics, food safety, and environmental monitoring, and an effective biosensor properly detects the biological and chemical reactions generated by the bio-interaction in the sample measured. The focus in the current study is the development of a laser scribing technique for graphene oxide (GO) in a vacuum chamber. The reduction of GO was investigated under four conditions involving the atmospheric environment, vacuum, and Nitrogen and Argon gases. A laser scribing technique which reduces GO to generate rGO was characterised using scanning electron microscopy (SEM), Raman spectroscopy and X-ray photoelectron spectroscopy (XPS) to visualise the morphological structures of rGO.

The SEM results demonstrated a spongier appearance for GO2 (laboratory prepared graphene oxide) compared to GO1 (commercial graphene oxide) material. Raman spectroscopic characterisation highlighted that, for both GO materials, the LSG_{N2} electrode showed improved response characteristics and a tendency to exhibit better closeness to single- layer graphene. Moreover, the XPS results showed that the percentage of oxygen decreased after the reduction process. The results of the electrochemical analysis suggested that GO2 has superior electrochemical activity compared to GO1. The LSG_{N2} electrode has been tested using solutions of potassium ferricyanide and 1,1'-ferrocene dimethanol, and the electrochemical behaviour of the electrode was acceptable for both according to cyclic voltammetry results, which indicates the reproducibility of the electrode. Likewise, the peak current ratio of LSG_{N2} for both solutions was better compared with the same electrode material prepared under the other conditions.

The ΔE_p for each redox species indicates higher values than the ideal Nernstian value of 59 mV. The Ψ values of all of the scan rates for the potassium ferricyanide and 1,1'-ferrocene dimethanol fall within the acceptable range of Ψ , indicating a quasi-reversible system which has been also confirmed by K^0 and M_{trans} values.

Acknowledgements

First of all, I am thankful to Allah almighty who grants me this unique opportunity to learn and attain this stage in my life successfully. This thesis, in its current form, is due to the assistance and guidance of many people.

I would like to express my sincere gratitude to my supervisory team Dr. John Hedley and Dr. Neil Keegan for their help, support, guidance and patience during my study.

I also want to thank our group members Hayder Ashelaish, Idris Musa, Elmira Alimohammadzadeh, Ayad Mahuof, Hasan Merie and Fadoo Unom for their help during my PhD research.

Deep thanks to my parents and my brothers and sisters for their calls and how they made me laugh, especially during the Covid-19 crisis. And I am sorry, beloved mum, for being away for ages but finally I did it, with your loving prayers.

Very special thanks to my wife, Rawyah Bihari for her unconditional love, care, support and delicious food. I really wish to thank you for encouraging and having faith in me to pursue my dream; I would not be here without you. Also, thanks to my lovely princess Meela and little prince Mohammed for colouring and shining my life with lots of joy and happiness.

I want to thank Prof. Lidija Siller and Dr. Isabel Arce Garcia for supporting me when I was bringing my samples and for always asking about my research.

Thanks to all my friends Dr. Ahmed Almoraya, Dr. Tarek Hosny, Dr. Ahmed Althobaiti, Dr. Haitham Hadidi, Mohammed Alamri, Ali Mahnashi, Jaber Sharahili, Feras Afifi, Abdulrahman Alhudhaibi, and Walid Algamdi who helped me a lot during my study.

Finally, I would like to express my sincere gratitude to my sponsor, Jazan University, for providing me with the opportunity to study at Newcastle University, UK, to pursue my PhD.

Abdullah Abdu Faqih

Declaration

I declare that this work has not been accepted for any degree or qualification and is not currently being submitted in candidature for any degree other than the degree of Doctor of Philosophy of Newcastle University.

Abdullah Abdu Faqih

List of publications:

Faqihi, A. and J. Hedley, Developing manufacturing process for the graphene sensors. *International Journal of Industrial and Manufacturing Engineering*, 2021, **15**(4): p. 171-174.

Contents:

Contents

Chapter 1. General Introduction.....	15
1.1 Introduction.....	15
1.2 Problem Statement.....	18
1.3 Aim and Objectives.....	18
1.4 Thesis Structure	19
Chapter 2. Literature Review	20
2.1 Biosensors.....	20
2.2 Biosensor Types.....	21
2.2.1 Optical detection Biosensors.....	21
2.2.2 Electrochemical Biosensors	22
2.2.3 Mechanical Biosensors	26
2.3 Graphene Background	26
2.4 Properties of Graphene	27
2.5 Graphene Production	28
2.5.1 Mechanical Exfoliation (ME)	29
2.5.2 Liquid Phase Exfoliation (LPE).....	29
2.5.3 Epitaxial Growth on Silicon Carbide SiC	29
2.5.4 Chemical Vapour Deposition (CVD).....	30
2.6 Graphene Applications in Different Types of Sensors	30
2.6.1 Electrochemical Sensors	31
2.6.2 Mechanical Sensors.....	32
2.6.3 Environmental Sensors	33
2.7 Methods of Reducing Graphene Oxide.....	34
2.7.1 Thermal Reduction Method	34
2.7.2 Use of a Laser to Reduce Graphene Oxide	35
2.7.3 Chemical Reduction Method	36
2.8 Conclusion	37
Chapter 3. Methodology	38
3.1 Introduction.....	38
3.2 Materials	38
3.2.1 Suspended Graphene Oxide	38
3.2.2 Polyethylene Terephthalate (PET) Film.....	39
3.2.3 Conductive Silver.....	40
3.3 Research Equipment	41
3.3.1 DVD LightScribe writer.....	41

3.3.2 Vacuum Chamber	41
3.3.3 Gas Cylinder	42
3.4 Materials Analysis	43
3.4.1 Raman Spectroscopy	43
3.4.2 Scanning Electron Microscopy (SEM)	46
3.5 Preparation of the Reduced GO Electrodes	47
3.6 Fundamental Method for Transforming GO to rGO	48
3.7 Electrochemistry of the Prepared Electrodes	49
3.7.1 Cyclic Voltammetry (CV)	50
Chapter 4. Material Characterisation	52
4.1 Introduction	52
4.2 Scanning Electron Microscopy	52
4.3 Raman Spectroscopy	55
4.3.1 Raman Spectroscopy for GO1 Electrodes	56
4.3.2 Raman Spectroscopy for GO2 Electrodes	60
Chapter 5. Experimental Results	68
5.1 Introduction	68
5.2 Cyclic Voltammetry of GO1 Electrodes in Potassium Ferricyanide Redox Species	68
5.3 Cyclic Voltammogram of GO1 Electrodes in 1,1'-ferrocene Dimethanol Redox Species	71
5.4 CV of GO2 Electrodes in Potassium Ferricyanide Redox Species	73
5.4.1 CV of LSG _{air} Electrode	73
5.4.2 CV of LSG _{uvc} Electrode	74
5.4.3 CV of LSG _{N₂} Electrode	75
5.4.4 CV of LSG _{Ar} Electrode	76
5.5 CV of GO2 Electrodes in 1,1'-ferrocene Dimethanol Redox Species	78
5.5.1 CVs of LSG _{air} , LSG _{uvc} , LSG _{N₂} , and LSG _{Ar} Electrodes	78
5.6 Conclusion	81
Chapter 6. Discussion of Results	82
6.1 Introduction	82
6.2 Electrochemical Performance of Each Electrode in Potassium Ferricyanide	82
6.2.1 Electrochemical Characteristics of the Prepared Electrodes	82
6.3 Electrochemical Performance of Each Electrode in 1,1'-ferrocene Dimethanol Redox Species	86
6.3.1 Electrochemical Characteristics of the Prepared Electrodes	86
6.4 Supporting Electrochemical Analysis of the Prepared Electrodes in Potassium Ferricyanide Redox Species	89
6.5 Supporting Electrochemical analysis of the Prepared Electrodes in 1,1'-ferrocene Dimethanol Redox Species	92
6.6 Electrochemical Performance	96

6.7 Conclusion	99
Chapter 7. Conclusion and Future Work	101
7.1 Conclusion	101
7.2 Recommendations and Future Work.....	104
7.3 Contribution to knowledge.....	104
References.....	105
Appendix.....	114

List of Figures:

Figure 1-1. Graphene-based sensor platform for health monitoring	17
Figure 2-1. A generic biosensor system.....	21
Figure 2-2. Surface Plasmon Resonance (SPR) sensor system	22
Figure 2-3. A simple electrochemical biosensor	24
Figure 2-4. Carbon-carbon atoms bonding in a graphene sheet	27
Figure 2-5. Top-down and bottom-up graphene synthesis	28
Figure 2-6. Graphene application in different research areas.....	31
Figure 2-7. Illustration of the fabrication process of the LSG	35
Figure 2- 8. Fabricated LSG electrode	36
Figure 3-1. The liquid form of GO1 and GO2	39
Figure 3-2. The cut-out shape of the PET film to fit the DVD.....	40
Figure 3-3. a) silver conductive paint, b) rGO electrode with attached copper conducting lead	40
Figure 3-4. a) the DVD Lightscribe writer, b) the DVD disc in a case	41
Figure 3-5. a) cylindrical vacuum chamber, b) the DVD Lightscribe writer in the vacuum chamber.....	42
Figure 3-6. Vacuum chamber setting: (a) Nitrogen and Argon gas cylinders; (b) vacuum chamber containing the laser-scribe DVD drive; (c) reader to monitor the pressure inside the chamber; (d) vacuum Pump; (e) laptop unit to transfer the design to the DVD writer.....	43
Figure 3-7. Comparison of Raman spectra: (a) between graphite and graphene; (b) 2D peaks of graphene and graphite	45
Figure 3-8. Raman spectra of GO and rGO	45
Figure 3-9. XPS spectra of: (a) GO film; (b) rGO film	47
Figure 3-10. rGO electrode design: (a) combined-shape electrode; (b) patch electrode.....	48
Figure 3-11. Electrode production process: (a) DVD disc; (b) GO layer over the disc; (c) the disc with dried GO layer placed in the LightScribe writer for scribing; (d) LSG electrode patterned in black.....	49
Figure 3-12. Typical cyclic voltammogram for an electrochemical system.....	51
Figure 4-1. SEM micrographs of the surface of each electrode material for rGO (from GO1) at a magnification of x10000, produced under: (a) atmospheric; (b) vacuum; (c) Nitrogen gas; and (d) Argon gas conditions.....	53
Figure 4-2. SEM micrographs of the surface of each electrode material at a magnification of x10000 for rGO (from GO2) produced under: (a) atmospheric; (b) vacuum; (c) Nitrogen gas; (d) Argon gas conditions.....	55

Figure 4-3. Raman spectra of the surface of each electrode material from GO1 under: (a) atmospheric; (b) vacuum; (c) N ₂ ; (d) Ar conditions.....	57
Figure 4-4. Raman shift of the GO1 electrodes produced under the different conditions.....	59
Figure 4-5. Raman spectra of: (a) LSGair; (b) LSGuvc; (c) LSGN ₂ ; (d) LSGAr.....	61
Figure 4-6. Reduced graphene oxide electrode from GO2 produced under different conditions.....	62
Figure 4-7. Raman spectra of the GO2 electrodes produced under different conditions.....	63
Figure 4-8. XPS data analysis for GO.....	64
Figure 4-9. XPS data analysis for LSG under the various manufacturing conditions: (a) air; (b) vacuum; (c) N ₂ ; (d) Ar.....	65
Figure 4-10. Survey scan XPS spectra of GO and LSG using: (a) air; (b) vacuum; (c) N ₂ ; (d) Ar conditions.....	66
Figure 5-1. Morphological appearance of: (a) the counter electrode; (b) one of the representative prepared electrodes; and (c) the reference electrode.....	69
Figure 5-2. Cyclic voltammograms for the prepared electrodes under different conditions (LSGair, LSGuvc, LSGN ₂ , and LSGAr) at a scan rate of 10mVs ⁻¹ in potassium ferricyanide redox species.....	70
Figure 5-3. Cyclic voltammograms for the prepared electrodes under different conditions (LSGair, LSGuvc, LSGN ₂ , and LSGAr) at a scan rate of 10mVs ⁻¹ in 1,1'-ferrocene dimethanol.....	71
Figure 5-4. Cyclic voltammograms of LSGair electrode at different scan rates in potassium ferricyanide redox species.....	73
Figure 5-5. Cyclic voltammograms of LSGuvc electrode at different scan rates in potassium ferricyanide redox species.....	74
Figure 5-6. Cyclic voltammograms of LSGN ₂ electrode at different scan rates in potassium ferricyanide redox species.....	76
Figure 5-7. Cyclic voltammograms of LSGAr electrode at different scan rates in potassium ferricyanide redox species.....	77
Figure 5-8. Cyclic voltammograms for LSGair at different scan rates in 1,1'-ferrocene dimethanol redox species.....	79
Figure 5-9. Cyclic voltammograms for LSGuvc at different scan rates in 1,1'-ferrocene dimethanol redox species.....	79
Figure 5-10. Cyclic voltammograms for LSGN ₂ at different scan rates in 1,1'-ferrocene dimethanol redox species.....	80
Figure 5-11. Cyclic voltammograms for LSGAr at different scan rates in 1,1'-ferrocene dimethanol redox species.....	80
Figure 6-1. Plot of peak-peak potential separation against scan rate for the electrodes prepared using four different conditions (LSGair, LSGuvc, LSGN ₂ , and LSGAr) in potassium ferricyanide redox species.....	90

Figure 6-2. Plot of peak current against scan rate for the electrodes prepared using four different conditions (LSGair, LSGuvc, LSGN2, and LSGAr) in potassium ferricyanide redox species. 91

Figure 6-3. Plot of peak current against square root of scan rate for the electrodes prepared using four different conditions (LSGair, LSGuvc, LSGN2, and LSGAr) in potassium ferricyanide redox species.....91

Figure 6-4. Plot of ΔE_p against scan rate for the electrodes produced under different conditions (LSGair, LSGuvc, LSGN2, and LSGAr) in 1,1'-ferrocene dimethanol redox species.....93

Figure 6-5. Plot of peak current against scan rate for the electrodes produced under the different conditions (LSGair, LSGuvc, LSGN2, and LSGAr) in 1,1'-ferrocene dimethanol redox species.....94

Figure 6-6. Plot of peak current against the square root of scan rate for the electrodes produced under the different conditions (LSGair, LSGuvc, LSGN2, and LSGAr) in 1,1'-ferrocene dimethanol redox species.....94

List of tables:

Table 4-1. Raman spectra of the manufactured LSG electrodes with GO1 and GO2 and other graphene electrodes.....59

Table 4-2. XPS analysis of the percentages of carbon and oxygen for GO and rGO using air, vacuum, N₂, and Ar conditions.....67

Table 5-1. Electrochemical responses shown in the cyclic voltammograms of different electrode devices manufactured with GO1 under different conditions (LSGair, LSGuvc, LSGN₂, and LSGAr) in both redox species (potassium ferricyanide and 1,1'-ferrocene dimethanol redox species).....72

Table 5-2. Electrochemical response results for all GO2 electrodes (LSGair, LSGuvc, LSGN₂, and LSGAr) in potassium ferricyanide redox species.....77

Table 5-3 Recorded results of electrochemical responses for all GO2 electrodes (LSGair, LSGuvc, LSGN₂, and LSGAr) in 1,1'-ferrocene dimethanol redox species.....81

Table 6-1. Response characteristics of the LSGair, LSGuvc, LSGN₂, and LSGAr electrodes in potassium ferricyanide redox species.....85

Table 6-2. Response characteristics of the LSGair, LSGuvc, LSGN₂, and LSGAr electrodes in 1,1'-ferrocene dimethanol redox species.....88

Table 6-3. R² values for the four manufactured electrodes (LSGair, LSGuvc, LSGN₂, and LSGAr) in potassium ferricyanide redox species.....92

Table 6-4. R² values for the manufactured electrodes (LSGair, LSGuvc, LSGN₂, and LSGAr) in 1,1'-ferrocene dimethanol redox species.....95

Table 6-5. Tested parameters of the optimum electrode devices compared with other published work.....98

Glossary

ΔE_p	Peak-to-potential separation
Ψ	Dimensionless kinetic parameter
BPPG	Basal-plane pyrolytic graphite
CV	Cyclic voltammetry
CNT	Carbon nanotube
CVD	Chemical vapour deposition
DPV	Differential pulse voltammetry
E_{pa}	Peak anodic potential
E_{pc}	Peak cathodic potential
EPPG	Edge-plane pyrolytic graphite
GCE	Glassy carbon electrode
GFET	Graphene field-effect transistor
GO	Graphene oxide
GQDs	Graphene quantum dots
I_{pa}	Peak anodic current
I_{pc}	Peak cathodic current
k^0	Electron transfer rate
LSG_{air}	Laser-scribe electrode under atmospheric condition
LSG_{UVC}	Laser-scribe electrode under vacuum condition
LSG_{N_2}	Laser-scribe electrode under Nitrogen gas condition
LSG_{Ar}	Laser-scribe electrode under Argon gas condition
LIG	Laser-induced graphene
LSG	Laser-scribed graphene
LSV	Linear sweep voltammetry
LPE	Liquid Phase Exfoliation
ME	Mechanical Exfoliation
M_{trans}	Mass transport
PET	Polyethylene terephthalate

PVD	Physical vapour deposition
rGO	Reduced graphite oxide
RI	Index of refraction
SLG	Single-layer graphene
SEM	Scanning electron microscopy
SPR	Surface Plasmon Resonance
SiC	Silicon Carbide
SEM	Scanning electron microscopy
TMDs	Transition metal dichalcogenides
UCLA	California at Los Angeles
XPS	X-ray photoelectron spectroscopy

Chapter 1. General Introduction

1.1 Introduction

In present times, given the increasingly polluted atmosphere as well as the day-to-day safety and comfort we experience, the detection and identification of atoms, molecules, and specific substances at low concentration levels is vital. Toxic substances in air, water, soil, or gases in the environment or in homes can be identified, alongside various dangerous biological substances in our body and food, by technological devices called sensors, including those called biosensors. A biosensor can be defined according to IUPAC definitions as “a device that uses specific biochemical reactions mediated by isolated enzymes, immunosystems, tissues, organelles or whole cells to detect chemical compounds usually by electrical, thermal or optical signals” [1]. It carries out biological detection via a linked transducer and transforms the biological response into an electrical signal. Stability, selectivity, and sensitivity are the dynamic and static characteristics that affect and dictate the quality and performance of biosensors [2-4]. To deal with the complexity of biological samples, the further development and engineering of highly effective and sensitive biosensors is required to match the need to detect traces of biological substances and the heightening complexity of damaging substances. For this purpose, miniaturised, flexible, transparent, portable, wearable, and multifunctional sensors hold great appeal [5, 6].

The demand to develop devices offering rapid and reliable results has led to the desire to acquire improved and novel sensing techniques. Reliable and prompt sensing should entail improvements in the system's efficiency and reductions in the throughput time to acquire results. Hence, this has motivated researchers to look for new materials and methods to ensure the quick, cheap, and easy determination of results. In the field of electronics, silicon has dominated the sensor industry in recent decades [7, 8]. It has the advantages of being an intrinsic semiconductor and is environmentally friendly and accessible, making it available for most electronic technologies and sensing applications in the modern era [9, 10]. The regular advances in technology have resulted in higher demand for material resources and has motivated the integration between nanostructured materials and existing technologies. Although current devices tend to be sufficiently small, it has become necessary to search for new materials to replace or supplement existing materials such as silicon. Recently, Graphene, which is a novel carbon material that could be replaced silicon, was introduced by Andre Geim and Konstantin Novoselov at the University of Manchester in 2004 [11]. They extracted

graphene by pressing Scotch tape onto graphite and pulling it off, resulting in exfoliated flakes a single-atom carbon atom thick. The carbon atoms in graphene form a hexagonal lattice, and it is the thinnest material known. They subsequently inspected its extraordinary properties such as electron mobility, and it has been used in the design of a graphene field-effect transistor (GFET) [12]. This work introduced a whole new field of research based on graphene and its properties.

The existence of graphene opens the door to various technologies and applications due to its extraordinary properties. As a result of its atomic structure, graphene has premium chemical and electronic properties [8]. Numerous studies have demonstrated advances in the use of reduced graphene oxide (rGO)-based sensors, illustrating rGO's suitability in the fabrication of sensors. All allotropic carbonic materials are made up of carbon atoms, and unique properties are exhibited by carbon allotropes due to their diverse ways of bonding and configurations; however, carbon also known to be a lightweight and generally multipurpose material. rGO and graphene oxide (GO) are among the most widely known carbonic materials derived from graphene [3, 6]. Although the mechanical and optical properties of GO experience a less significant effect, its conductive properties are substantially lower compared to graphene. Nevertheless, the conversion of GO into rGO via further reductive exfoliation treatment enables the restoration of properties akin to those of graphene [6]. Upon selecting GO or graphene, rGO is turning into an ideal option between the two. This is the case because various photo-assisted thermal, microwave, and electrochemical techniques enable the seamless production of sufficient quantities of low-cost GO which is also a good conductor and exhibits properties similar to those of graphene.

Multi-step combined methods which may involve solar mediated, radiation-induced, and serigraphy-guided reduction can be utilised to enhance the generation of rGO [6, 13-17]. Furthermore, the presence of structurally damaged regions, where oxidised chemical groups adorn the graphene-like basal plane that makes up its heterogeneous structure and lead to rGO's typical conductive and optoelectronic characteristics, means that its mechanical properties approach those of pristine graphene. The usage of reduced graphene oxide in storage and optoelectronic devices alongside a multitude of catalytic, biological, sensorial, and environmental applications is possible due to its properties being similar to graphene, thus highlighting its practical appeal [6]. Due to its excellent properties, graphene is suitable for significant applications in health monitoring systems where miniaturisation, biocompatibility, low cost, and quick and reliable results are important in the diagnosis and treatment of ailments.

A concise illustration is presented in figure 1-1 showing a graphene-based sensor platform for health monitoring.

Electrochemical sensors are now types of chemical sensors which play an important role in our day-to-day lives. Their sensing schemes are based on several means of electrochemical recognition that range from electrochemical to an amperometry impedance processes [18]. They are used in many areas, and mainly for biochemical and biomedical applications; for example, as gas sensors [19], the detection of heavy metals in water quality analysis [20], and for the sensing of alcohol [21]. Electrochemical sensors have found applications in biological and chemical warfare, food monitoring, medical diagnostics (including corona virus testing), manufacturing, the automotive sector, and home and environmental monitoring [22-24]. It is important to state that rGO electrodes can find applications not only in the fabrication of supercapacitors but also in the area of electrochemistry in the above-mentioned fields for specific sensing purposes.

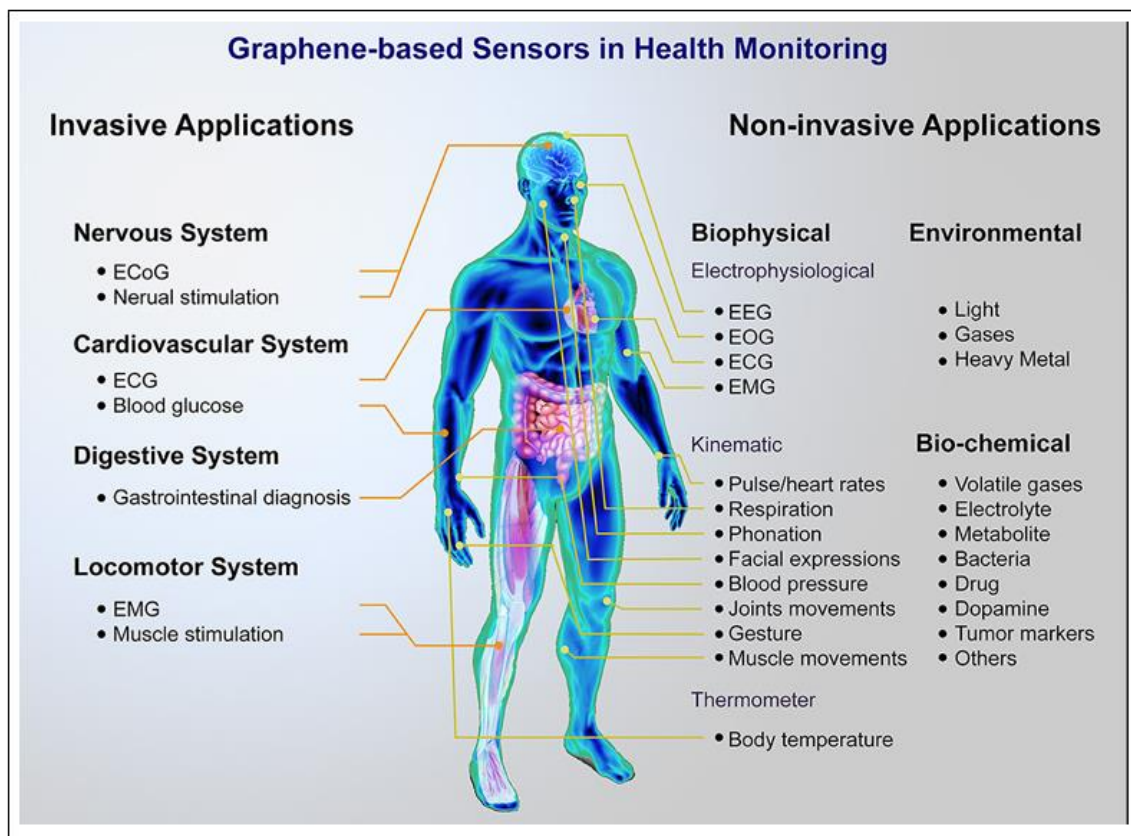


Figure 1-1. Graphene-based sensor platform for health monitoring [25].

1.2 Problem Statement

Some sensors are mainly dependent on the use of pure graphene due to its beneficial properties. However, the process of graphene production can be time-consuming and expensive, and very advanced equipment is required for effective production. The high production costs of graphene have led to the search for a more economical material that possesses properties that are similar or closely comparable to those of graphene while also being cheaper and easier to fabricate. Various techniques for the production of rGO have been explored due to its premium properties similar to those of pure graphene.

1.3 Aim and Objectives

- Aim

This work aims to design a low-cost and simple technique for the fabrication of interconnect capacitors and electrode devices made of reduced graphene oxide to be used in the field of biosensing. Another reason for an exploration of the currently applied manufacturing methods is to establish techniques for and approaches to the cost-effective production of rGO. In addition, improved repeatability in the manufacturing process is sought along with the optimum fabrication conditions so that the graphene produced can be customised for better use in electrochemical or biological sensors.

- Objectives

The key objectives of this work are:

- The fabrication of an electrode as a sensing device under atmospheric and vacuum conditions, as well as in the presence of gases such as Nitrogen (N₂) and Argon (Ar).
- Optimization of the methods used to produce these electrode devices and how their quality can be improved.
- The design of the electrode of choice followed by the preparation of reduced graphene oxide from graphene oxide using the light-scribe method under the above-mentioned conditions.
- Study the characteristics of the surfaces of the fabricated devices.
- Carry out an instrumental analysis to investigate the viability of the devices using cyclic voltammetry, which is an electrochemical technique for the investigation of redox reactions at electrode-solution interfaces.
- Creating high-performance electrochemical electrodes for diagnostics and biosensing applications.

1.4 Thesis Structure

This thesis contains chapters that are structured as presented below:

Chapter 1 introduces the subject and research problem of the study and describes the objectives of the thesis. It details the motivations for the research and the significance of the problems currently encountered, and a brief overview of the classes of techniques available is also given. The study's objectives are also outlined, with a brief explanation of the techniques developed.

Chapter 2 reviews the existing literature, evaluating different models and offering an overview of graphene-based techniques and the methods developed to reduce graphene oxide.

Chapter 3 gives a concise understanding of the materials and equipment used in the design and production of the sensing device. This chapter also presents brief insights into the electrode production process and the fabrication approach employed, with figures included to explain the implementation techniques in detail.

Chapter 4 gives a complete investigation and analysis of the obtained characterised results. The accuracy and viability of the proposed techniques used for device production are shown, and in addition graphical representations and some analysis of the results are also presented.

Chapter 5 presents the results of the tests carried out on the rGO electrode, the results were categorized to aid understanding of the test outcome leading to the determination of the performance electrode device that suits the proposed application.

Chapter 6 presents the results of electrode tests conducted using CV and a discussion of the analysis to aid in the selection of the optimum electrode.

Chapter 7 concludes the thesis and evaluates the limitations and advantages of the developed models. A summary of each of the techniques developed is provided, outlining the main ideas and contributions of the work completed and its relevance. It then highlights possible avenues for future research and offers recommendations based on the experience of the present study.

Chapter 2. Literature Review

2.1 Biosensors

The effort to develop easy-to-manufacture electrodes with superior electrochemical performance capabilities will be beneficial for biosensing and diagnostics. Biosensors are increasingly applied to monitor health and diagnose disease, which means that such electrodes are key to the usability and reliability of biosensors [3, 26]. As their name suggests, biosensors are biological sensing units incorporated into analytical devices. These devices require physiochemical transducers capable of capturing highly sensitive and specific biological events in a straightforward manner to provide complex bioanalytical measurements [26, 27]. Their potential applications are almost limitless and cover most analytical tasks, including drug discovery, diagnostics for health, food safety, monitoring of the environment, process controls, and use in the security and defence industries [26].

Biosensors are a product of an earlier concept known as the Clark oxygen electrode [28]. Clark theorised that the electrochemical detection of hydrogen peroxide (H_2O_2) or oxygen could be exploited by incorporating suitable immobilised enzymes in a wide variety of bioanalytical instruments. An early example was applied to the detection of glucose levels in diabetic patients, where a simple platinum electrode became an effective analytical tool through the incorporation of immobilised Glucose Oxidase (GOx) [28, 29]. A biosensor system consists of the following three components: (a) a detector to identify a biological target such as antibodies, bacteria, DNA, or enzymes; (b) a transducer to convert energy from one form related to the biological element which requires recognition to another form as a signal); (c) an output system to address signal amplification and display. These components are depicted in figure 2-1 [26, 30].

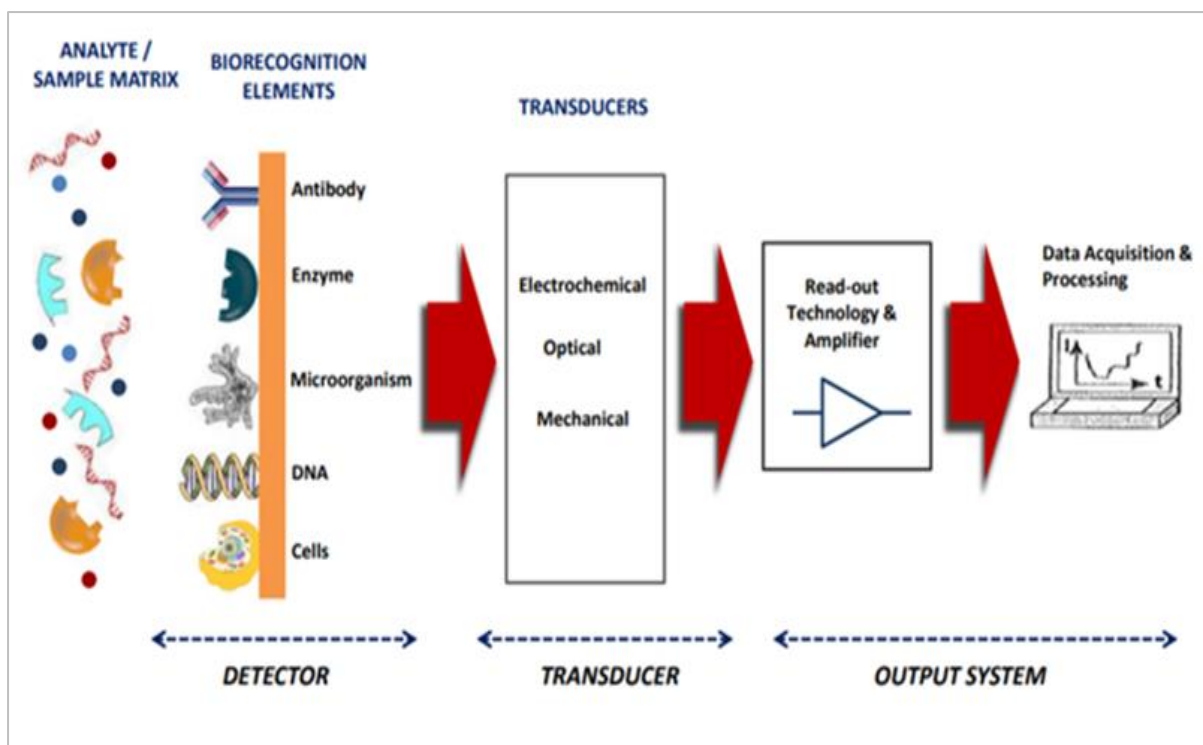


Figure 2-1. A generic biosensor system [30].

2.2 Biosensor Types

There are different types of biosensors, some are classified based on their biorecognition elements while others are categorised according to their transducer, which may be electrochemical, optical, thermal, or piezoelectric. The next section gives a brief overview of some of the biosensors used for biomedical applications.

2.2.1 Optical detection Biosensors

Optical biosensors offer advantages in comparison to conventional models in that they are capable of detecting many biological and chemical compounds directly both in real-time and label-free. These small devices have proved to be cost-effective while simultaneously offering high specificity and sensitivity [31, 32]. Optical biosensors use a light source and other optical components to generate a light beam with specific characteristics such as high specificity and sensitivity, small size, and cost-effectiveness [33, 34]. For example, Surface Plasmon Resonance (SPR) biosensors use a surface plasmon wave generated by the oscillation of charge density taking place at the interface between the dielectric and metal to measure the light produced by the luminescence process. In this case, the light beam is targeted at a modulating agent with a modified sensing unit and a photodetector. In other words, SPR sensors (figure 2-2) detect changes in refractive index (RI; also referred to as the index of refraction which

represents the degree to which a ray of light bends when it passes from one medium to another) as a variation of resonance angle (RA) within the area of detection [31, 35, 36]. However, there are other types of optical biosensors that have been used by a lot of researchers such as bioluminescent optical fibre biosensors, evanescent wave fluorescence, ellipsometric, interferometric, and reflectometric interference spectroscopy and surface-enhanced Raman scattering biosensors [31].

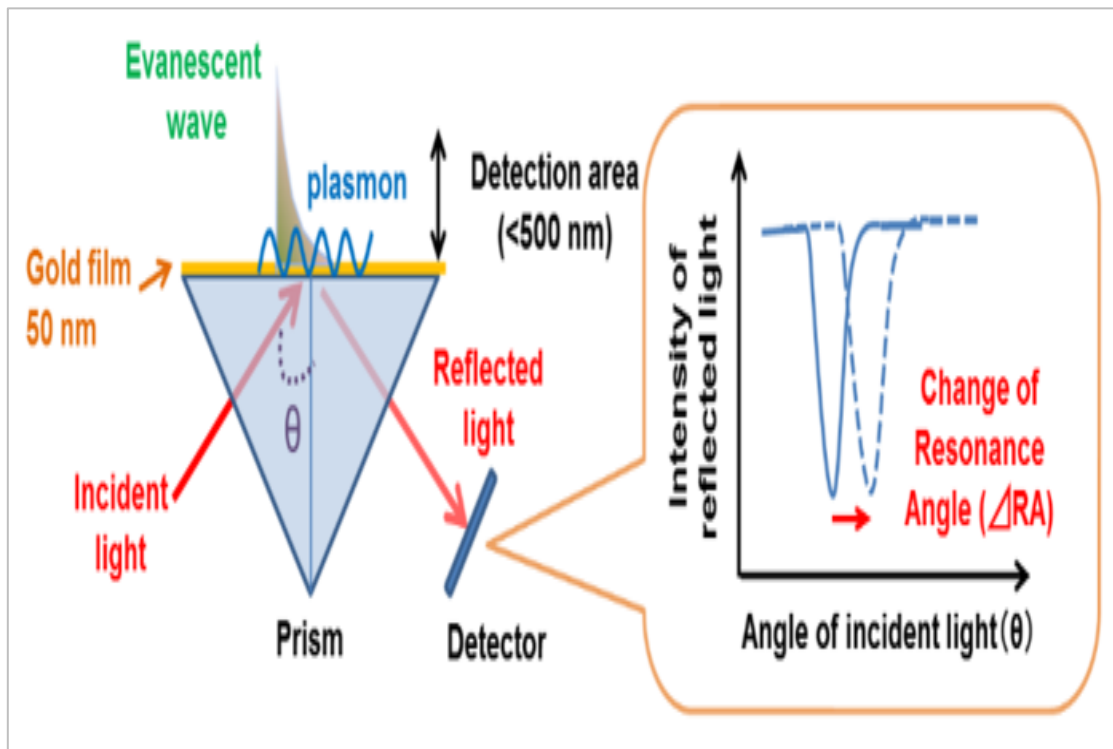


Figure 2-2. Surface Plasmon Resonance (SPR) sensor system [35].

2.2.2 Electrochemical Biosensors

Through electrochemistry, researchers can examine diverse systems such as molecules and the materials involved research fields such as clean energy and substrate activation in biological systems. In particular, electrochemistry can help give a better understanding of the role of catalysts and catalytic efficiency as well as chemical reduction and oxidation (redox) processes. Chemical research uses electrochemical techniques such as coulometry, voltammetry, potentiometry, and amperometry to assess redox potentials, assemble or synthesise materials, examine the efficiency and functions of catalysts, and determine the reversibility of a chemical process [37].

There have been significant developments in the synthesis, characterisation and processing as well as applications of nanomaterials utilised in the design of electrochemical sensors and

biosensors which exhibit heightened sensitivity. Furthermore, sensors must be reusable, specific, and highly sensitive to a particular analyte. Electrochemical biosensor technology offers unique advantages, resulting in increasingly wide application compared to traditional detection methods [38]. In the development of electrochemical biosensors, there has been a considerable focus on nanostructured carbon-based materials, including fullerenes (C₆₀) [38], carbon nanotubes [39], carbon quantum dots [40, 41], graphene [38], and carbon nitride [42], due to their high durability and biocompatibility, excellent optical, electrical, and thermal conductivity, mechanical strength, and large surface area. Studies have shown that, given the outstanding performance of electrochemical sensors, this type of biosensor can match or outdo traditional methods [38, 43]. Exceptional electrochemical, electrical, and mechanical properties have been observed in graphene along with its derivatives such as reduced graphene oxide (rGO). Moreover, given its large surface area as well as a framework rich in oxygen and defects, graphene can be developed as nanocomposites with quantum dots and polymers, metal/semiconductor nanoparticles, and metal oxides. There has been increasing use of these nanocomposite materials, including in applications such as electrochemical biosensing platforms [44]. Biomedical and environmental protection applications as well as those in clinical diagnosis all have significant use for electrochemical sensors and biosensors. Such sensors have extensive capabilities in sensing, for example, cancer biomarkers, sugars, neurotransmitters, by-products of purine metabolism, toxins in food or drinking water, antioxidants, and lipids, and the detection of all of these substances is crucial for human health [27, 45].

In electrochemical detection methods, the electrochemical biosensor is developed to identify and rapidly detect primarily biocomponents, including enzymes and antibodies for modifying electrodes [46]. A reaction between the original biocomponents and the specific target analyte is then confirmed and measured. The electronic system subsequently assesses the electrical signals generated, developing the information that is observed directly. Linear sweep voltammetry (LSV), differential pulse voltammetry (DPV), and cyclic voltammetry (CV) are methods commonly used to detect electrochemical sensor. Figure 2-3 illustrates the principle of electrochemical sensors as carbon nanomaterials used to identify metabolic disease biomarkers [38].

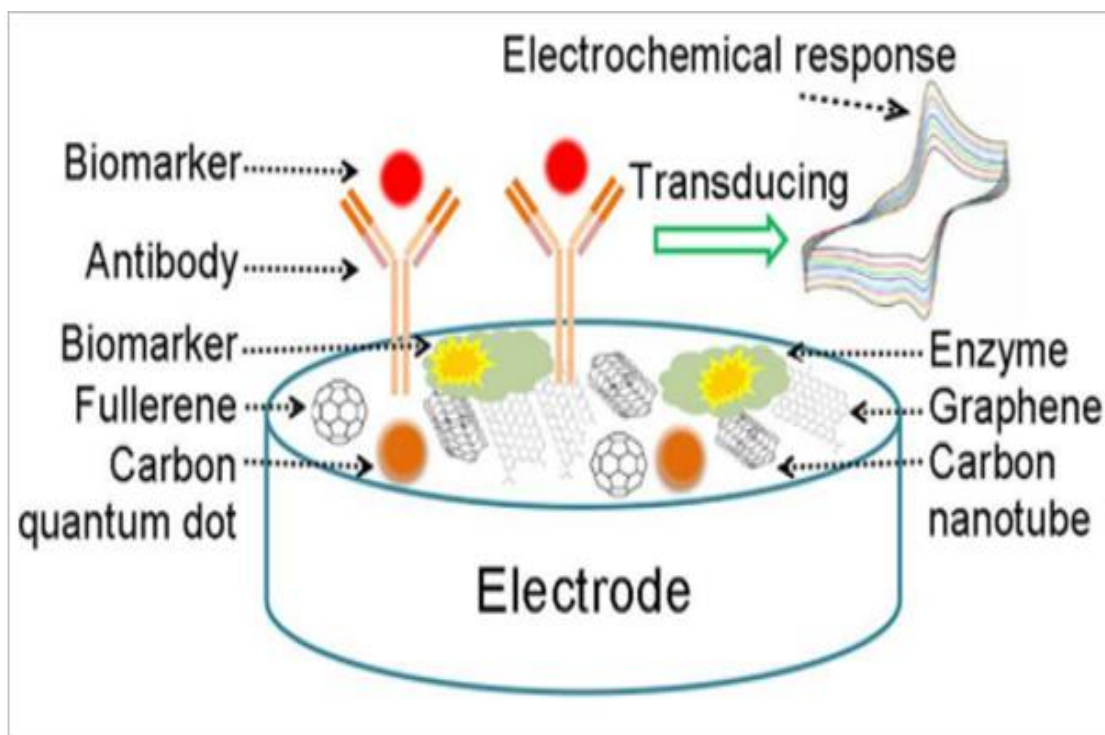


Figure 2-3. A simple electrochemical biosensor [38]

In order to effectively analyse the results from these kinds of sensors, several analytical steps need to be followed and various factors need to be taken into account. For this kind of sensor, it is important to consider the ideal Nernstian one-electron transfer process with a value of peak-to-peak separation potential (ΔE_p) of 59mV [47, 48]. This is obtained by using Equation 2.1 [49] where this value for an electrochemical system indicates that it is a reversible system:

$$\Delta E_p = E_{pa} - E_{pc} \dots\dots\dots 2.1$$

In order to further determine the reversibility, quasi-reversibility or irreversibility of system, it is important to determine the heterogeneous electron transfer at the electrode surface (k^0), which is more simply referred to as the electron transfer rate [48, 50]. Once the k^0 is fast enough to sustain the concentrations of the oxidation and reduction, electroactive species forms at the values needed by the applied overpotential that is based on the Nernst equation, this process is referred to as a reversible and is called a Nernstian system [50]. Otherwise, the electrochemical reversibility is a condition in which the rate of electron transfer is considerably greater than the rate of mass transport, and the electron transfer process (or current) is solely determined by the mass transport as the slower step. From this, it then follows that a system with a value of k^0 greater than 0.05cms^{-1} is referred to as a reversible electron transfer process [51]. For a slow electron transfer reaction, specifically when k^0 is smaller than 10^{-5}cms^{-1} , the electrode process is mainly controlled by the rate of electron transfer and is referred to an irreversible electron

transfer reaction [47]. This simply means that, when the rate of electron transfer is smaller than the diffusion constant, the electrochemically generated species diffuses from the surface of the electrode and does not exist at the electrode surface to undergo a reverse electron transfer reaction during the reverse scan. However, when the value of k^0 lies in the range from 10^{-5} to 0.05 cm s^{-1} ($0.05 > k^0 > 10^{-5} \text{ cm s}^{-1}$), both the electron transfer reaction and the mass transfer process determine the overall rate of electrode process and the electron transfer reaction is therefore called a quasi-reversible process [50].

In order to estimate the value of k^0 , the dimensionless kinetic parameter Ψ was first determined using Equation 2.2 [52, 53], and substituting it in Equation 2.5 where the value for k^0 would be determined for each electrode:

$$\Psi = \frac{(-0.6288 + 0.0021 X)}{(1 - 0.017 X)} \dots\dots\dots 2.2$$

where X equals the ΔE_p of the system multiplied by the number of electrons involved in the electrochemical reaction, n , expressed in mV as shown in equation 2.3 [54]:

$$X = \Delta E_p \times n \dots\dots\dots 2.3$$

To precisely determine the value of X, it is imperative to determine the value of n in equation 2.3 since the value of ΔE_p has been determined above for each electrode. The value of n can be determined for each electrode using Equation 2.4 below [55]:

$$\Delta E_p = 2.218 \frac{RT}{nF} \dots\dots\dots 2.4$$

where F is the Faraday constant, R is the universal gas constant, T is the absolute temperature, and n is the number of electrons.

Inputting this number of electrons in Equation 2.3 will yield an X value that is equal to the individual ΔE_p for each electrode from which the dimensionless kinetic parameter Ψ of each electrode was estimated, and this value can then be used to determine the system process. It is, however, important that, if $\Psi > 10$, this indicates the electrochemical reversibility of the system whereas if $10 < \Psi < 10^2$ the system is considered to be quasi-reversible while if $\Psi < 10^2$ the system is irreversible [47, 53]. Now, to estimate the electron transfer rate (k^0), Equation 2.5 is employed.

$$K^0 = \Psi \times \sqrt{\frac{\pi D n \nu F}{RT}} \dots\dots\dots 2.5$$

where v is the scan rate (in Vs^{-1}), F is the Faraday constant, R is the universal gas constant, T is the absolute temperature, and D is the diffusion coefficient of the oxidation of the electroactive species which has been approximated to be $5.4 \times 10^{-6} \text{ cm}^2 \text{ s}^{-1}$ for potassium ferricyanide [56, 57]. It is important to note that if the system that has a value of k^0 greater than 0.05 cms^{-1} , it is counted as having a reversible electron transfer process and thus is a reversible system [50]. As a reversibility of any system means its ability to recover or return to its original background and/or baseline condition, after exposure to an analyte, which is an important trait to any biosensor to be reproducible and repeatable [58-61]. But for slower electron transfer reactions, and particularly if k^0 is smaller than 10^{-5} cms^{-1} which is considered the normal value of the diffusion constant, the electrode process is here largely controlled by the rate of k^0 and this situation is termed an irreversible electron transfer reaction [50]. By and large, when the value of k^0 lies in the ranges from 10^{-5} to 0.05 cms^{-1} , both electron transfer and the mass transport process determine the overall rate of electron process and hence the electron transfer is therefore termed a quasi-reversible process [47, 50]. The mass transport for these electrodes can be determined by equation 2.6:

$$M_{trans} = \sqrt{\frac{\pi D n v F}{RT}} \dots\dots\dots 2.6$$

2.2.3 Mechanical Biosensors

The chemical interactions between the analyte and sensor are used to classify four broad categories of mechanical biosensors. Fingerprint assays use an array of less selective functionalised layers to determine a target according to its distinctive binding affinities to a collection of sensors whereas affinity-based assays depend upon highly specific interactions between specific antigens and antibodies in which the identification and capture of the target on the device surface is highly specific (with high affinity). Meanwhile, spectrometric assays identify the target through its mass or optical properties, and separation-based assays use spatiotemporal separation arising from the different chemical affinities of flowing analytes and immobilised species [62, 63].

2.3 Graphene Background

The discovery of graphene materials has enormous potential for overcoming issues in the disciplines of life sciences, energy, and the environment linked to performance, functionality, and durability. Furthermore, graphene has recently attracted a lot of attention as a potential

candidate for biosensors because of its exceptional electrochemical and mechanical strength, good adsorption performance, and flexibility [64, 65].

Graphene is basically the only form of carbon (and solid materials in general) where each of its atom is exposed to chemical reactions from two sides due to its 2-dimensional (2D) structure. Typical carbon-carbon atom bonding in a graphene sheet is shown in figure 2-4. It is acknowledged that carbon atoms at the edge of graphene sheets possess special chemical reactivity, and graphene has the highest ratio of edge carbons in comparison with similar materials such as carbon nanotubes. In addition, its chemical reactivity increases due to the various types of defect which are very common within the sheet [66].

Graphene can be produced in various ways depending on the synthesis method used, such as chemical vapour deposition (CVD) or chemical synthesis to form materials such as graphene oxide (GO) and reduced graphene oxide (rGO). It has remarkable qualities that make it the first choice for a variety of applications such as the design of transparent conductive electrodes [67].

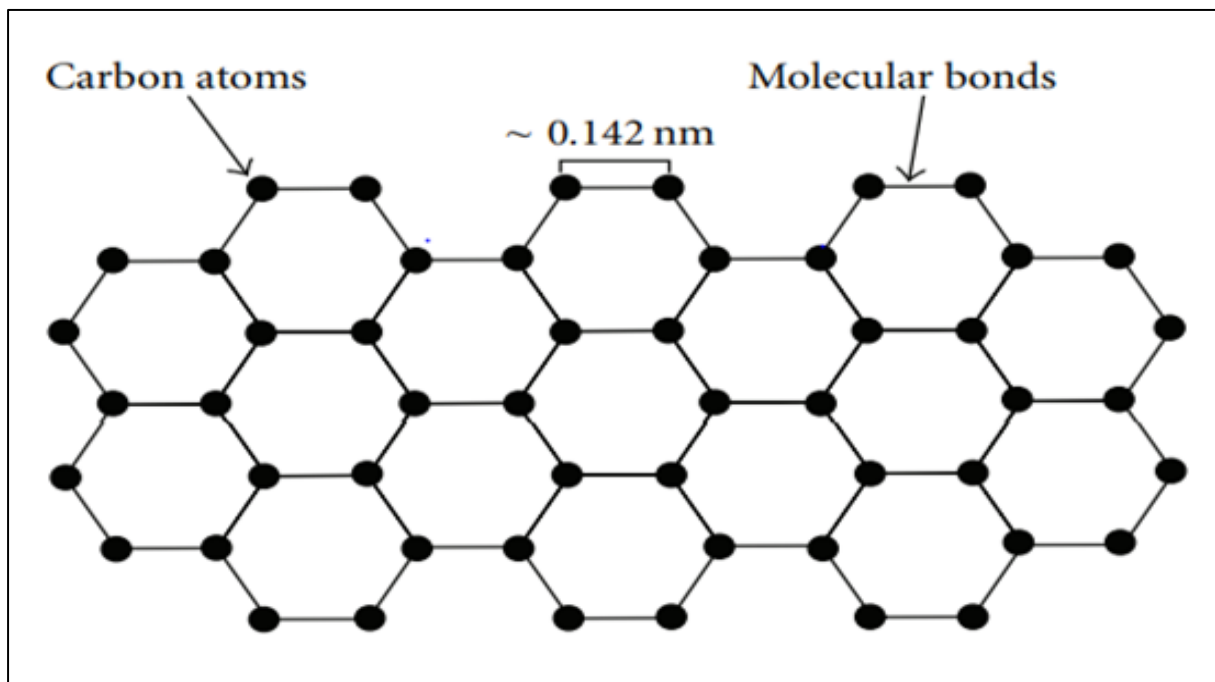


Figure 2-4. Carbon-carbon atoms bonding in a graphene sheet [68, 69].

2.4 Properties of Graphene

Given the unique properties of the material compared to other carbon allotropes and functional materials, the thermal properties of graphene have encouraged its use in electronic devices and particularly those for heat management. The thermal conductivity of graphene mainly depends on its diffusive and ballistic conditions at higher and lower temperatures respectively [70-72].

For example, the conductivity of suspended monolayer graphene at room temperature is higher than that of graphitic carbon [70, 73, 74]. In addition, graphene excels over carbon nanotubes in heat conduction when obtained using mechanical exfoliation [75]. Furthermore, calculations have demonstrated the dependence of its conductivity on the width of graphene nanoribbons and the roughness of its edges.

Its mechanical properties largely depend on the purity of the material. Graphene is among the strongest materials known, with a Young's modulus of approximately 1.0 TPa and tensile strength of 130GPa when defect-free [73]. Chemical cross-linking between the flakes in graphene oxide paper also enhances its mechanical stiffness and tensile strength [76]. Other unique properties include high electron mobility at room temperature ($2.5 \times 10^5 \text{ cm}^2 \text{ V}^{-1} \text{ s}^{-1}$), impermeability to gases, high thermal conductivity above $3,000 \text{ Wmk}^{-1}$, zero bandgap, and high optical absorption [77]. Furthermore, graphene-based materials have been reported to possess a surface area of $2630 \text{ m}^2 \text{ g}^{-1}$ and this property is useful for sensing applications where surface area is of importance for the efficiency of the sensing scheme [78, 79].

2.5 Graphene Production

Methods for the production of graphene can be divided into top-down and bottom-up categories, as shown in figure 2-5. Mechanical exfoliation and liquid phase exfoliation are examples of top-down procedures, whereas epitaxial growth on silicon carbide SiC and chemical vapour deposition (CVD) are bottom-up methods [80]. The following section provides a brief background for these methods used in the synthesis of graphene.

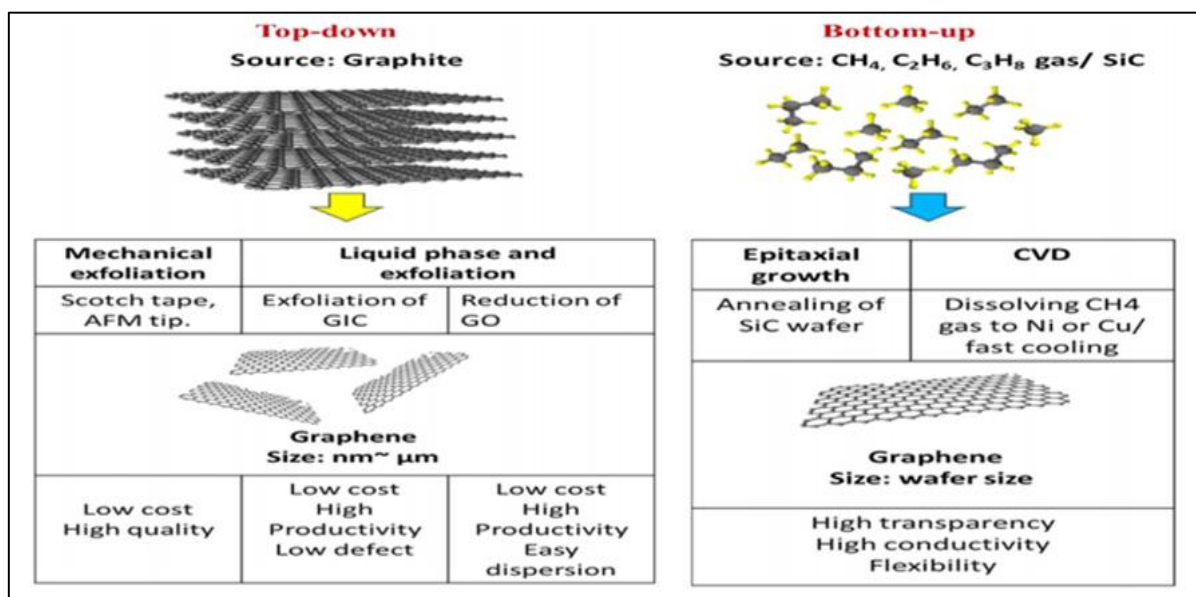


Figure 2-5. Top-down and bottom-up graphene synthesis [80].

2.5.1 Mechanical Exfoliation (ME)

Graphene is prepared by the exfoliation of graphite within the top-bottom concept. The exfoliation technique is a commonly used way to synthesise graphene from graphite or other carbon sources. Mechanical exfoliation is also referred to as the Scotch tape method, which is a traditional technique that has been employed for decades. The graphite is placed as a substrate and repeatedly peeled using the tape until a monolayer is collected. Although this process is simple, it has some challenges facing with smaller final products and structural defects [81].

2.5.2 Liquid Phase Exfoliation (LPE)

Liquid phase exfoliation is a promising scaling method in which graphene is disseminated in a suitable solvent and exfoliated using ultrasonication or shear forces. The surface energy of the solvents used should be around 40 nN.m^{-1} and finding a suitable one may be difficult due to their toxicity, corrosiveness, and high boiling point and cost. Experiments have been conducted using solvents with low boiling points such as methanol, ethanol, acetone and acetonitrile [82]. Water is another solvent utilised in LPE with a high value of surface tension (72 mN.m^{-1}); thus, it must be used with caution. Moreover, water is hydrophilic and graphene is hydrophobic and, as a result, some surfactants such as sodium cholate and sodium dodecylbenzene sulfonate are utilised with a water solvent [83, 84]. In such cases, non-ionic surfactants are more appropriate compared to ionic ones because the former have more extended hydrophilic regions and hydrophobic tails, resulting in steric repulsion [85]. During the LPE process, the bubbles expand and contract and hence the distributed graphite exfoliates to a few layers of graphene. The exfoliation of graphite to produce graphene is also caused by fluctuations in pressure [82].

2.5.3 Epitaxial Growth on Silicon Carbide SiC

Graphene is also produced by heating silicon carbide (SiC) to 1100°C , where the size of the resulting graphene flakes depends on the size of the SiC wafers used. The characteristics of the SiC surface also affects the graphene's thickness, mobility and carrier density [86]. This type of graphene tends to have weak antilocalisation compared to exfoliated graphene [87]. However, epitaxial graphene has similar properties to that from the peeling-off method but is not as high as exfoliated graphene [38]. Moreover, epitaxial graphene is high in quality, but can be costly due to the expensive SiC substrate. In addition, the yield is low and therefore it is not appropriate for industrial manufacturing [86].

2.5.4 Chemical Vapour Deposition (CVD)

Chemical vapour deposition (CVD) is a commonly employed materials processing technology where single layers or thin-films of the desired material are formed on a heated substrate by means of a chemical reaction of gas-phase precursors [88]. In contrast to physical vapour deposition (PVD) methods which involve techniques such as evaporation and sputtering, CVD has a clear advantage by depending on chemical reactions that permit tuneable rates of deposition as well as giving high-quality products with excellent conformality [88]. In addition, the introduction of low-dimensional materials such as carbon nanotubes, graphene, and 2D transition metal dichalcogenides (TMDs) in the electronics industry has led to more strict requirements for the successful CVD of these materials possessing high purity and finer structures. CVD, however, permits the tuning of the structures and properties of the resulting products [89, 90] and several advanced CVD systems and their variants have been developed. Typically, CVD does not need high-vacuum working environments, making it a prevalent technology in electronics, optoelectronics, surface modification, and biomedical applications [88, 91].

2.6 Graphene Applications in Different Types of Sensors

Graphene has found application in different research areas due to their sterling qualities as shown in figure 2-6, and other areas are still being explored. To begin with sensors are devices used to monitor or detect events in physical environments. Therefore, for these devices to be effective with high efficiency, materials are required whose properties will allow for the smooth and effective conversion of the relevant physical events into useful and readable information. Graphene is now used as a sensing material due to its large surface-to-volume ratio, high electrical and thermal conductivity, and excellent transparency and mechanical properties [92]. In addition, the ability to regulate the synthesis of graphene in terms of numbers of layers and dimensions and the addition of doping elements improves the ease of adjustment of its properties. Recently, graphene has been developed to meet the requirements of various sensing applications and purposes such as in gas, electrochemical, magnetic field, and mechanical sensors [93-95].

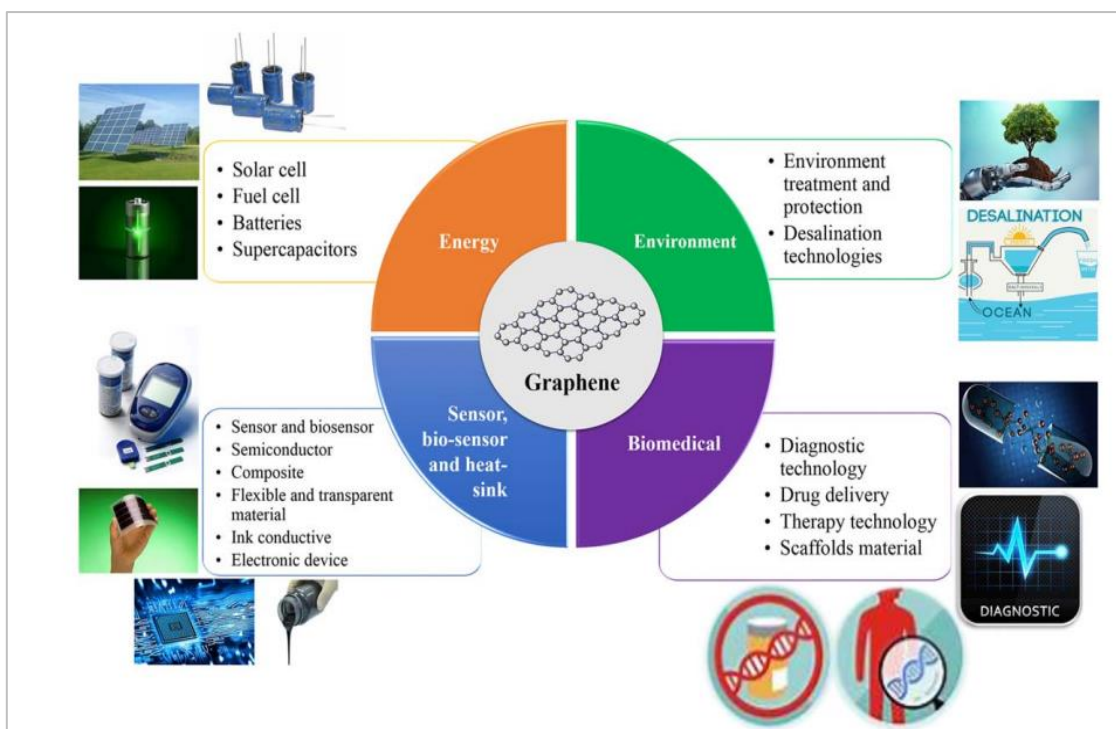


Figure 2-6. Graphene application in different research areas [96].

2.6.1 Electrochemical Sensors

For medical and biological applications, the precise monitoring of chemical or biological processes is critical. Electrochemical sensors can in theory achieve this purpose by transforming a chemical or biological response into a processable and quantifiable signal [93]. Intensive studies and developments of electrochemical sensors over the last two decades have enabled the fabrication of various devices. Following the successful introduction of numerous electrochemical sensors, there is now a noticeable shift to and increasing demand for the development of flexible and wearable sensors of this kind [93, 97]. The emergence and preparation of free-standing and elastic innovative materials are important in the development and production of flexible electrochemical sensors. There have been advances in flexible electronic devices, and particularly electrochemical sensors, as the technology is deployed to address real-world concerns such as in-situ sensing to tackle health and environmental problems [97]. Flexible electrode-based devices are more versatile and adaptable than traditional devices. They also take up less space and may be compatible with shape-targeted systems such as the human body and rough or irregular-shaped substrates [98, 99]. Flexible electrodes need to have excellent conductivity in sensing electrons and thermal energy as well as stability and mechanical strength [100, 101].

Carbon nanotube (CNT)-based devices previously dominated research and development due to the mechanical strength of their unique one-dimensional nano-channels [102, 103]. Nevertheless, owing to various serious technical drawbacks such as high production costs, the complex process of achieving high-density vertically aligned CNTs, chemical and biocompatibility issues, and challenges in realising large-scale production, CNT-based flexible electrodes are limited primarily to fundamental interests [102-104]. The recent increase in the synthesis and procession of 2D graphene and its derivatives provides new and intriguing potential for construction of a novel class of flexible electrodes with essential physiochemical properties [105, 106]. Graphene paper with outstanding mechanical properties, variable conductivity and diverse functionality could aid in the study and development of the next generations of flexible electrode-based sensors and other electronic devices [25, 107, 108]. Moreover, GO is a chemically modified form of graphene material the preparation of which by oxidation and exfoliation is accompanied by extensive modification of the basal plane. It has so far been largely ignored in the field of electrochemical sensing, and has been considered predominately as a precursor in graphene synthesis. Moreover, the modified form of GO often referred to as rGO is a kind of graphene material that has been reductively processed using chemical, thermal, microwave, photo-chemical, photo-thermal or microbial/bacterial approaches to reduce its oxygen content [109]. It is now attracting interest and being considered for application as a cheaper alternative to graphene.

2.6.2 Mechanical Sensors

Graphene-based mechanical sensors are used to detect physical changes in materials [110, 111]. He Tian and his team [112] developed an ultra-sensitive resistive pressure sensor for electronic skin sensing systems using laser-scribed graphene (LSG). The authors reported 0.96 kPa sensitivity in 0-50 kPa pressure range which was attributed to the large spacing between the layers of graphene and the LSG V-shaped microstructure. Park et al [113] developed a highly stretchable strain sensor to monitor the movements of various body parts, and Cheng et al. [114] presented a highly sensitive strain sensor to detect human walking movements, squatting, and sound recognition. Their results included response times less than 100 msec and durability over more than 1000 cycles. A similar approach was used by Yang et al. [115] to prepare strain sensors to diagnose human health based on traditional Chinese medicine. They reported ultrahigh sensitivity under minor strain and the accurate detection of pulse differences in three adjacent positions. Wang et al. [116] developed fibre graphene assemblies based on a fabric structure where GO is combined with polyester fabric before reducing it to rGO. They reported

good sensitivity with a high response time of 50 msec, making it appropriate for the detection of ground plantar pressure distribution.

2.6.3 Environmental Sensors

Graphene-based sensors are used widely for environmental sensing purposes in daily life and industrial processing [95]. Chehura et al. [117] developed a humidity sensor using tilted fibre Bragg gratings sensors (FBGs) coated with a GO layer of thin film. Their results showed that the maximum reported sensitivity was about 0.129 dB/%RH in the range of relative humidity from 10% to 80%. Smith et al. [118] utilised changes in the electrical resistance of CVD-grown single-layer graphene in the design of a high-performance humidity sensor, and their results included response and recovery times lower than 1s. Shehzad et al. [119] used the graphene/Si Schottky junction for a multimode humidity sensor where adsorbent water molecules affect the sensor's intrinsic properties, and it was shown to exhibit a sensitivity to humidity of 17% when forward-biased, 45% in the case of reverse bias, and 26% and 32% in capacitive and resistive modes respectively.

Zhu and his co-workers [120] utilised wrinkled graphene to develop a high-performance humidity sensor. The wrinkled morphology of the graphene improved evaporation because the aggregation of water microdroplets was prevented, and a response time of 12.5ms was reported which appropriately rapid for the monitoring of sudden changes in respiratory rate and depth. However, although fast response times have been reported for such sensors based on pristine graphene, their long-term stability was not investigated because humidity modifies its interlayer interaction and thus the sensitivity of the sensors is affected. Other researchers have used GO due to its high proton-conductive sensitivity to water molecules. Bi et al. [121] used microscale interdigitated electrodes to deposit GO film. Sensitivity towards humidity was measured using an LCR meter and values of 15-95% were found compared to typical capacitive sensors, with a fast response time of 10.5s, and a 41s recovery time. Borini et al. [122] investigated the effect of GO thickness on the sensor's response towards humidity, and the results showed an ultrafast response to a modulated humid flow with a film thickness of 15nm. Reduced graphene oxide (rGO) was used by Guo et al [123] in the development of a highly sensitive humidity sensor. A PET substrate was used to deposit GO employing a two-beam laser interference method, and in addition to long-term stability an excellent sensitivity in the RH range of 30% to 90% was reported for this sensor along with a response time of 28s and a recovery time of 48s. Phan et al. [124] used the rapid thermal annealing technique to investigate

the influence of degree of reduction on GO sensitivity. They demonstrated that resistivity decreased when temperature increased, and the sensor responses also decreased because the film could not adsorb water molecules. Graphene quantum dots (GQDs) were also used by Ruiz et al [125], and their results showed an exponential dependence of sensitivity in the RH range of 15-80% and a response time of 5s. A similar approach was used by Alizadeh et al. for two sensing mechanisms and response times of 10s were reported for values of RH between 0-52% and 52-97%. Various other graphene-based sensors are being researched and developed, such as those using chemically modified graphene and graphene/polymer composites for biochemical applications.

2.7 Methods of Reducing Graphene Oxide

Reduced graphene oxide material is becoming prominent as a useful and promising material for graphene-based applications. The reduction of graphene oxide for use as an alternative to graphene and other 2D materials has recently attracted attention among researchers, and these rGO materials have found application in sensors, supercapacitors, and electrodes [126, 127]. This turn towards rGO is mainly due to its lower cost, hydrophilic affinity, ease of handling, and the possibility of mass production of devices[128]. Several methods exist to produce this material, and the following sections give an overview of these techniques.

2.7.1 Thermal Reduction Method

Many researchers have investigated methods for the reduction of graphene oxide. Thermal reduction is an effective approach that can be used to reduce graphite oxide at elevated temperatures. The decomposition of oxygen atoms and exfoliated graphite oxide can occur at temperatures in excess of 2000 °C [14]. There are some drawbacks in using this type of technology, such as the small size of the graphene sheet and presence of defects [14, 129, 130]. Carbon atoms are eliminated from the graphene sheet during the breakdown of oxygen atoms, resulting in a smaller sheet, while its electrical conductivity declines during the thermal exfoliation of graphite oxide due to loss of mass and structural defects [14, 78]. During this process, a film or powder is produced from the graphene oxide solution before it is subjected to annealing [14, 78, 131]. To achieve a suitable graphene oxide structure, a high temperature is required. For example, GO films annealed at 500 degrees Celsius have lower electrical conductivity than those annealed at 1100 degrees Celsius, but the disadvantages of this approach include that it consumes a significant amount of energy and it takes a long time if to film expansion is to be avoided [14, 132].

2.7.2 Use of a Laser to Reduce Graphene Oxide

The laser-induced reduction of graphene oxide can remove oxygen components and increase the material's electrical conductivity, and figure 2-7 shows the illustration of the fabrication process of the LSG, and figure 2-8 shows the fabricated LSG electrode of this work. When a graphene oxide solution is exposed to a pulsed laser, the oxygen functional group is swiftly reduced, which ultimately enhances the material's electrical and mechanical properties. Additionally, the graphene oxide solution changes from a yellow-brown colour to black, which indicates reduction [133]. Due to its lower cost and the advantages of mass production potential, this method is attracting a lot of research interest and several kinds of laser system are being explored.

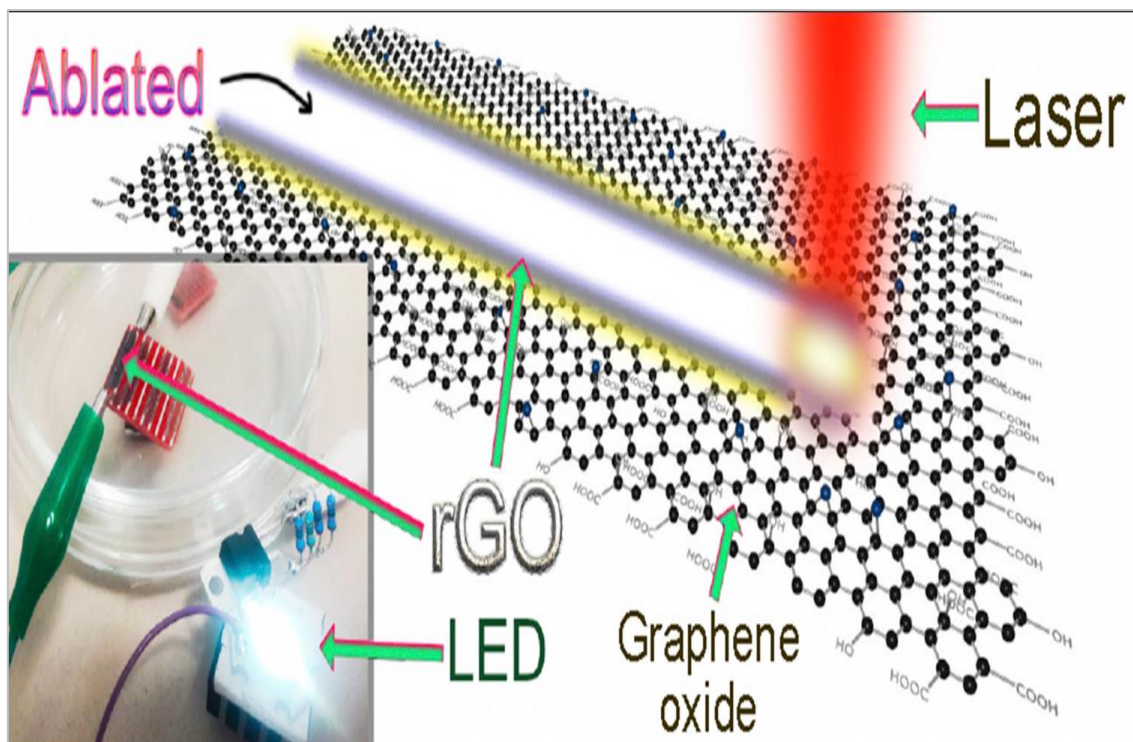


Figure 2-7. Illustration of the fabrication process of the LSG [134]

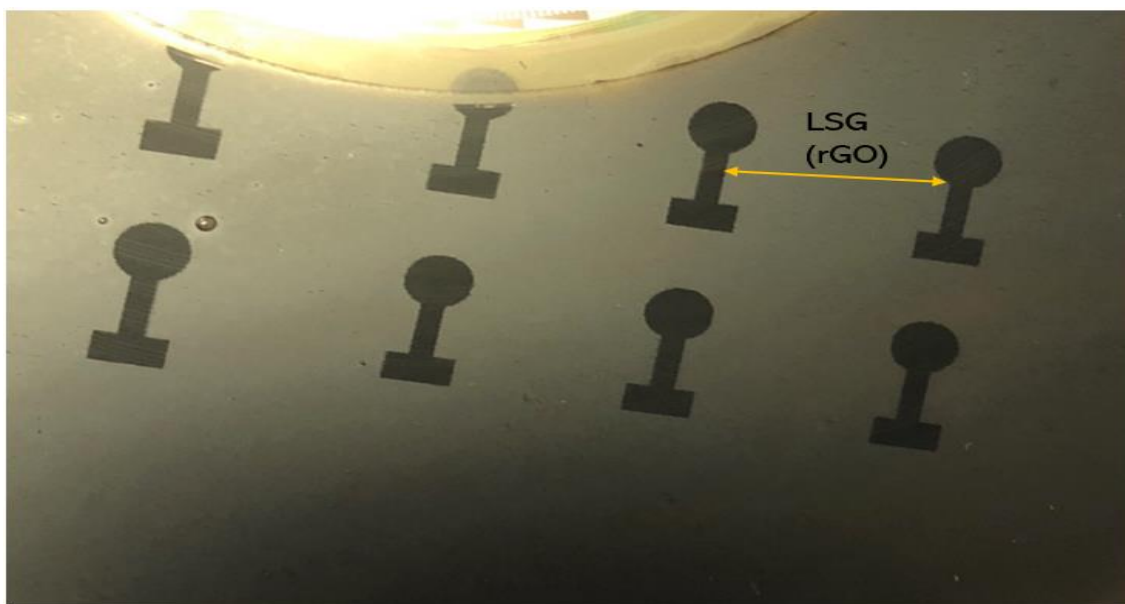


Figure 2-8. Fabricated LSG electrode.

2.7.3 Chemical Reduction Method

This reduction method utilises various chemical reactants, and the most commonly used chemical reagent for the reduction of GO is hydrazine hydrate [135]. Some other well-known chemical reactants that can effectively be used to restore GO to graphene include hydroquinone, iron powder, hexamethylenetetramine, sodium borohydride, hydroiodic acid, sodium, and potassium alkaline solutions [135]. This reduction method can be carried out in liquid media or a vapour environment at moderate or room temperatures [14, 135]. One additional advantage of the chemical reduction method is the prospect for synchronised chemical modification in synthesising the material. New studies show that the level of reduction achieved by this method could be significantly improved by exploiting the solvothermal method, which is itself a combination of chemical and thermal methods with supercritical settings [135, 136].

From the review of literature above, including various areas of application for graphene and its rGO counterpart, the present research work focuses on the development of techniques for the manufacture of rGO with a view to the establishment of a repeatable production process and the optimum type of electrode for electrochemical sensing applications. This will allow the achievement of the study's aims and objectives as stated in chapter one.

2.8 Conclusion

This chapter considers relevant work in the literature so as to fully understand the methods used for the reduction of GO as well as its sensing and biochemical sensing applications. It started with the background of biosensors, where several types of devices were reviewed including optical detection, electrochemical, and mechanical biosensors. Then the focus shifted to a review of the background of graphene, and its properties and synthesis methods which include ME, LPE, CVD, and epitaxial growth on Silicon Carbide (SiC). Then the applications of graphene in several sensor types were discussed, such as in optical detection, electrochemical, and mechanical biosensing. The chapter also reviewed the methods used in reducing graphene oxides, which are thermal, laser, and chemical reduction, as well as solvothermal methods.

Chapter 3. Methodology

3.1 Introduction

Techniques such as inkjet and screen printing are widely used in the development of platforms in electrochemical biosensing for the elaboration of bare electrodes [137, 138]. Electrochemical biosensors based on laser-scribed graphene electrodes have recently shown tremendous potential because of their electronic properties, porous structure, and large surface area that can support charge transfer [139]. Graphene oxide (GO) is converted into reduced graphene oxide (rGO) using the laser-scribing technology. The LightScribe DVD drive (with a laser power of 5mW and a wavelength of 788nm) can be used to pattern the surface and produce rGO from GO [140].

3.2 Materials

This section focuses on the materials used in the production of the electrodes and sensing devices in this study and these are discussed in the following subsections.

3.2.1 Suspended Graphene Oxide

Suspended GO1 is a two-dimensional (2D) material which is an oxidised form of graphene with Oxygen (O) functional groups attached to its branches [141]. It was purchased from Graphenea (San Sebastian, Spain) with a concentration of 4 mg/ml.

The second GO2 material is a more viscous liquid which was kindly provided by the University of California at Los Angeles (UCLA) and has been diluted in deionised water to 75 mg/ml in a sealable container as a working solution recommended in previous work [142]. The mixture was then hand-shaken for a period of 5 to 10 minutes and the suspended solution obtained was then used in the fabrication of the electrode. The liquid form of GO1 and GO2 are presented in figure 3-1.



Figure 3-1 The liquid form of GO1 and GO2

3.2.2 Polyethylene Terephthalate (PET) Film

Polyethylene terephthalate (PET or PETE) is a general-purpose class of thermoplastic polyester polymers. These resins are well-known for their various excellent properties such as high mechanical strength, and good thermal stability and chemical resistance [143]. Transparent PET film was purchased from the Viking Office Depot, UK served as the flexible base for electrode production with 210 mm x 297 mm as A4 sheet with a thickness of 115 micro- meter. The PET film was attached to the LightScribe DVDs using a few drops of 3M adhesive spray and the cut-out shape of the PET film to fit the DVD can be shown in figure 3-2. This adhesive material provided a fast and secure bond between the flexible transparent PET substrate and the DVD, thus forming a secure and stable base during the electrode fabrication.

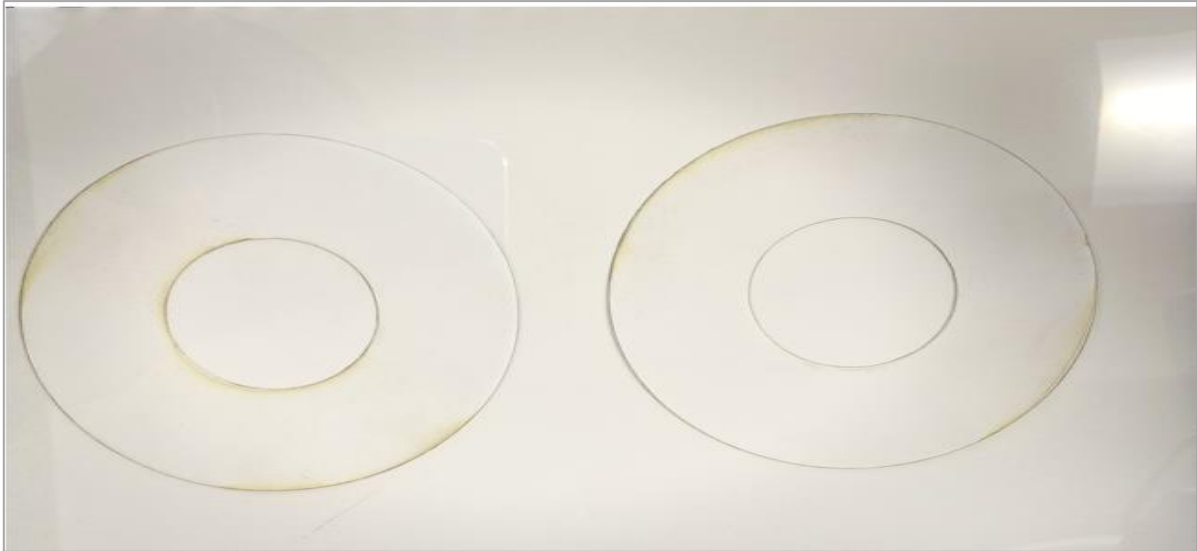


Figure 3-2 The cut-out shape of the PET film to fit the DVD

3.2.3 Conductive Silver

186-3600 silver conductive paint was obtained from RS Components (Northamptonshire, UK) and used to make the electrode contact point. Figure 3-3 shows a silver conductive paint and rGO electrode with attached copper tape through the using of this paint. The paint is used for painting onto an electrical screen or the creation of electrical connections to non-solderable surfaces. It has a good volume resistivity of $0.001 \Omega/\text{cm}$ when completely solidified. It can also provide excellent resistance against corrosion. This adhesive was painted onto the electrode with a brush and kept at room temperature for 10 min until touch-dry so as to be ready to use.

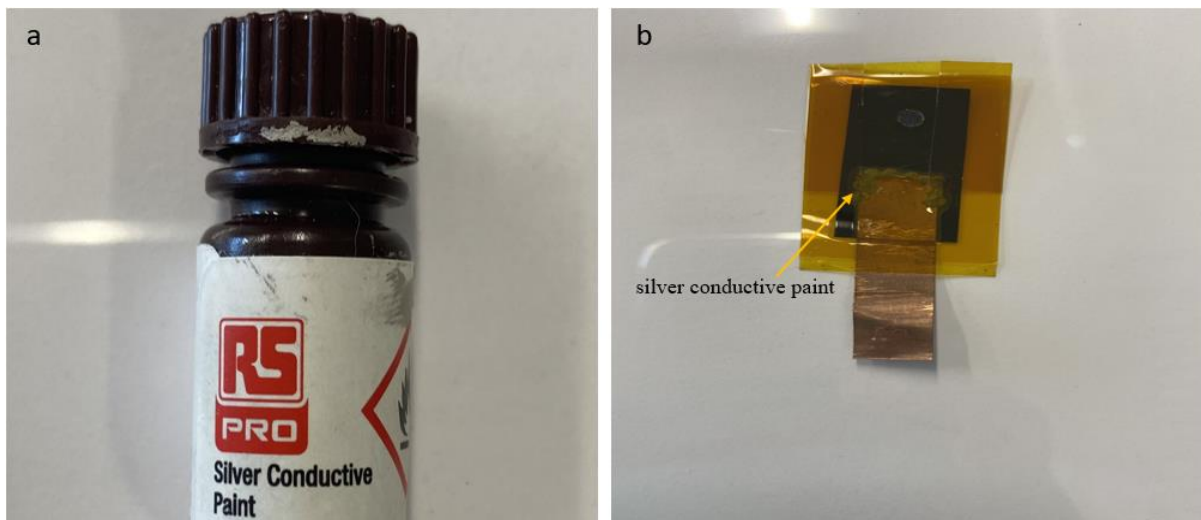


Figure 3-3 a) silver conductive paint, b) rGO electrode with attached copper tape through the using of silver conductive paint.

3.3 Research Equipment

The following sections describe the equipment used for the production of electrodes and device manufacture during the current research.

3.3.1 DVD LightScribe writer

LightScribe (Hewlett-Packard Company HP, USA) is a direct disc labelling system that precisely burns DVDs loaded with GO materials quickly and easily. It includes a personal computer (PC) LightScribe DVD drive with specially coated compact disc (CD) or DVD discs and advanced disc-labelling software [144, 145]. For this work, a set of ten DVD LightScribe discs were purchased online. The substrates were placed in the writer, and the LightScribe software was run to transfer the electrode design to the writer, and the LightScribe laser then imprinted the electrode design on the surfaces of the discs. Figure 3-4 shows the DVD LightScribe writer and the DVD disc in a case.



Figure 3-4 a) the DVD Lightscribe writer, b) the DVD disc in a case

3.3.2 Vacuum Chamber

Laser-scribing under vacuum conditions was used in addition to conventional ambient conditions to determine if different methods could improve the resulting quality of the electrodes. The vacuum chamber was designed in the laboratory at Newcastle University using Autodesk Inventor software. The soft copy-designed chamber was physically manufactured by Bill Quay Precision Engineering Factory, Newcastle, UK. Figure 3-5 shows the cylindrical vacuum chamber and the DVD LightScribe writer inside the vacuum chamber. It is worth mentioning that all of the components of the vacuum chamber including the chamber chassis, lid, pump bolts, and a pump (Edwards RV12, England) with a pressure sensor (Edwards, INST

CONT 40 W, England), were made of stainless steel so as to be efficient and cost-effective, since it is a significantly strong material and can withstand high pressure, in addition to being cost effective as it can be used several times for long time periods. Upon manufacturing this equipment, the chamber was installed in the Micro-Electro-Mechanical Systems (MEMS) Laboratory, Merz Court, Newcastle University, and was connected to an instrument controller to observe the pressure inside the chamber.



Figure 3-5 cylindrical vacuum chamber (left), the DVD Lightscribe writer in the vacuum chamber (right).

3.3.3 Gas Cylinder

Most of the electrodes produced under vacuum conditions without any additions appeared to have become charred. Thus, in order to ensure the production of electrodes of better quality, a cooling down in the chamber during production was necessary. For that reason, either N_2 or Ar gases were used at 0.5 mbar. Figure 3-6 presents an illustration of the chamber setting with the gas cylinders.

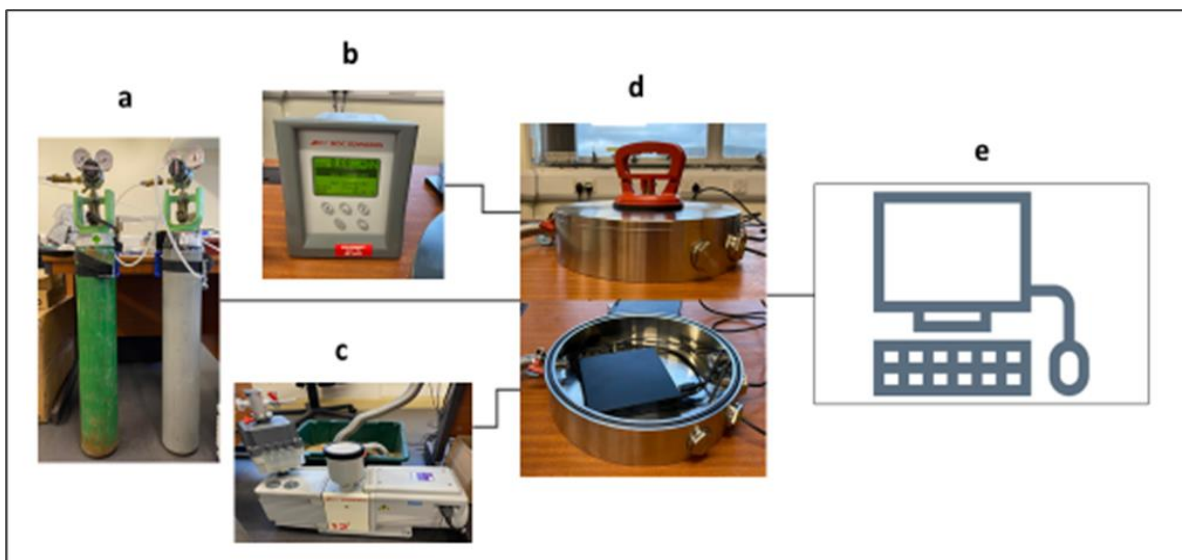


Figure 3-6. Vacuum chamber setting: a). Nitrogen and Argon gas cylinders, b). Pressure controller to monitor the pressure inside the chamber, c). Vacuum pump, d). Vacuum chamber with the laser-scribe DVD drive placed inside, e). PC unit to transfer the design and control printing process.

3.4 Materials Analysis

Different techniques have been utilised to study the properties, structure, and quality of graphene to assist in the determination of the desired characteristics. Specific properties of some materials are particularly desired when used for electrochemical applications. Its electron mobility and electrical conductivity are suitable for either electrochemical or electronic applications using the material produced, while on the other hand mechanical strength could be suitable for piezoelectric applications. In the determination of suitable material properties, certain standard tests and measurement techniques need to be used for any specific application. These analyses include the spectral analysis of device material using Raman and XPS spectroscopy, assessment of the surface topology of the manufactured material using scanning electron microscopy (SEM), and an evaluation of electrochemical behaviour using cyclic voltammetry (CV).

3.4.1 Raman Spectroscopy

Raman spectroscopy is a beneficial tool in the field of materials science which can be used to characterise material properties without causing damage to the sample. Moreover, the Raman spectra of a graphene or graphene oxide sheet may be used to determine its atomic structure, number of layers, edge type, disorder type, and attached functional groups. The Raman shift, peak form, position, and intensity can all be used in the investigation of these features [146]. The recorded Raman spectra of graphene and graphite at an excitation wavelength of 514 nm are shown in figure 3-7 (a). As can be observed, two primary features were captured at

wavenumbers of 1580cm^{-1} and 2700cm^{-1} which correspond to the G and 2D bands respectively. The position and broadness of a 2D band can be used in the calculation of the number of graphene layers present [147, 148]. The form of the 2D band in graphite differs from that of graphene, as can be seen in figure 3-7 (b). The 2D band in graphite has two peaks whereas in graphene it has just one sharp peak. This is because there are fewer layers in graphene and a different electron-phonon scattering process takes place [149].

On the other hand, the Raman spectra of graphene oxide in the range of 1100cm^{-1} to 3000cm^{-1} has three significant peaks called D, G, and 2D, which occur at wavenumbers of 1300cm^{-1} , 1580cm^{-1} and 2680cm^{-1} respectively [146] as presented in figure 3-8. The existence of a D band suggests that there is a fault in the graphene sheet. On the other hand, the appearance of the G band at 1580cm^{-1} is caused by scattering in the E_{2g} mode [146]. As a result of the functionalisation of the graphene, the G band may exhibit a blue shift from 1580cm^{-1} in graphite to more than 1593cm^{-1} in graphene oxide [149, 150]. The presence of a 2D band in the Raman spectra is conclusive proof of the presence of graphene. The G band of a single layer of graphene, for example, was discovered to be around 2685cm^{-1} with a value of full width at half maximum (FWHM) of 25cm^{-1} . The intensity ratio of the D and G bands in a graphene sheet offers information about structural flaws. The ratio of I_d/I_g , for instance, rises after annealing takes place due to a loss of carbon atoms [149].

In this work, Raman spectroscopy was used to characterise the electrodes produced in order to distinguish their quality levels depending on the number of graphene layers. The Raman spectra were performed at Newcastle University using a Horiba Jobin Yvon HR800 Raman spectrometer with a 532 nm excitation laser.

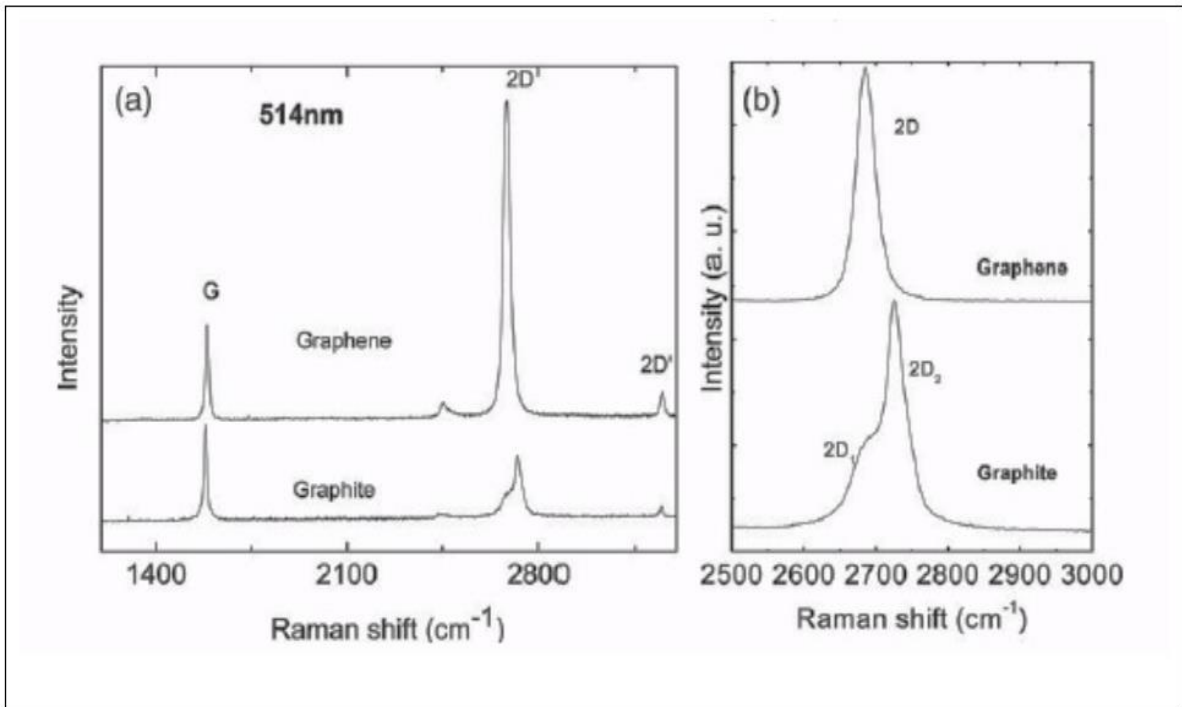


Figure 3-7. Comparison of Raman spectra: (a) between graphite and graphene; (b) 2D peaks of graphene and graphite [150].

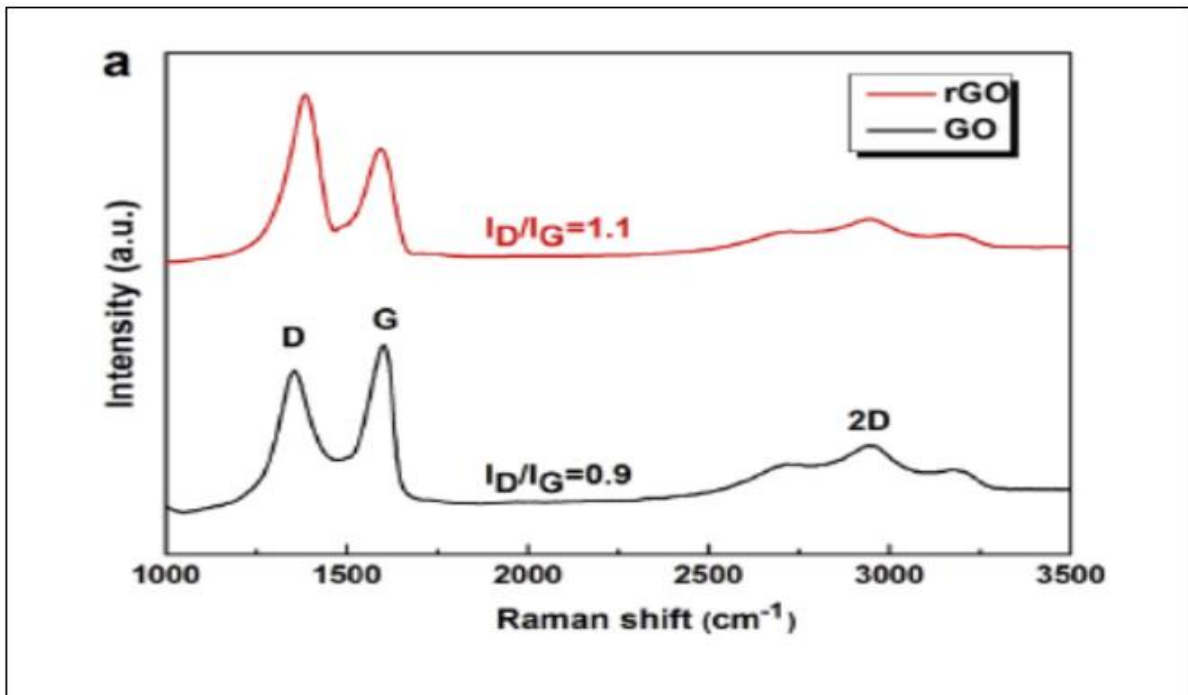


Figure 3-8. Raman spectra of GO and rGO [151]

3.4.2 Scanning Electron Microscopy (SEM)

SEM is one of the most versatile tools available for the characterisation, examination and analysis of the morphology and microstructure of materials. In scientific research, light microscopy has been and will continue to be of great importance. However, since the discovery that electrons can be deflected by a magnetic field as shown in numerous experiments, electron microscopy has been developed by replacing the light source with a high-energy electron beam [152]. In SEM, a concentrated electron beam is applied to a sample, and the electron signals generated are extracted and used to provide a picture of the sample surface. The sample for this technique should be electrically conductive in order to avoid overcharging with electrons [153].

SEM depicts images of GO flakes and layers which exhibit a wavy, folded morphology and thin layers. The SEM pictures will indicate whether or not the rGO material is made up of separate sheets that are inextricably linked. In this work, SEM enabled the close observation of the surfaces of the electrodes and their topology.

In the current work, the SEM photographs were performed at Newcastle University using Jeol JSM 5610LV machine fitted with an X-act EDX detector from Oxford Instruments, Japan.

3.4.3 X-ray Photoelectron Spectroscopy

X-ray photoelectron spectroscopy (XPS) is widely used for the rapid evaluation of features when preparing GO and achieving efficiency in reduction procedures. This surface-sensitive technique gives information about the oxidative state and chemical composition of available elements [154]. XPS is used in studies of graphene to identify how close a given sample is to pure graphene. In theory, graphene requires the maximum carbon and minimum oxygen in its structure, or otherwise purity is determined by the extent of its structural defects [155]. In XPS, sampling depth is crucial, and the measurement equipment tends to be limited vertically to be between 5-10 nm which is significantly higher than the thickness of pristine graphene at ≈ 0.35 nm [156]. In this method, high-resolution elemental spectrum analysis is employed to fit the curve of the XPS carbon's C1 spectra so as to identify the relevant chemical bonds or functional groups based on the distribution of peaks demonstrating the binding forces [157].

However, for rGO, XPS analysis is considered to be a beneficial method to confirm levels of reduction and the quality of the precursor material [158]. For instance, figure 3-9 shows the XPS spectra of the GO film before and after the reduction process. Figure 3-9a shows that there are several functional groups at different binding energies, which are C-C at ~ 284.7 eV, C-O at ~ 286.0 eV, carbonyl C at ~ 287.7 eV, and carboxylate carbon O-C=O at 289.2 eV. On the

other hand, as shown in figure 3-9b, the intensity and atomic ratio of the reduced GO film are substantially reduced. This is followed by substantial rises in C-C intensity [14, 159, 160]. In order to determine the suitability of the electrode material produced for the intended application, the XPS of the device can be carried out to determine the chemical composition at the surfaces.

In the current work, XPS data for the four prepared electrodes (LSG_{air} , LSG_{uv} , LSG_{N_2} and LSG_{Ar}) were obtained using an instrument from Kratos Axis Nova, UK according to the following parameters:

1. The survey was conducted using a dwell time of 100 ms, pass energy of 150 eV, and step size of 0.2 eV.
2. The O1s was measured using 526-538 eV, 0.05 eV step size, 300 ms dwell time, and 40 eV pass energy.
3. The C1s was measured using 279-290 eV, 0.05 eV step size, 300 ms dwell time, and 40 eV pass energy.

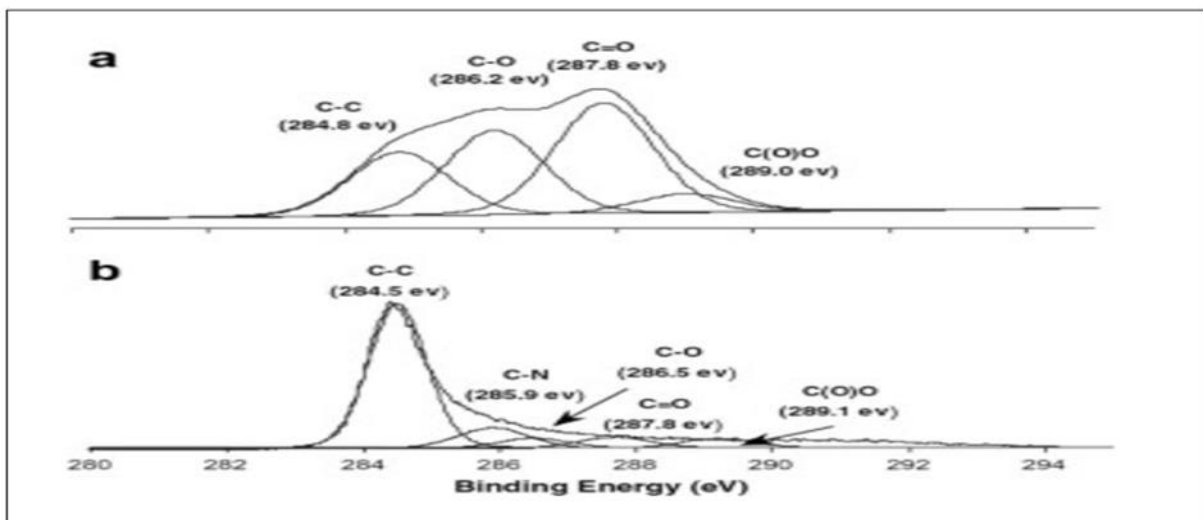


Figure 3-9. XPS spectra of: (a) GO film; (b) rGO film [14]

3.5 Preparation of the Reduced GO Electrodes

The rGO sensing platform consisted of electrodes initially created using Autodesk Inventor Professional 2018 software and produced using the LightScribe on GO-coated discs. Where the LightScribe technique is a direct disc labelling technology which uses the DVD disc writer capability to etch or inscribe a pattern that offers an easy approach to burn accurately silk-screen quality labels. It merges the LightScribe-enabled DVD drive of PC with uniquely coated DVD discs and improved disc-labelling software [161]. Figure 3-10 illustrates the different

geometries of the electrodes that have been manufactured according to previous work [158-160]. In order to prepare an easy-to handle electrode so as to facilitate its characterisation using SEM, Raman, and XPS spectroscopy, the electrode was designed as shown in figure 3-10a. On the other hand, the electrodes shown in figure 3-10b have been designed for the CV analysis as this provides a larger contact area which facilitates the analysis process.

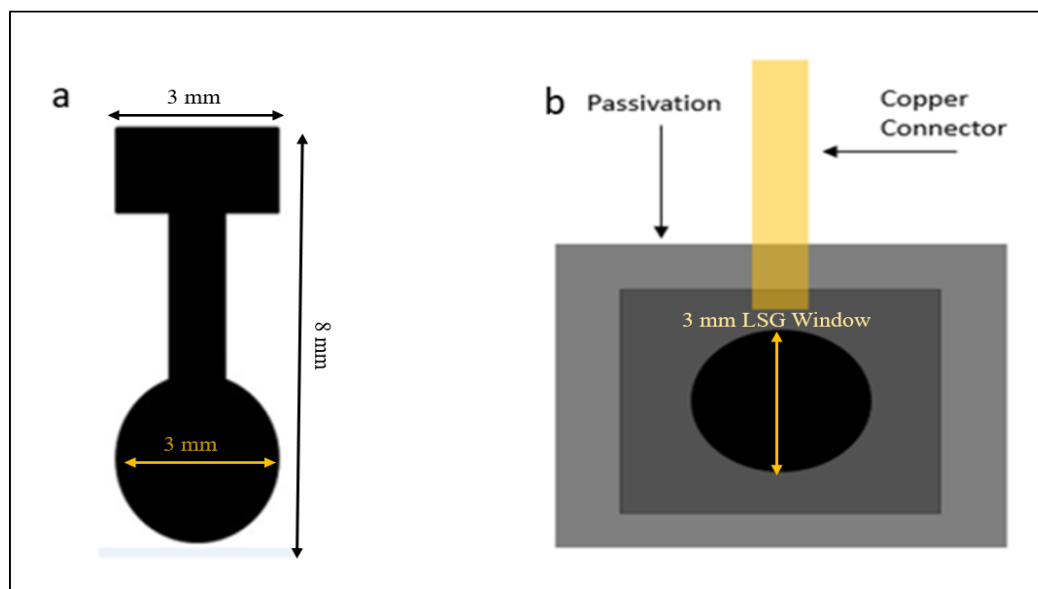


Figure 3-10. rGO electrode design: (a) combined-shape electrode; (b) patch electrode.

3.6 Fundamental Method for Transforming GO to rGO

Laser-scribing technology converts GO into rGO using a laser beam. The significant advantages of the light-scribe in GO reduction are that the process is rapid, simple, and effective [140]. The laser thermally reduces an insulating GO film at predefined positions, resulting in bespoke conducting LSG electrodes [162]. The one-step patterning method can be performed in any laboratory that has basic computer facilities because it does not require the expensive lithography which is required for the screen-printing and microfabrication of electrochemical sensors [163].

For this work, the first step in the fabrication of the sensor device involved the preparation of the substrate, which is the PET foil film. These films were glued onto a supporting DVD disc using the 3M adhesive, followed by the homogeneous drop-casting of 15 ml of the liquid GO onto the PET substrate. The liquid GO was left to dry for 48 hours at room temperature in a dust-free room. Subsequently, the design made using Autodesk software was transferred to LightScribe Template Labeler Version 1.18.27.10 (Hewlett-Packard). The DVD disc was inserted bottom-up inside the LaserScribe writer and the selected patterns for each sensing

electrode device were separately loaded from the computer. In order to yield a well-designed sensing electrode, the pattern was scribed 10 cycles onto the surface. Each cycle took about 15 minutes to be completed. Moreover, the production process was improvised to enhance the quality of the sensor devices. Some devices were produced under atmospheric and vacuum conditions, while other devices were fabricated in the presence of Nitrogen (N_2) or Argon (Ar) gases in a vacuum chamber. Figure 3-11 illustrates the basic process of the production of the laser-scribed graphene (LSG) under all production conditions.

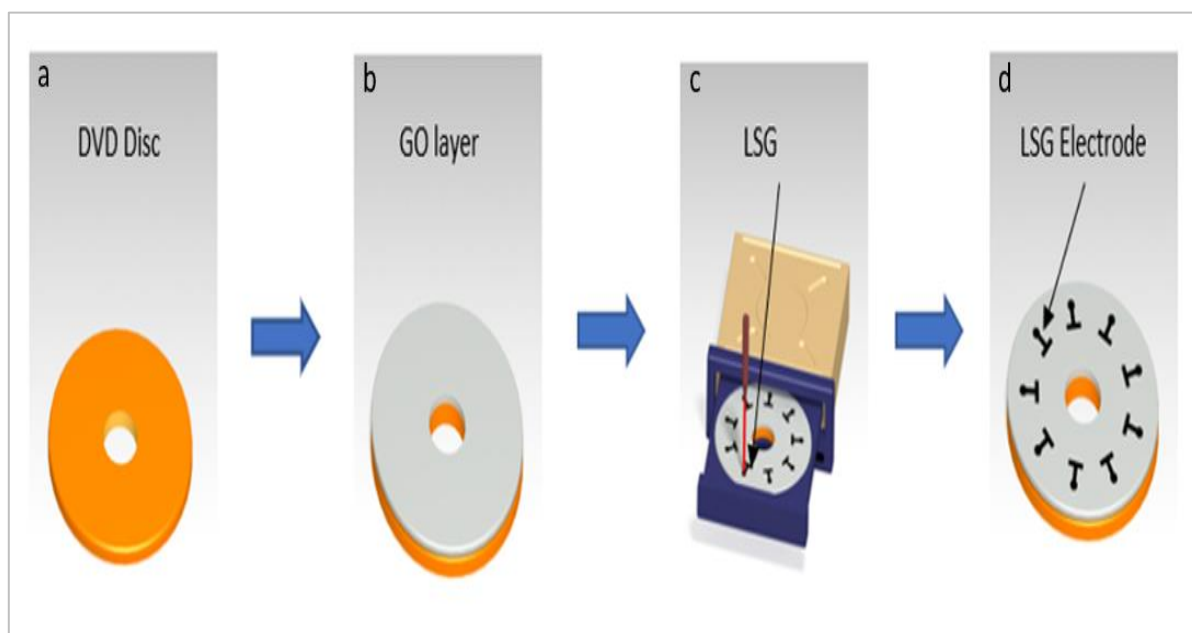


Figure 3-11. Electrode production process: (a) DVD disc; (b) GO layer over the disc; (c) the disc with dried GO layer placed in the LightScribe writer for scribing; (d) LSG electrode patterned in black.

3.7 Electrochemistry of the Prepared Electrodes

The electrochemistry of the four prepared electrodes (LSG_{air} , LSG_{uvc} , LSG_{N_2} and LSG_{Ar}) used for this work involved the utilisation of a three-electrode system that consists of a platinum counter electrode, a standard Ag/AgCl reference electrode, and the produced LSG working electrodes. Electrochemical measurements were obtained using the Autolab electrochemical workstation (Netherlands). Two redox species (1,1'-ferrocene dimethanol and potassium ferricyanide both at concentration of 0.001M) were used for the electrochemistry in this work. For the CV experiments with each redox species, 3 replicas of each electrode in addition to 3 CV runs for each replica were applied. When investigating the effect of scan rate on peak current and peak-peak potential separation (ΔE_p), CV was performed at five different scan rates of 10, 25, 50, 75 and 100 $mV s^{-1}$. Experiments comparing the different working electrodes were performed using the redox species mentioned above. When 1,1'-ferrocene dimethanol was

used, the potential cycled between 0.6 V and 0.0 V, while in the case of the potassium ferricyanide redox species, the potential cycled between 0.6 V and -0.15 V.

3.7.1 Cyclic Voltammetry (CV)

This section highlights the cyclic voltammetry (CV) of the electrode devices produced under various conditions with the two types of redox species used in the electrochemical analysis of the devices. The aim here is to analyse the performance of the devices and their suitability for electrochemical applications. The response performance shown in the voltammogram is key in determining the performance, effectiveness, efficacy, and suitability of the device for the intended application [164]. Cyclic voltammetry (CV) is an effective electrochemical method which is commonly used to examine the reduction and oxidation (redox) processes of various molecular species [18]. CV is vital in the study of electron transfer-initiated chemical reactions and has become an important and widely used electroanalytical system in numerous areas of chemistry. It is used in the study of redox processes to analyse electrochemical reactions that occur between ions and the surface atoms of electrodes under investigation for known reaction intermediates and to determine the qualitative properties of the transfer of charge reactions between electrolyte ions and electrons from the surface of the electrode [20]. The ‘duck-shaped’ plot generated by cyclic voltammetry is a typical electrochemical response observed in a CV experiment, as shown in figure 3-12, which is often referred to as a cyclic voltammogram. In the typical example shown in figure 3-12, the electrochemical process is such that the scan starts at a lower value of potential and then sweeps to higher and more positive oxidative potentials [48]. At the onset of oxidation, the current exponentially increases as the analyte is oxidised at the working electrode surface. Here the process is under electrochemical control, with the current linearly increasing with increasing voltage until it reaches a peak at a point called the anodic [165] peak current (I_{pa}) for the oxidation process at some anodic peak potential (E_{pa}). From this point onwards in this forward scan, increased potentials slow down the electrochemical process and decrease the current as the potentials are scanned to a more positive potential until a steady state is reached, where further increases in potential no longer affect the observed current [165]. Afterwards, the scan reverses potentials (reductive scan) and continues; this reduction process mimics that for oxidation, except with an opposite scan direction, until a cathodic peak current (I_{pc}) at some cathodic peak potential (E_{pc}) is reached. After this point the current begins to rise in value.

In this work, two redox species, potassium ferricyanide and 1,1'-ferrocene dimethanol, were investigated and the results are presented in chapters 5 and 6. The CV of the manufactured device was performed in the Institute of Cellular Medicine at Newcastle University.

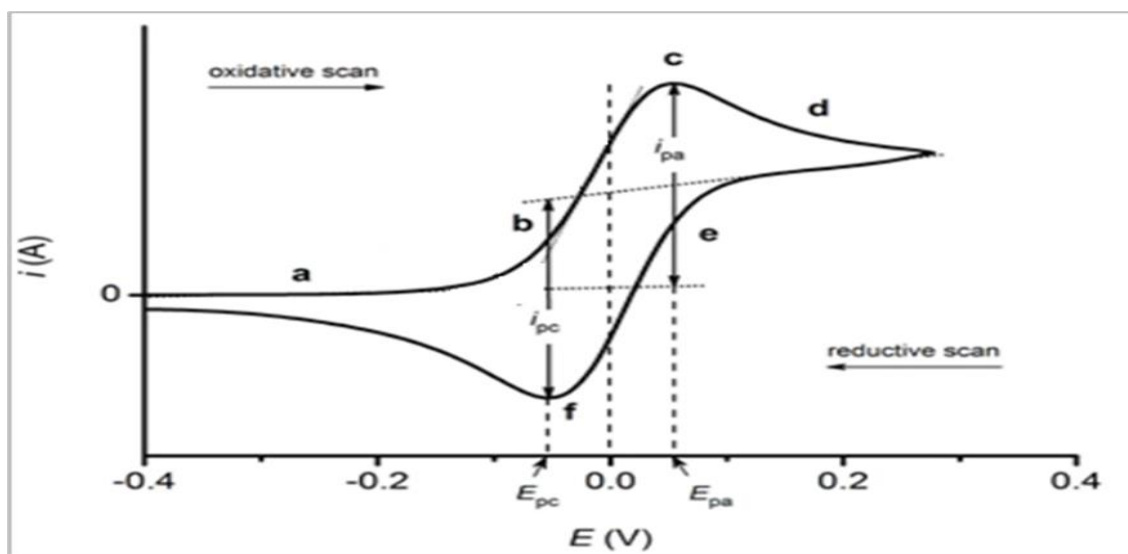


Figure 3-12. Typical cyclic voltammogram for an electrochemical system [165].

Chapter 4. Material Characterisation

4.1 Introduction

One of the ways in which the materials used in the production of the electrode can be studied is by looking their features at microscale as well as the composition of atoms in their structure. This examination helps to give insights into the chemical, mechanical and biological properties, leading to a better understanding of their expected performance and efficacy in the proposed application. For this work, the material characterisation was carefully designed to serve the purpose of the research. For both prepared materials (GO1 and GO2), the most important characterisation techniques were performed in order to properly describe both materials in addition to investigating the characteristics that would allow the selection of a preferred material. The characterisation included a assessment of surface morphology using scanning electron microscopy (SEM) and Raman Spectroscopy, and in addition X-ray photoelectron spectroscopy (XPS) was performed for the most promising material selected.

4.2 Scanning Electron Microscopy

In this work the rGO electrodes were produced under four different manufacturing conditions as described in chapter 3. The SEM was used to check the morphologies of the rGO electrode devices. It is important to demonstrate that the two graphene oxide samples were used to produce separate electrode devices in order to determine the best GO that gives the most suitable electrode device. The morphological images obtained for the rGO electrode sample (from GO1) prepared using the four manufacturing schemes are presented in figure 4-1. The micrographs obtained were sufficiently magnified to precisely observe the surface of each electrode material. Figure 4-1 shows the SEM images for rGO produced under atmospheric (LSG_{air}), vacuum (LSG_{vac}), Nitrogen gas (LSG_{N_2}), and Argon gas (LSG_{Ar}), conditions. All of the micrographs of these electrodes were obtained at the same magnification of x10000, which facilitates a clearer visualisation of the morphology of the electrode surface.

The micrographs of rGO presented in figure 4-1 show that all of the rGO surfaces included crumpled thin sheets which accumulated to form material with a disordered structure. However, the material produced under atmospheric, vacuum, and vacuum with Argon gas conditions had more crumpled sheets. This crumpling or folding of the thin sheets might be due to the pre-existence of wrinkles and the random curving of the sheets in the graphene oxide

[166]. Furthermore, when undergoing rapid deformation during thermal reduction technique, wrinkles and curves could be transformed into folds in the rGO electrodes [166].

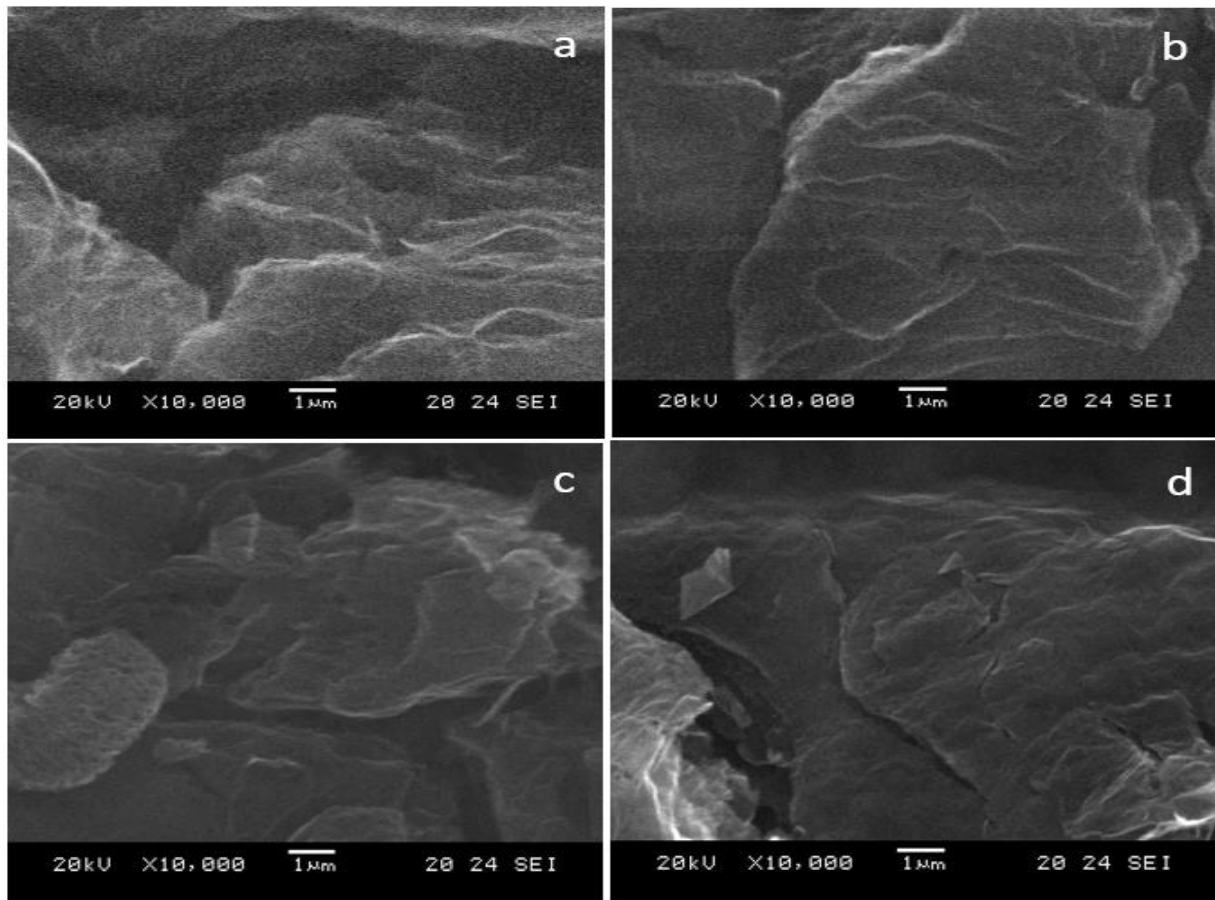


Figure 4-1. SEM micrographs of the surface of each electrode material for rGO (from GO1) at a magnification of x10000, produced under: (a) atmospheric; (b) vacuum; (c) Nitrogen gas; and (d) Argon gas conditions.

Similarly, the second graphene oxide, GO2, was obtained and prepared in the same manner as for GO1. The morphological images obtained for these electrode samples prepared using the four schemes (LSG_{air} , LSG_{uvc} , LSG_{N_2} , and LSG_{Ar}) for GO2 are presented in figure 4-2. The SEMs indicate an appropriately magnified image of the surface of each electrode material obtained from GO2. Figure 4-2 shows the SEM images for the LSG_{air} , LSG_{uvc} , LSG_{N_2} , and LSG_{Ar} electrodes at the same magnification of x10000 that was used for GO1 in order to allow an unbiased comparison.

A comparison of the materials from these two GO samples using the SEM images might not immediately indicate any significant difference, but from visual observation it can be noted that the materials in figure 4-2 possess more wrinkles (or folds or deformations). This characteristic can be quite beneficial for the material, since research has shown that folds can alter the electronic structure of graphene and can lead to a pseudomagnetic field in the graphene material and modulate its surface properties and transparency [167]. Since graphene has only

recently been considered for application in electrodes for electrochemical sensing applications due to its enhanced electronic properties, high surface area and conductance, folded and wrinkled surfaces are advantageous for these applications. These properties make the sheets less stiff, which hinders stacking and allows increased surface area to be retained, hence enhancing the electrochemistry of the material leading to better electron transfer and electroactivity in the electrode [167].

It has also been reported that folds on graphene can lead to enhanced chemical activity and the possession of low thermal conductivity, which suggests the potential for thermoelectric applications. They also provide improved interlocking, better interaction with the host polymer within a composite, tuneable wettability, and high transparency, all of which could make them suitable for the fabrication of other graphene structures [167, 168]. These merits possessed by GO2 over GO1 as observed from the SEM images could provide the basis for the choice of which form of GO to be used in the manufacturing of rGO electrodes devices. Further comparison has been performed, as described in the following sections, to determine and confirm which of the tested GO materials would produce the optimum rGO electrodes to be preferentially used in the intended electrochemical and biological applications.

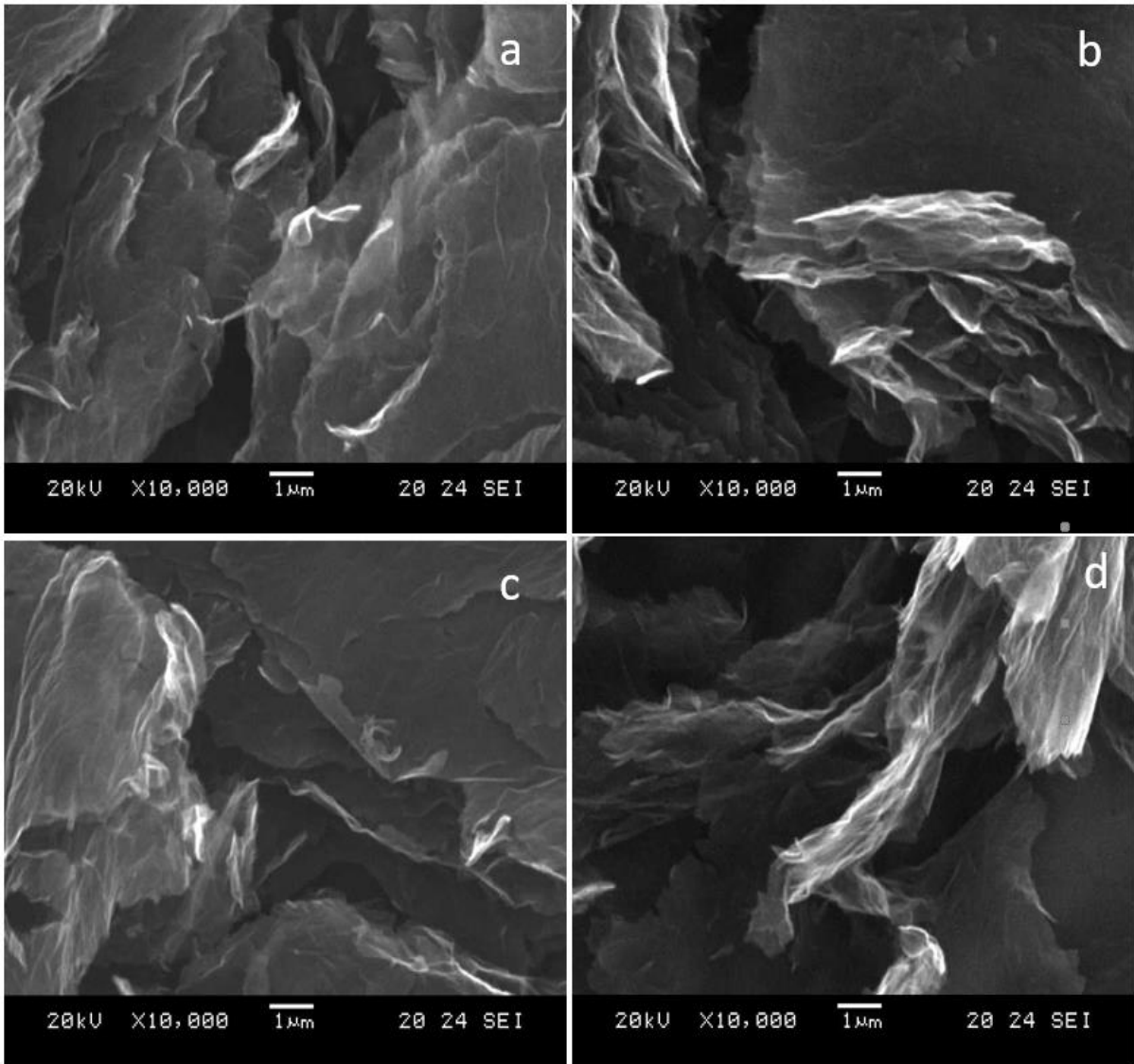


Figure 4-2. SEM micrographs of the surface of each electrode material at a magnification of x10000 for rGO (from GO2) produced under: (a) atmospheric; (b) vacuum; (c) Nitrogen gas; (d) Argon gas conditions.

4.3 Raman Spectroscopy

Raman spectroscopy is used to investigate defects, doping, thermal conductivity, and strain in graphene and other related materials. It provides information based on the inelasticity (or Raman) scattering of a molecule illuminated by a monochromatic light [64, 141, 147]. In this research the Raman spectra of the produced devices were conducted using a scan spectrum from 1000 cm^{-1} to 3000 cm^{-1} with the Argon laser beam set to a value of 514 nm. Since there two types of GO were used (GO1 and GO2), the Raman spectra of the electrodes are presented separately as recorded for the different manufacturing conditions in atmosphere, a vacuum chamber, Nitrogen gas, and Argon gas conditions.

4.3.1 Raman Spectroscopy for GO1 Electrodes

This section presents the results of Raman spectroscopy of the rGO produced from the first graphene oxide material (GO1) under the different manufacturing conditions.

Figure 4-3 shows Raman spectra for the surface of each electrode material at a laser excitation of 514 nm. From the figure, three prominent fundamental vibrations can be observed for the D band, the G band and 2D band in the range of 1345-1350 cm^{-1} , 1580-1582 cm^{-1} and 2670-2682 cm^{-1} respectively for the various conditions used in the production of the electrodes. The D vibration band is the peak which highlights defects in the sample [169-171]. It can be observed in table 4-1 that, the D band for the LSG_{air} electrode occurs at 1346.88 cm^{-1} and that for the LSG_{uvc} electrode occurs at 1349.25 cm^{-1} . Similarly, the D bands for LSG_{N_2} and LSG_{Ar} at 0.5 mbar occur at 1345.92 cm^{-1} and 1348.42 cm^{-1} respectively. On the other hand, the G band is an in-plane vibrational mode relating to sp^2 hybridized carbon atoms [147], and for the LSG_{air} electrode it occurs at 1577.89 cm^{-1} while for the LSG_{uvc} electrode it occurs at 1582.09 cm^{-1} . Likewise, the G bands for the LSG_{N_2} and LSG_{Ar} electrodes occur at 1582.11 cm^{-1} and 1581.17 cm^{-1} respectively. The D and G bands in the Raman spectra in figure 4-3 represent the disorder and tangential bands respectively [147, 172].

Meanwhile, the 2D band which is the second order of the D band and occasionally denoted as an overtone of the D band, is simply the result of a two-phonon lattice vibrational process [148]. This band is significantly broader and shifted to a higher wavenumber (Raman shift) as compared to the D and G bands. From figure 4-3 and table 4-1, it can be observed that the 2D band for the LSG_{air} electrode occurs at 2680.76 cm^{-1} and that for the LSG_{uvc} electrode occurs at 2680.76 cm^{-1} , whereas the 2D band for the LSG_{N_2} electrode occurs at 2673.91 cm^{-1} and that for the LSG_{Ar} electrode occurs at 2686.88 cm^{-1} . This 2D band is usually a strong band in graphene and graphene-based materials and it can be used to determine the layer status of graphene as monolayer, double layer, or multilayer since it is highly sensitive to the stacking of graphene layers [148, 169].

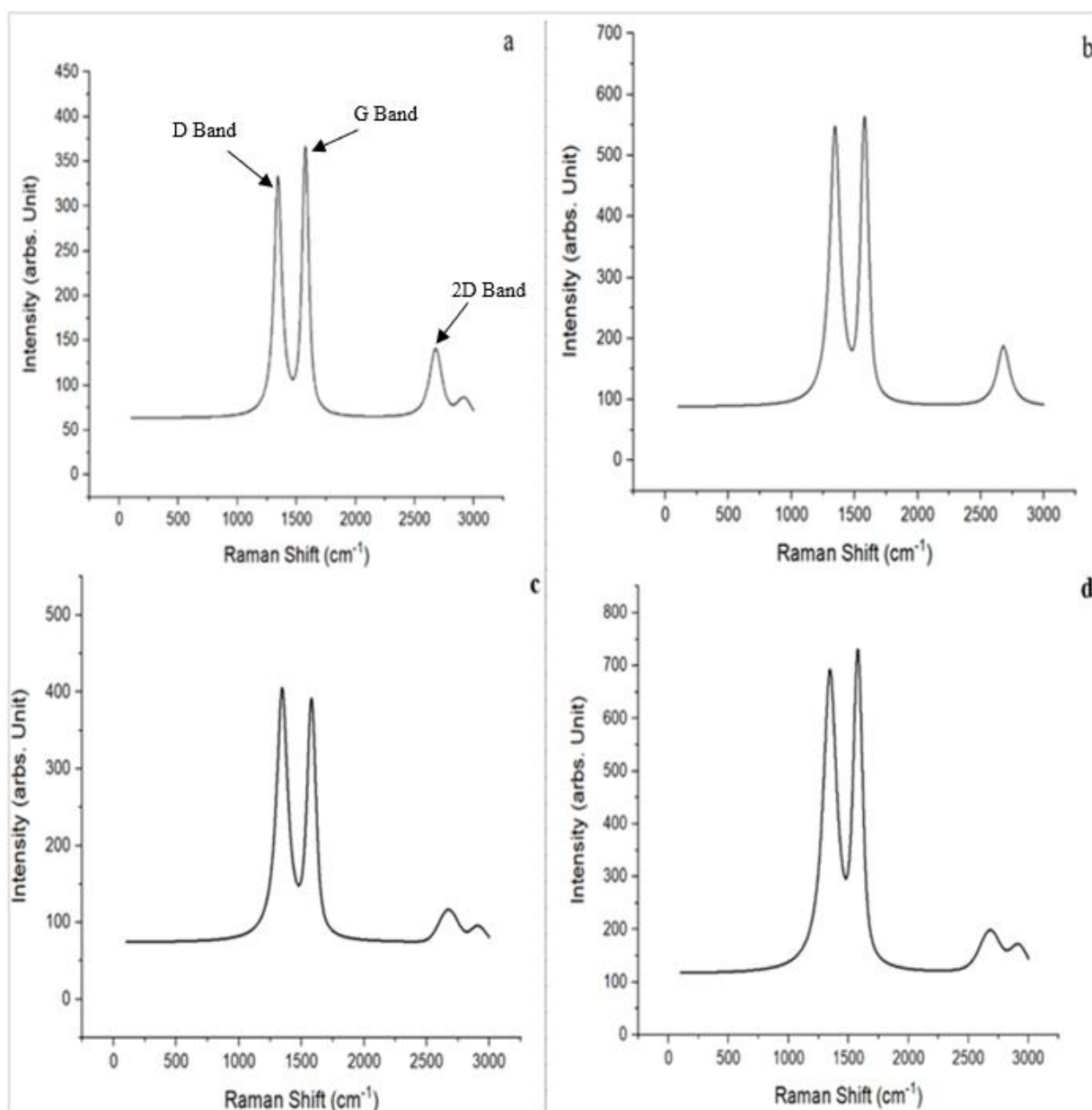


Figure 4-3. Raman spectra of the surface of each electrode material from GO1 under: (a) atmospheric; (b) vacuum; (c) N_2 ; (d) Ar conditions.

It is important at this point to determine how close the prepared electrodes are to single-layer graphene (SLG), since this possesses excellent chemical, electrical and mechanical properties [173-176]. For such an examination, a summary of results from the Raman spectra are presented in table 4-1. It has been previously mentioned in the literature that the Raman spectrum of single-layer graphene has specific wavenumbers for the D, G, and 2D bands. It has been observed that the wavenumber of the D band value for SLG is around 1350 cm^{-1} , its G band occurs at about 1580 cm^{-1} , and its 2D band occurs at approximately 2670 cm^{-1} [147, 148, 169, 177, 178].

From table 4-1, it can be observed that, the electrode material that has its D band closest to the D band of SLG is the LSG_{uvc} electrode while the electrodes with G bands closest to that of SLG are those produced under the vacuum conditions (LSG_{uvc}, LSG_{Ar}, and LSG_{N2}) as compared with LSG_{air}. Likewise, the electrode whose 2D band is closely related to that of SLG is the LSG_{N2} electrode. The vibration data using a mean value of 5 samples from table 4-1 was plotted for the D, G and 2D bands and the results are shown in figure 4-4. From this figure, the electrode that possess the highest G band intensity is the LSG_{Ar} electrode, with the LSG_{air} electrode having the lowest G band intensity. It can also be deduced from this plot that the electrode with the lowest 2D band intensity is the LSG_{N2} electrode, while that with the highest 2D band intensity is LSG_{Ar}.

In this work, the 2D band is of interest since other research has also concluded that a higher 2D band intensity of an electrode indicates lower graphene layering, and also that a higher Raman shift in the 2D band of the electrode suggests higher graphene layering [148, 150, 179]. From the results presented thus far, it can be observed that the LSG_{N2} electrode possesses a 2D band Raman shift of 2673.91 cm⁻¹ which is close to the value of single-layer graphene whose 2D band Raman shift is approximately 2670 cm⁻¹. This electrode also exhibits a G band Raman shift of 1582.11cm⁻¹, which is again very close to SLG's Raman shift of about 1580 cm⁻¹.

It has been found that the 2D band is useful in the differentiation between SLG and multi-layer graphene and that the 2D band of SLG is a single symmetric peak with a full width at half maximum (FWHM) of 30 cm⁻¹ [141]. Meanwhile, the 2D band of a graphene material that has successive layers is split into several overlapping bands. The present results as shown in figure 4-4 strongly accord with those previous findings, as the 2D band of the electrode prepared under nitrogen gas conditions has a single symmetric peak with the complete absence of overlapping bands, which proves that the electrode material is closer to SLG.

The D/G band intensity ratio gives insight into the structural disorder present such as edge defects and ripples [180] [181]. As shown in table 4-1, the electrode material with the lowest density of defects is that manufactured under atmospheric conditions, while the LSG_{N2} electrode possesses the highest defect density indicating that this material has more active regions. This makes it suitable for electrochemical applications as it is endowed with specific sensor sites for molecular adsorption [180, 182]. From the results obtained, it can be concluded that the LSG_{N2} electrode is preferred for uses related to electrochemical and biosensor applications.

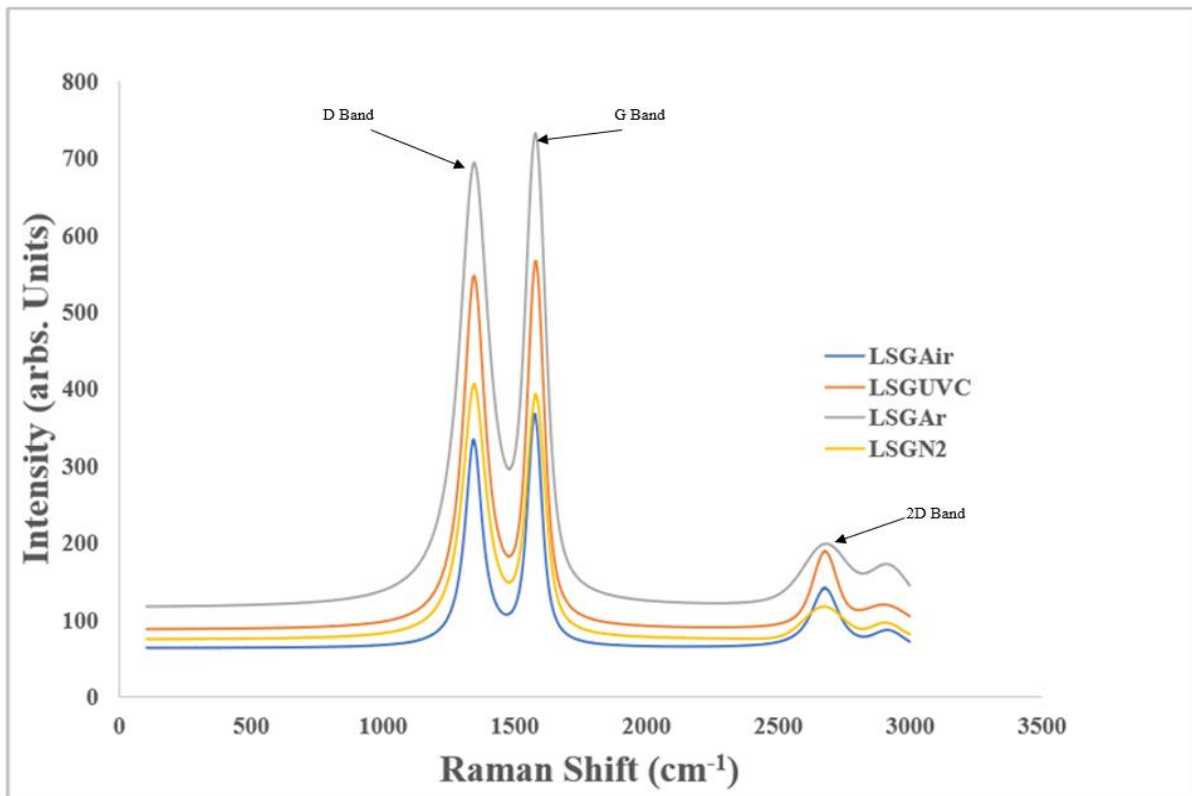


Figure 4-4. Raman shift of the GO1 electrodes produced under the different conditions.

Table 4-1. Raman spectra of the manufactured LSG electrodes with GO1 and GO2 and other graphene electrodes.

Graphene oxide (GO)	Electrode	D Band cm^{-1}	G Band cm^{-1}	2D Band cm^{-1}	I_d	I_g	I_d/I_g	Ref
GO1	LSG _{air}	1346.88	1577.89	2680.76	331.25	365.16	0.90714	This work
	LSG _{uvc}	1349.25	1582.09	2680.76	542.76	562.28	0.96528	This work
	LSG _{Ar}	1348.42	1581.17	2686.88	692.07	729.03	0.9493	This work
	LSG _{N2}	1345.92	1582.11	2673.91	405.16	390.46	1.03765	This work
	SLG	1350	1580	2670	-	-	-	[147, 148, 169, 177, 178]
	MLG	1355	1583	2710	4	6.8	0.58824	[183]
	rGO	1339.2	1587.3	2663.3	7750	4650	1.66667	[184]
GO2	LSG _{air}	1343.51	1578.83	2677.2	627.26	662.26	0.94715	This work
	LSG _{uvc}	1345.92	1575.07	2677.2	682.78	716.94	0.95235	This work
	LSG _{Ar}	1341.1	1576.95	2680.42	726	726.92	0.99873	This work
	LSG _{N2}	1348.42	1578.83	2690.1	699.31	681.7	1.02583	This work

4.3.2 Raman Spectroscopy for GO2 Electrodes

This section presents the results of Raman spectroscopy for GO2. Figure 4-5 shows the Raman spectra for the surface of each electrode material at a laser excitation of 514 nm. It is clear from figure 4-5 and table 4-1 that the D band for the LSG_{air} electrode occurs at 1343.51 cm⁻¹ and that for the LSG_{uvc} electrode occurs at 1345.92 cm⁻¹. Likewise, the D band for the LSG_{N2} electrode occurs at 1348.42 cm⁻¹ with that for the LSG_{Ar} electrode at 1341.10 cm⁻¹. On the other hand, the G bands for the four electrodes occur at 1578.83cm⁻¹, 1575.07 cm⁻¹, 1578.83 cm⁻¹, and 1576.95 cm⁻¹ respectively.

It can also be observed from figure 4-5 and table 4-1 that the 2D bands for the LSG_{air} and LSG_{uvc} electrodes occur at 2677.20 cm⁻¹, while the 2D bands for the LSG_{N2} and LSG_{Ar} electrodes occur at 2690.10 cm⁻¹ and 2680.42 cm⁻¹ respectively. This 2D band as above is usually a strong band in graphene and graphene-based materials and therefore it can aid in the determination layering in graphene since it is extremely sensitive to the stacking of graphene layers [148, 169].

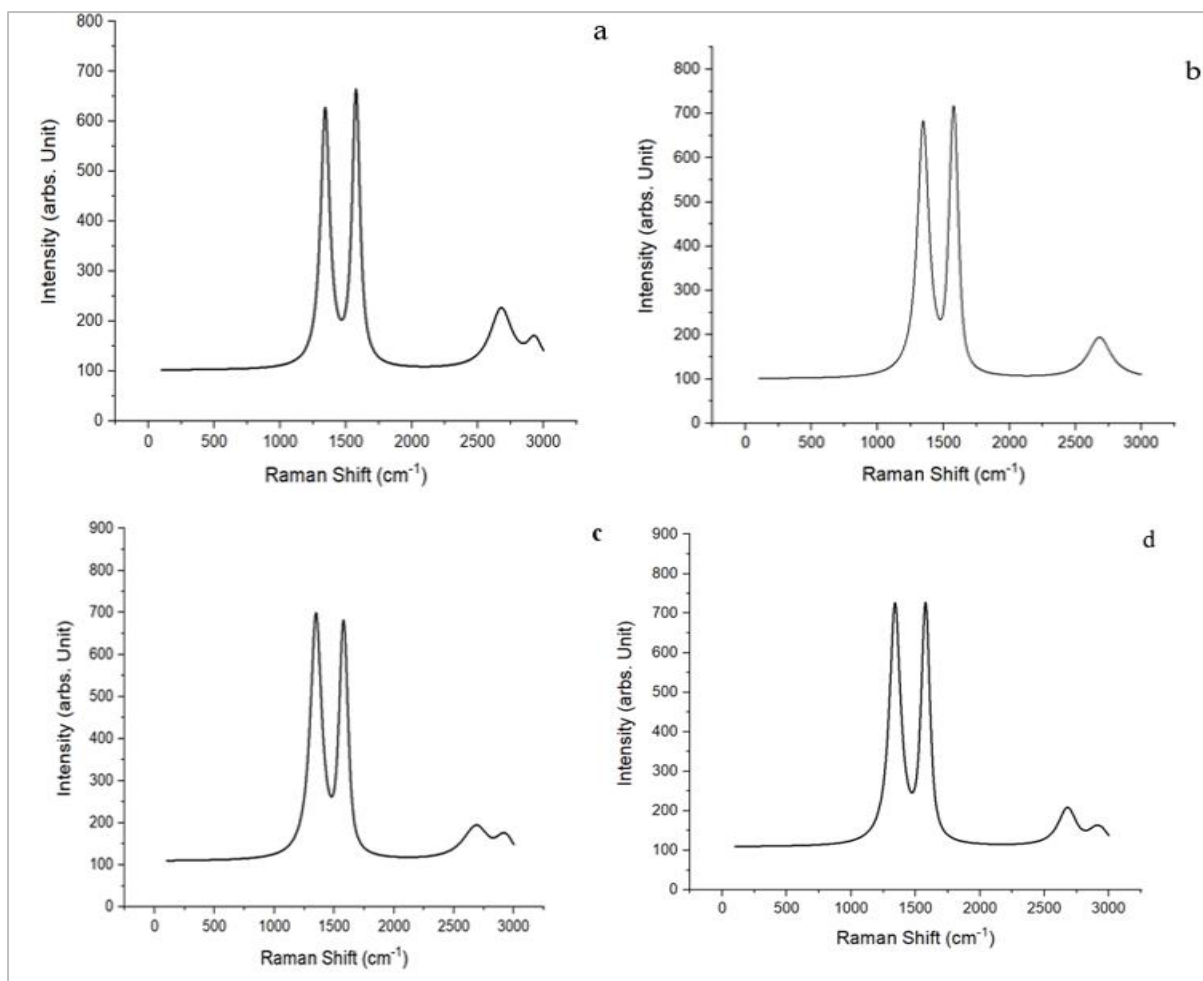


Figure 4-5. Raman spectra of: (a) LSG_{air}; (b) LSG_{uvac}; (c) LSG_{N₂}; (d) LSG_{Ar}.

For the selection of the optimum choice among the prepared GO2 electrodes, it is better to investigate which of them has properties closest to those of SLG. From table 4-1, it can be seen that the electrode material exhibiting a Raman shift in its D band closest to that of SLG is that produced in nitrogen gas conditions, at 1348.42 cm^{-1} . Meanwhile, the electrodes whose G band wavenumbers are closest to that of SLG are LSG_{air} and LSG_{N₂}, at 1578.83 cm^{-1} . Likewise, the electrodes whose 2D band is closest to that of SLG, at 2677.20 cm^{-1} , are those produced under atmospheric and vacuum conditions (LSG_{air} and LSG_{uvac}). The recorded vibration data for the D, G and 2D bands are plotted as shown in figure 4-6. From this figure, it is evident that the electrode possessing the highest G band intensity is the LSG_{Ar} electrode, while that produced under atmospheric conditions has the lowest G band intensity. It can also be seen from this plot that the electrodes with the lowest 2D band intensity are LSG_{N₂} and LSG_{uvac}, while that with the highest 2D band intensity is the electrode produced in air. However, according to the literature, it is more appropriate to describe how close a material is to SLG according to the position of its G band wavenumber. It has been found that an

increase in the intensity and lower wavenumber of the G band indicates multiple graphene layers [148, 150, 185]. From the data in table 4-1, it can be seen that the G band intensity of LSG_{N_2} and LSG_{air} are the lowest recorded among the prepared electrodes, whereas the G band wavenumber of the LSG_{N_2} electrode has the highest value.

As mentioned earlier, the 2D band of single layer graphene can be shown to have a single symmetrical peak but for graphene that has more layers the peak is split into several overlapping bands [148, 150, 179, 185]. This matches our results which show that the electrode prepared in nitrogen gas conditions is the one closest to SLG.

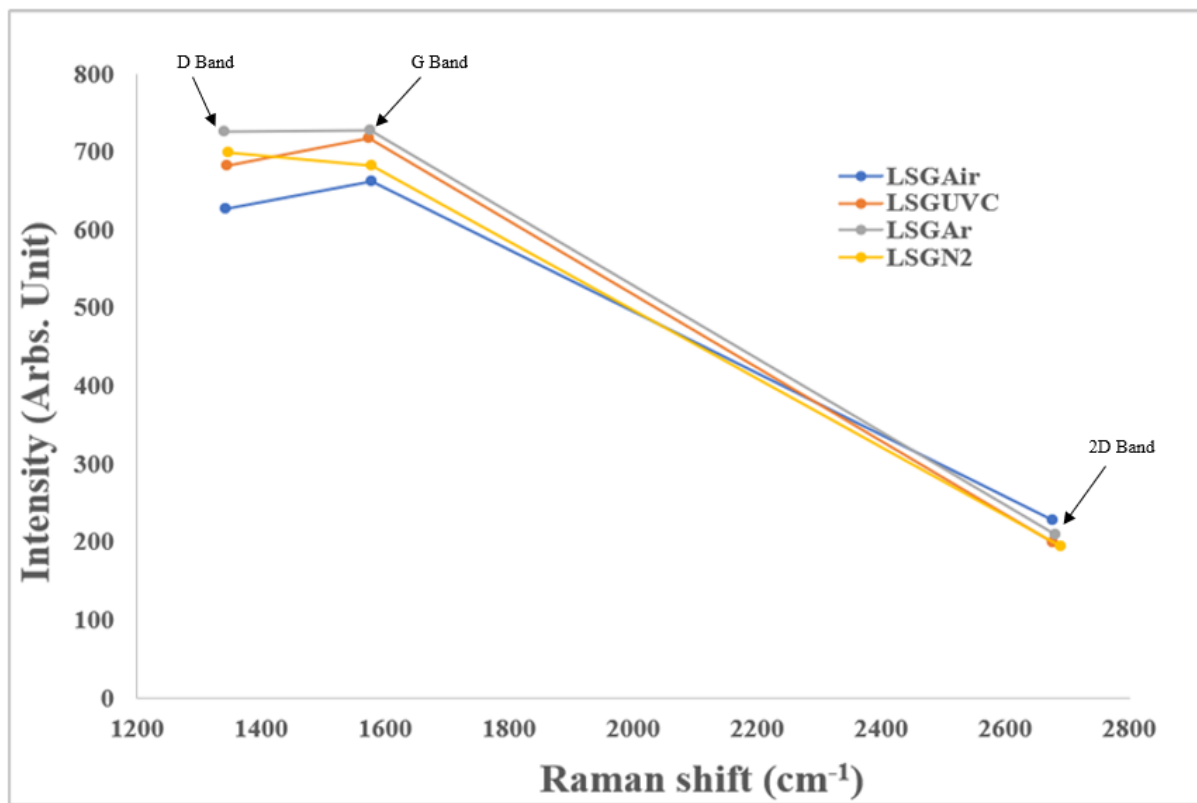


Figure 4-6. Reduced graphene oxide electrode from GO2 produced under different conditions.

Furthermore, to choose the best possible electrode obtained from the GO2 sample, the intensity and wavenumber of the 4 electrodes were plotted in order to determine which one exhibits the desired response in this case, indicating fewer graphene layers. This plot is shown in figure 4-7, from which it can be observed that all of the electrodes possess identically broad Raman shifts in their 2D band, with the electrode produced under atmospheric conditions having the highest value of intensity. The band for the electrode produced in nitrogen possesses the lowest intensity but is slightly broader than those of the other electrodes, although the 2D Raman shift of the LSG_{uvc} electrode has the second lowest intensity. However, in comparing G band intensity, it can be observed that the G band Raman shift of the electrode produced under

vacuum conditions in the presence of Argon gas is higher than that produced in simple vacuum. This indicates that the LSG_{Ar} electrode possesses more layers than the LSG_{uvc} electrode, which accords with other published data [148, 179]. Overall, according to the literature, the determination of the number of layers in a material is mostly based on the value of the 2D Raman shift [148, 150]. It can be observed that the electrode produced under vacuum conditions possesses the lowest 2D band Raman shift of 2677.20 cm⁻¹, which is quite close to that of single layer graphene with a 2D band wavenumber of approximately 2670 cm⁻¹. Meanwhile, its G band Raman shift of 1575.07cm⁻¹ is close to that of SLG at a value of about 1580 cm⁻¹ [148, 179]. However, as mentioned above, the D/G band intensity ratio gives more insight into aspects of the nature of the material, where a smaller value indicates fewer defects [180]. It can be deduced from table 4-1 that the electrodes with the smallest density of defects are those manufactured under atmospheric and vacuum conditions, while the LSG_{N₂} and LSG_{Ar} electrodes possesses the highest defect densities [181] indicating that these electrodes have more active regions and thus they are more suitable for electrochemical applications [180, 182]. From these data, it can be concluded that the LSG_{N₂} electrode is closest to SLG, indicating that it is the optimal choice for electrochemical applications.

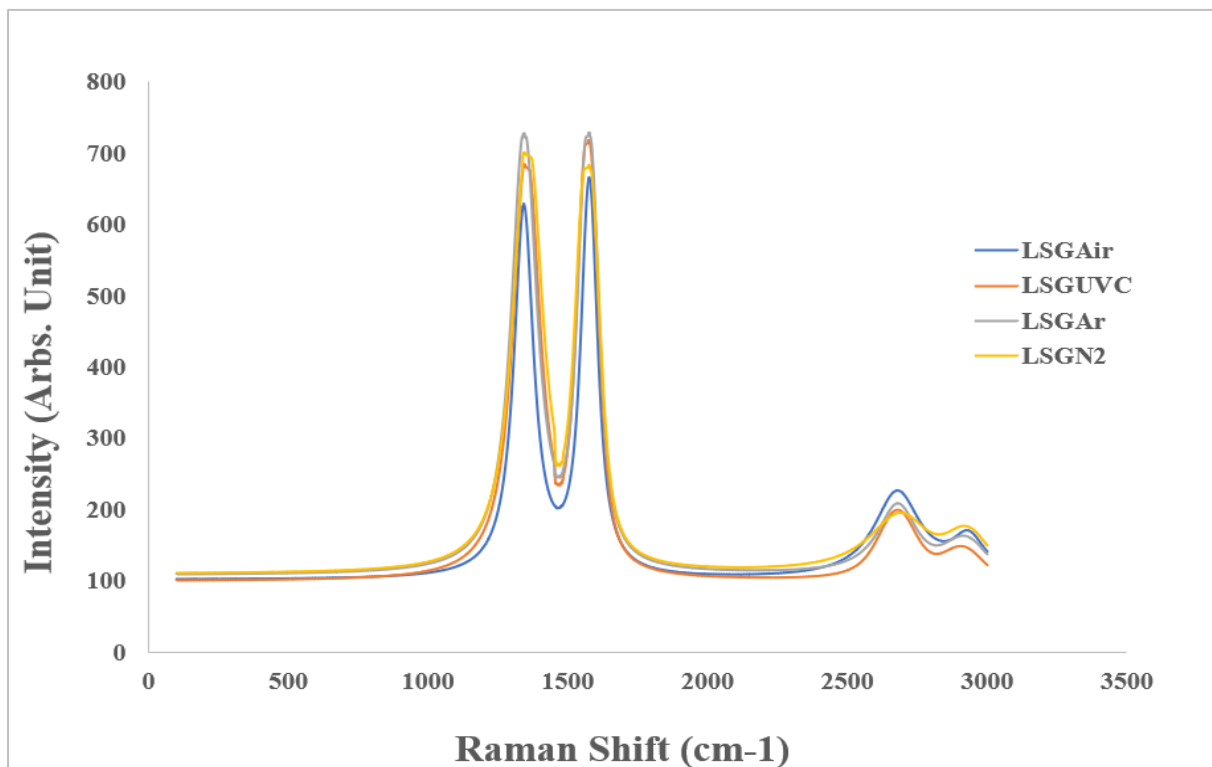


Figure 4-7. Raman spectra of the GO2 electrodes produced under different conditions.

To determine the optimum LSG_{N2} electrode device from the GO1 and GO2 samples, the two electrodes were compared as shown in table 4-1. It can be observed that the two GO samples possess similar characteristics, since their Id/Ig ratios are similar which indicates that they have similar defect densities and possess similar numbers of layers. Meanwhile, the D and G band wavenumbers of the GO2 sample indicate values closer to SLG, and from subsequent cyclic voltammetry experiments the response characteristics for the GO2 electrode devices indicate superior electrochemistry. Hence, from the above results in addition to the SEM micrographs of the two GO materials, it can be concluded that the two materials are very similar in terms of response characteristics. But, in general, the LSG_{N2} electrode manufactured using the GO2 sample showed the most suitable results from the electrochemical analysis conducted using cyclic voltammetry. This has guided its selection in the manufacture of rGO for the subsequent research work in this study.

4.4 X-ray Photoelectron Spectroscopy (XPS)

XPS is an important technique that is extensively used as a quantitative method to investigate the presence of elements on the surface of a material, their percentage, and chemical states [186, 187]. In our case, it is considered to be a useful technique in the characterisation of reduced graphene oxide to show its residual oxygen content in addition to the oxygen/carbon ratio following laser reduction.

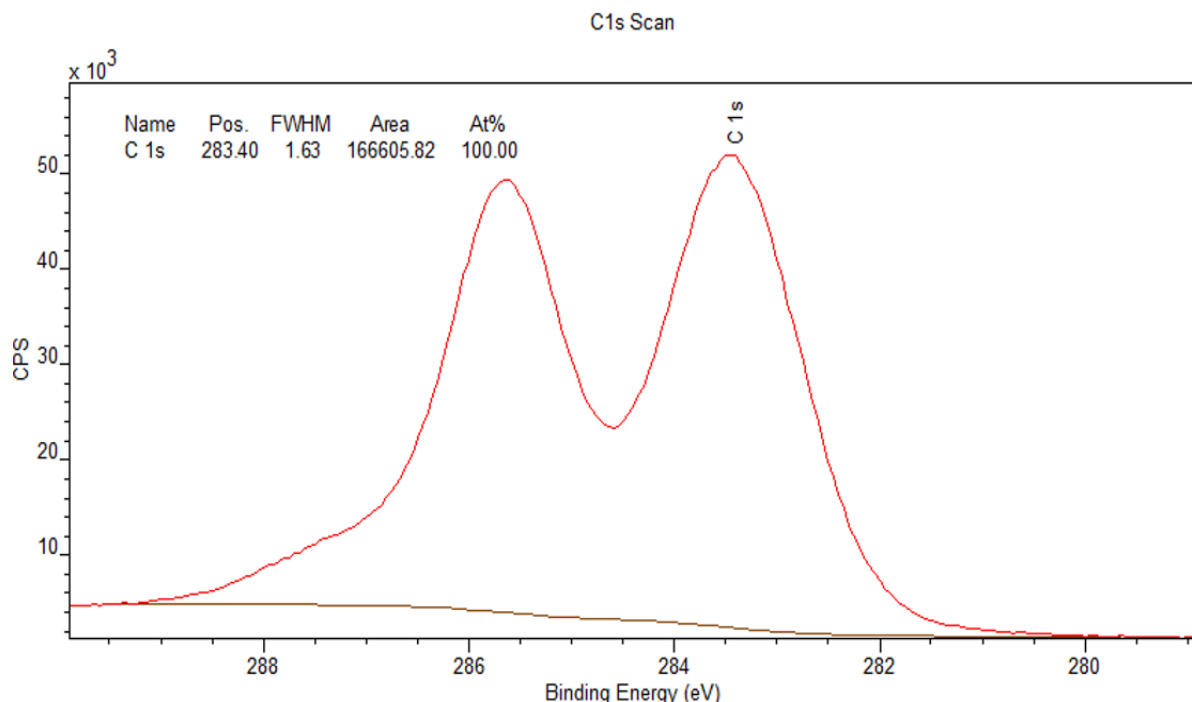


Figure 4-8. XPS data analysis for GO

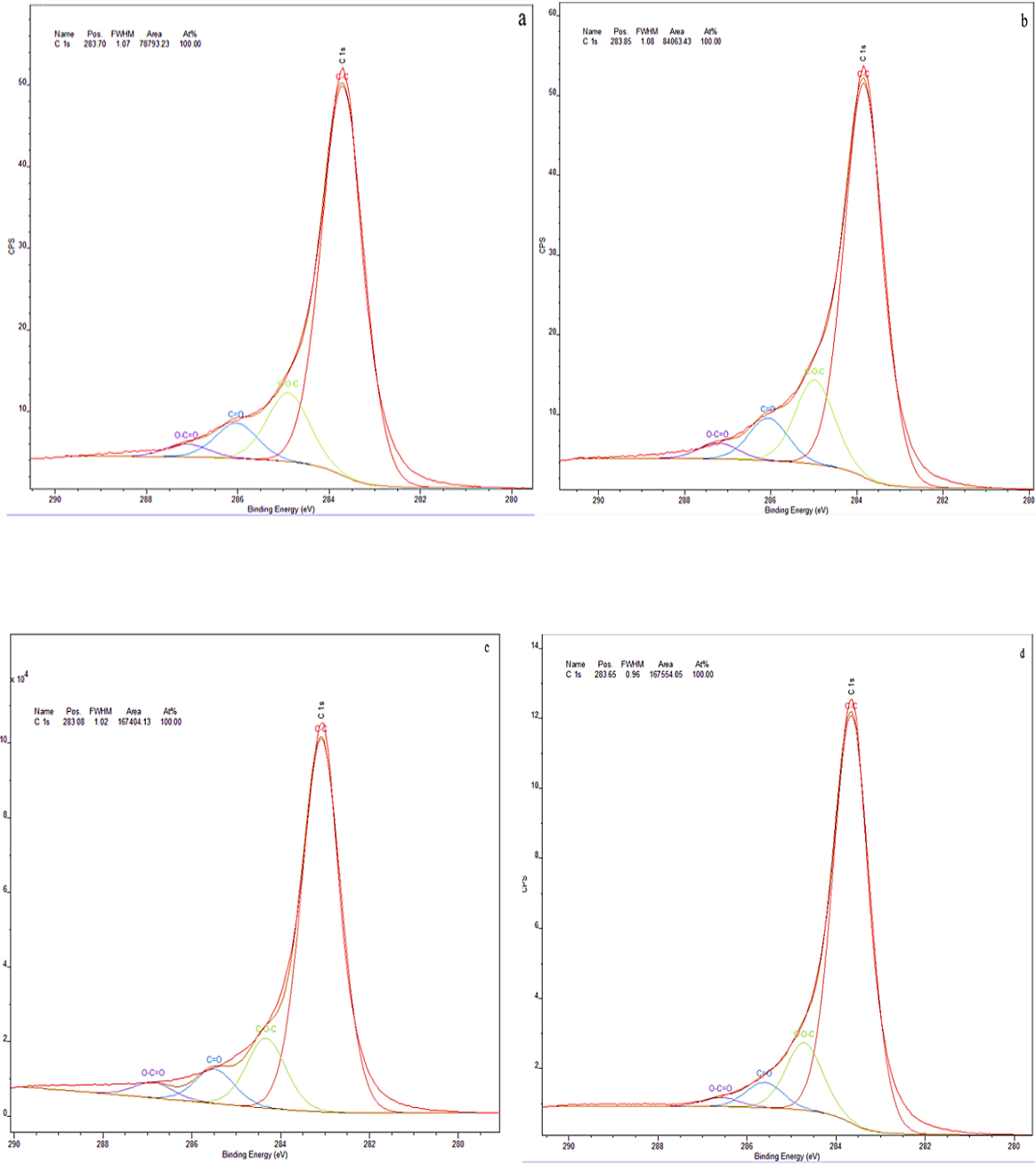


Figure 4-9. XPS data analysis for LSG under the various manufacturing conditions: (a) air; (b) vacuum; (c) N₂; (d) Ar.

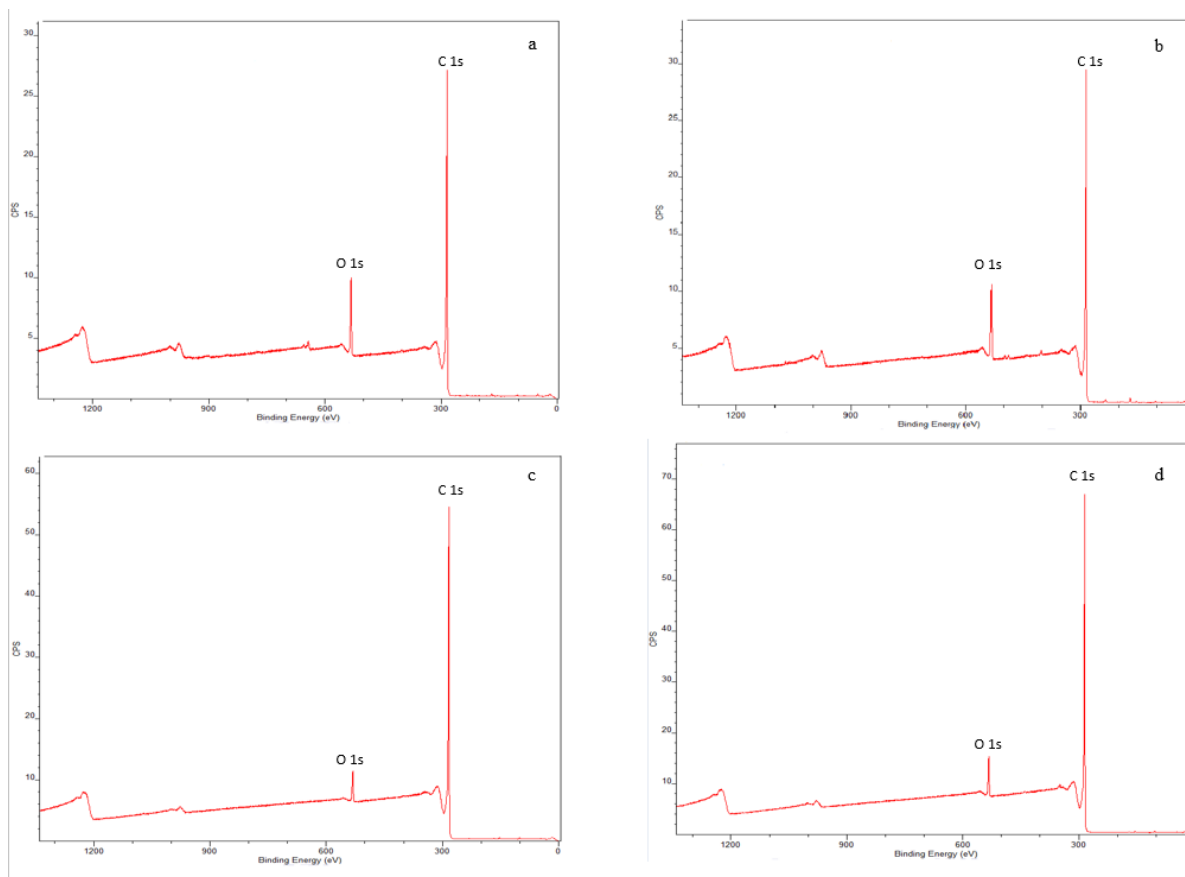


Figure 4-10. Survey scan XPS spectra of GO and LSG using: (a) air; (b) vacuum; (c) N₂; (d) Ar conditions.

As shown in figures 4-8 to 4-10, a decrease and a shift in the O1s peak were observed after the reduction of GO to rGO using LSG, which indicates the loss of oxygen molecules during the reduction process. It is also shown that, at the location C1s, its double peak changed into a prominent single peak after the reduction of GO into rGO, which considered to represent evidence of the alteration in bond configurations. It is also shown that, the ratio between carbon-oxygen and carbon-carbon bonds was greater in GO than rGO, which showed the largest peak at the sp² bonded carbons accompanied by lowered carbon-oxygen bonds. Figures 4-8 to 4-10 demonstrate more variable amounts of oxygen in the prepared rGO in the different electrodes compared with GO. The results from table 4-2 suggest that the use of atmospheric conditions during the laser scribe reduction process leads to a reduction in oxygen percentage from 30.13 to 9.27%, while very similar changes in levels from 30.13 to 9.93 were found under vacuum conditions. However, the N₂ and Ar conditions during the reduction process resulted in lower oxygen content from 30.13 to 4.95% and from 30.13 to 5.88% respectively. A greater reduction in the oxygen content of a material is advantageous for use in various electrochemical reactions, especially for materials that have oxygen-derived functional groups as surface

species which will thus provide an acceptable level of electron transfer on the electrode surface [188].

These results demonstrate that the order of preference of the four conditions applied regarding oxygen content would be: $N_2 > Ar > air > vacuum$. These results match those obtained from SEM and Raman spectra, proving that the reduction of GO in N_2 gas conditions represents the optimal electrode preparation condition and suggests its promise in biosensor applications.

The percentages of both carbon and oxygen in GO and rGO using the four mentioned preparation conditions are summarised in table 4-2

Table 4-2. XPS analysis of the percentages of carbon and oxygen for GO and rGO using air, vacuum, N_2 , and Ar conditions.

Electrode preparation condition	GO		rGO	
	Carbon%	Oxygen%	Carbon%	Oxygen%
Air	69.87	30.13	90.73	9.27
Vacuum			89.96	10.04
N_2			95.05	4.95
Ar			94.12	5.88

4.5 Conclusion

According to the results obtained, it can be concluded that the reduced GO₂ material has a more crumpled and wrinkled surface than GO₁, especially when N_2 gas is used as demonstrated by SEM micrography. This suggests that the LSG _{N_2} material possesses a more defective surface, indicating enhanced potential for chemical activity and better interaction with the host polymer within a composite. In addition, the Raman spectra of both GO₁ and GO₂ materials were very similar in terms of response characteristics. However, the material produced from GO₂ in nitrogen gas showed intensities of and shifts in the G, D, and 2D bands that are extremely close to those of SLG, and this could be a more promising material for electrochemical applications. Moreover, the data from XPS analysis demonstrated that the oxygen content of the rGO produced using N_2 gas represented the lowest percentage recorded among the tested conditions. These results indicate that the LSG _{N_2} electrode could potentially be applied as an electrochemical device.

Chapter 5. Experimental Results

5.1 Introduction

It is vital to evaluate the suitability of a device produced for its specific potential application. Hence, it was crucial to perform specialised tests of the prepared LSG_{air} , LSG_{uvc} , LSG_{N_2} , and LSG_{Ar} devices to determine how they compare with each other and their possibility for future diagnostic, industrial and research applications. To do this, however, the most suitable technique for examination was explored and, for this work, cyclic voltammetry (CV) was chosen as a powerful and popular electrochemical technique commonly utilised to investigate the oxidation and reduction (redox) processes of molecular species. It is also a vital technique that is often employed to study chemical reactions instigated by electron transfer, including catalysis [48]. The analysis of the electrochemical reactions between the ions and surface atoms of the electrodes under investigation can therefore aid in understanding the reaction intermediates formed, thereby leading to a determination of the stability of reaction products. This provides qualitative information on the reaction mechanisms at the electrode and the qualitative properties of the charge transfer reactions between redox species ions and electrons from the electrode surface [49]. CV involves a three-electrode electrochemical cell, and the process is based on varying the voltage applied to a working electrode in the forward and reverse directions at specific scan rates whilst observing the current [189]. This technique entails a linear and a cyclic alteration of electrode voltage between the reference and working electrodes within a voltage range (the potential window) and the current that flows between the working electrode and counter electrode is then measured. The cyclic voltammogram gives a plot of the current against the potential applied, which provides the best visualisation of the redox process on the electrode device [49, 189]. The following sections present the results of experiments conducted with the devices produced in this research.

5.2 Cyclic Voltammetry of GO1 Electrodes in Potassium Ferricyanide Redox Species

In this work the LSG material was characterised electrochemically using CV with a standard three-electrode electrochemical cell employing Ag/AgCl as the reference electrode, a platinum rod with a diameter of 3 mm as the counter electrode, and the manufactured LSG electrodes as the working electrodes, as mentioned in chapter 3. One of the representative prepared electrodes using the LSG technique in addition to the reference and the counter electrodes can

be seen in figure 5-1. It is important to examine the preliminary results obtained from the CV experiments conducted using the chosen redox species, in this case potassium ferricyanide solution. In this work, the LSG electrode device was manufactured using the GO1 material, and figure 5-2 shows the cyclic voltammograms of the different manufactured rGO electrodes in the potassium ferricyanide redox species. The results illustrate that the electrode material manufactured under vacuum in the presence of Argon gas (LSG_{Ar}) shows the best electrochemical activity, with visible peak currents and peak-peak separation potential which indicate irreversible electrochemical behaviour exhibited by all of the electrodes except LSG_{Ar} , where the scan rate has been changed several times and the same results were obtained.

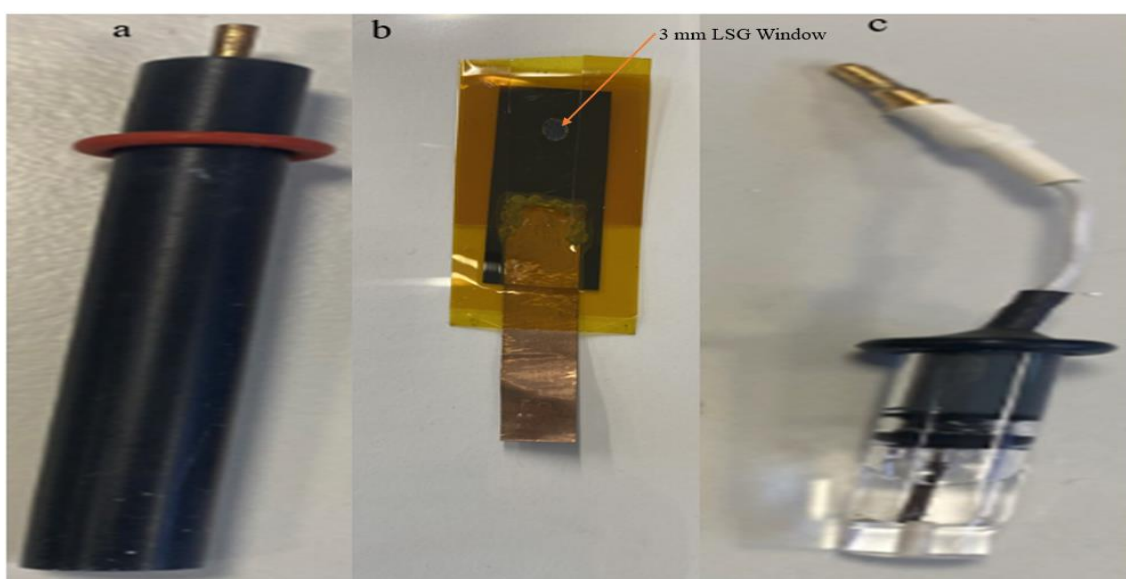


Figure 5-1. Morphological appearance of: (a) the counter electrode; (b) one of the representative prepared electrodes; and (c) the reference electrode.

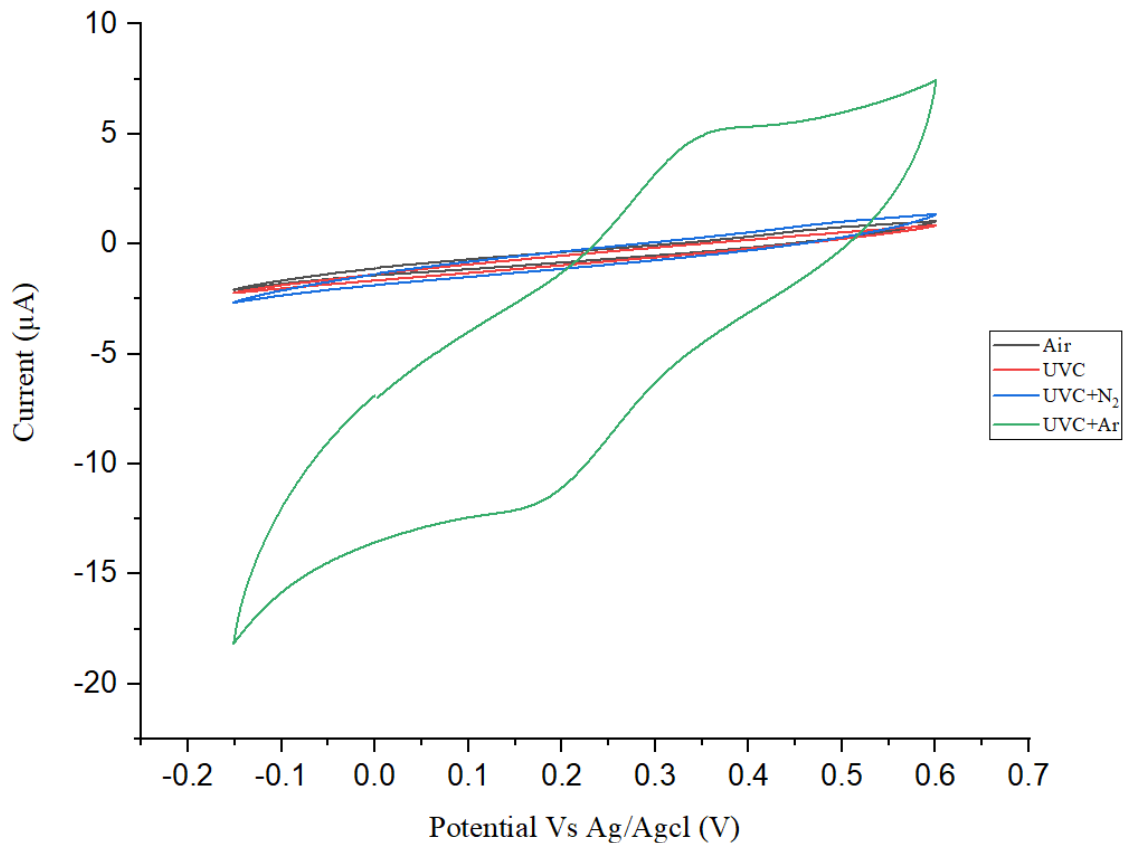


Figure 5-2. Cyclic voltammograms for the prepared electrodes under different conditions (LSG_{air} , LSG_{uvc} , LSG_{N_2} , and LSG_{Ar}) at a scan rate of $10mVs^{-1}$ in potassium ferricyanide redox species.

From figure 5-2 and table 5-1, the response characteristics of the LSG_{Ar} electrode is the only one in which pronounced electrochemical activity is detected compared to the LSG_{air} , LSG_{uvc} , and LSG_{N_2} electrodes. From this it can be concluded that the CV of the LSG_{Ar} electrode in potassium ferricyanide redox species is the only one which exhibits the relevant significant peaks associated with known cyclic voltammograms in terms of electrochemical behaviour.

For the LSG_{Ar} electrode, an anodic peak current (I_{pa}) of $4.86 \mu A$ occurred at an anodic peak potential (E_{pa}) of $0.3467 V$, while its cathodic peak current (I_{pc}) of $-11.7 \mu A$ occurred at a cathodic peak potential (E_{pc}) of $0.1782 V$.

5.3 Cyclic Voltammogram of GO1 Electrodes in 1,1'-ferrocene Dimethanol Redox Species

This section looks at the performance of the rGO electrodes manufactured using GO1 graphene in the 1,1'-ferrocene dimethanol redox species. Its electrochemical activity is compared with that in the potassium ferricyanide redox species using the same electrode devices manufactured using GO1. Figure 5-3 shows the CV curves from the tests of all of the prepared electrodes. The results indicate that the electrode manufactured under vacuum conditions (LSG_{UVC}) shows a pronounced peak current and peak-to-peak separation potential with a rapid electrochemical response, indicating better electrochemical activity than the other electrodes tested. The electrode device LSG_{Ar} has slower electrochemical activity shown by its peak currents and peak-to-peak separation potential. These two electrodes exhibited better electrochemical behaviour than the other two electrode devices manufactured in air (LSG_{air}) and in the presence of Nitrogen gas (LSG_{N_2}). The latter two electrodes showed poor electrochemical activity as illustrated by their cyclic voltammogram in figure 5-3, indicating an irreversible response.

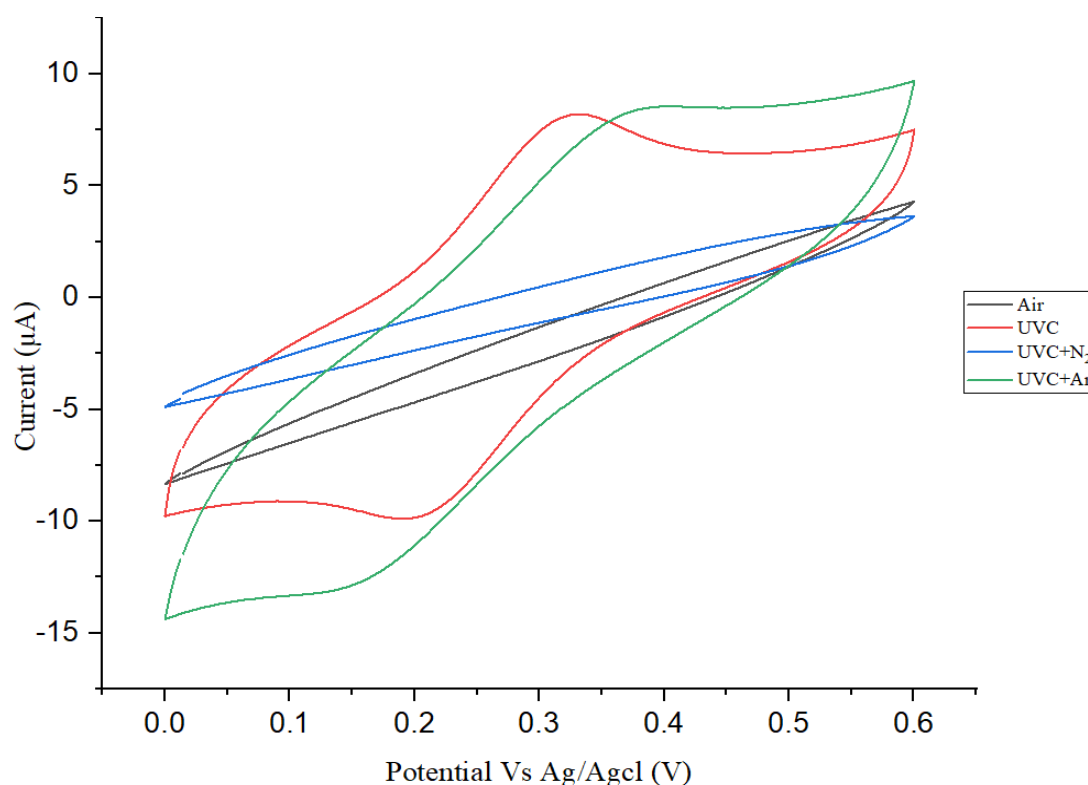


Figure 5-3. Cyclic voltammograms for the prepared electrodes under different conditions (LSG_{air} , LSG_{UVC} , LSG_{N_2} , and LSG_{Ar}) at a scan rate of 10mVs^{-1} in 1,1'-ferrocene dimethanol.

The results shown in table 5-1 indicate better responses by two of the prepared electrodes (LSG_{uvc} and LSG_{Ar}) in 1,1'-ferrocene dimethanol compared with the potassium ferricyanide cyclic voltammograms, since both electrodes were detected as active electrodes. It can be seen that the I_{pa} of 8.17 μA occurred at an E_{pa} of 0.3271 V for the LSG_{uvc} electrode device, with an I_{pc} of -9.85 μA occurring at a value of E_{pc} of 0.2002 V. Meanwhile, for the LSG_{Ar} electrode device, the I_{pa} of 8.12 μA occurred at an E_{pa} of 0.3662 V, with its I_{pc} of -12.8 μA occurring at an E_{pc} of 0.1538 V. According to these results, it can be deduced that use of the 1,1'-ferrocene dimethanol redox species led to better electrochemical behaviour exhibited by the electrode devices LSG_{uvc} and LSG_{Ar} as compared to its potassium ferricyanide redox species counterparts. The results of further comparisons are presented in subsequent sections to highlight the most suitable redox species to be used in this work.

However, it is important to state that fewer CV experiments were conducted for GO1 as an electrode material due to the evidence provided in chapter 4 in which the Raman spectroscopy and SEM results for GO2 indicated that it is superior to GO1 as a graphene oxide material, where this superiority is based on GO concentration. The presentation of the results in this section corroborates the findings in chapter 4 and also allows a comparison of the different concentrations found in GO1 and GO2.

Table 5-1. Electrochemical responses shown in the cyclic voltammograms of different electrode devices manufactured with GO1 under different conditions (LSG_{air} , LSG_{uvc} , LSG_{N_2} , and LSG_{Ar}) in both redox species (potassium ferricyanide and 1,1'-ferrocene dimethanol redox species).

Redox Species	Electrode Type	E_{pa}	E_{pc}	I_{pa}	I_{pc}
Potassium ferricyanide	LSG_{air}	N/A	N/A	N/A	N/A
	LSG_{uvc}	N/A	N/A	N/A	N/A
	LSG_{N_2}	N/A	N/A	N/A	N/A
	LSG_{Ar}	0.3467	0.1782	4.86	-11.7
1,1 ferrocene dimethanol	LSG_{air}	N/A	N/A	N/A	N/A
	LSG_{uvc}	0.3271	0.2002	8.17	-9.85
	LSG_{N_2}	N/A	N/A	N/A	N/A
	LSG_{Ar}	0.3662	0.1538	8.12	-12.8

5.4 CV of GO2 Electrodes in Potassium Ferricyanide Redox Species

This section presents the results concerning the electrochemical behaviour of the electrode devices manufactured using GO2 from CV performed with the potassium ferricyanide. This material is an inner-sphere redox species that is known to be sensitive to surface oxides [188]. In this section the results presented include a comparison of the scan rate used in the electrochemistry of each electrode device.

5.4.1 CV of LSG_{air} Electrode

The electrochemistry of this electrode device is represented in figure 5-4, which includes a comparison of the electrochemical activity of the electrode with respect to scan rates increasing from 10 mVs⁻¹ to 100 mVs⁻¹. As a general trend, it can be observed that, as the scan rate increases, the peak-to-peak separation potential at which the peaks of the anodic and cathodic currents occurred increases. It can be observed that the value of the peak current usually tends to increase with increasing scan rate for all scan rates except 75 mVs⁻¹ which shows the highest recorded peak current.

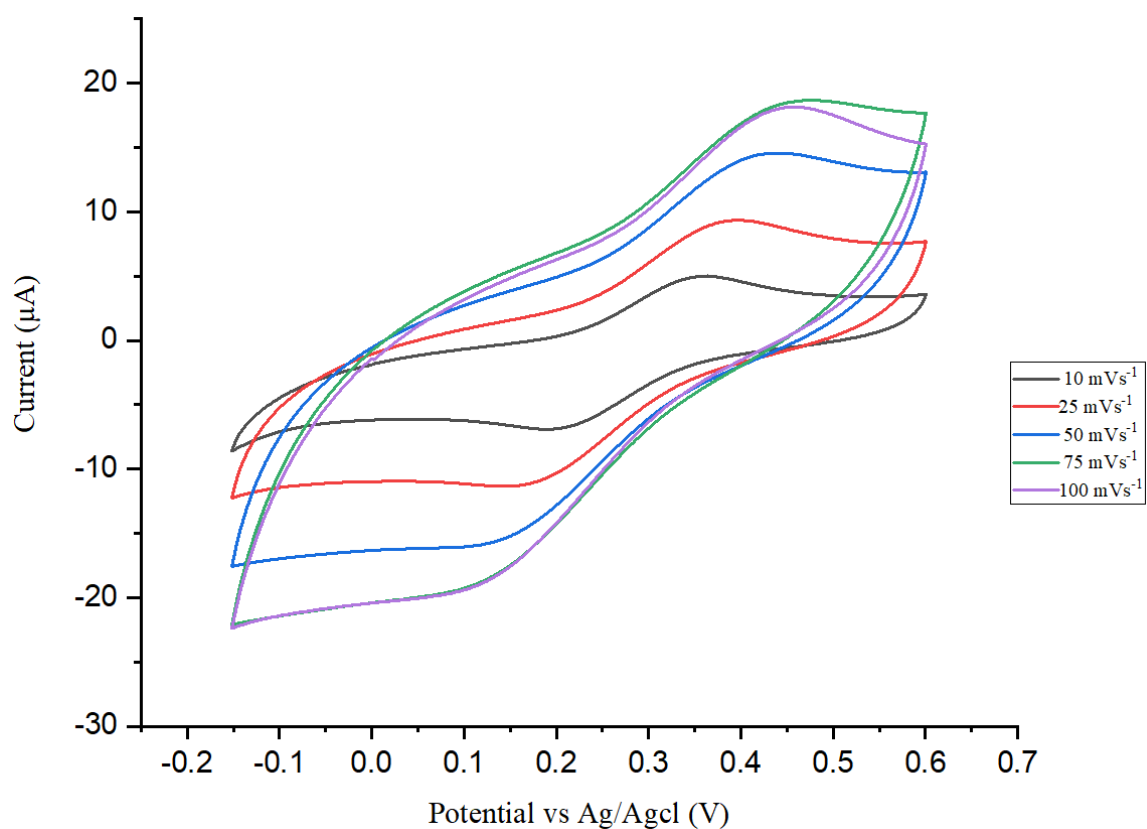


Figure 5-4. Cyclic voltammograms of LSG_{air} electrode at different scan rates in potassium ferricyanide redox species.

To further highlight the performance of the electrodes, a comparison was conducted of the response characteristics shown in the cyclic voltammogram for each electrode, and the results for each of the electrodes are shown in table 5-2 below. This table shows that the results for potassium ferricyanide indicates values of peak potential which are very close together. At the scan rates applied, it can also be observed that the values of anodic peak current for ranges from 5.11 μA to 18.67 μA with a cathodic peak current in the range from -5.3 μA to 19.76 μA . These readings represent quite high values of peak oxidation and reduction current, which indicate a porous material [142].

5.4.2 CV of LSG_{uvc} Electrode

An assessment of the effect of scan rate on the electrochemical activity of this electrode will explain the nature and quality of the device manufactured using this technique. The same scan rate from 10 mVs^{-1} to 100 mVs^{-1} was also applied to this electrode, as represented in figure 5-5. Overall, as the test scan rate increases, both the I_{pa} and I_{pc} peak currents increase proportionally. Similarly, the peak potential of the electrode also increased with scan rate. The figure also shows that the rate of electrochemical activity for electrode device decreases as the scan rate increases. These results can also be considered to reflect the effect of scan rate on the quality of the electrode device and its suitability for electrochemical sensing applications.

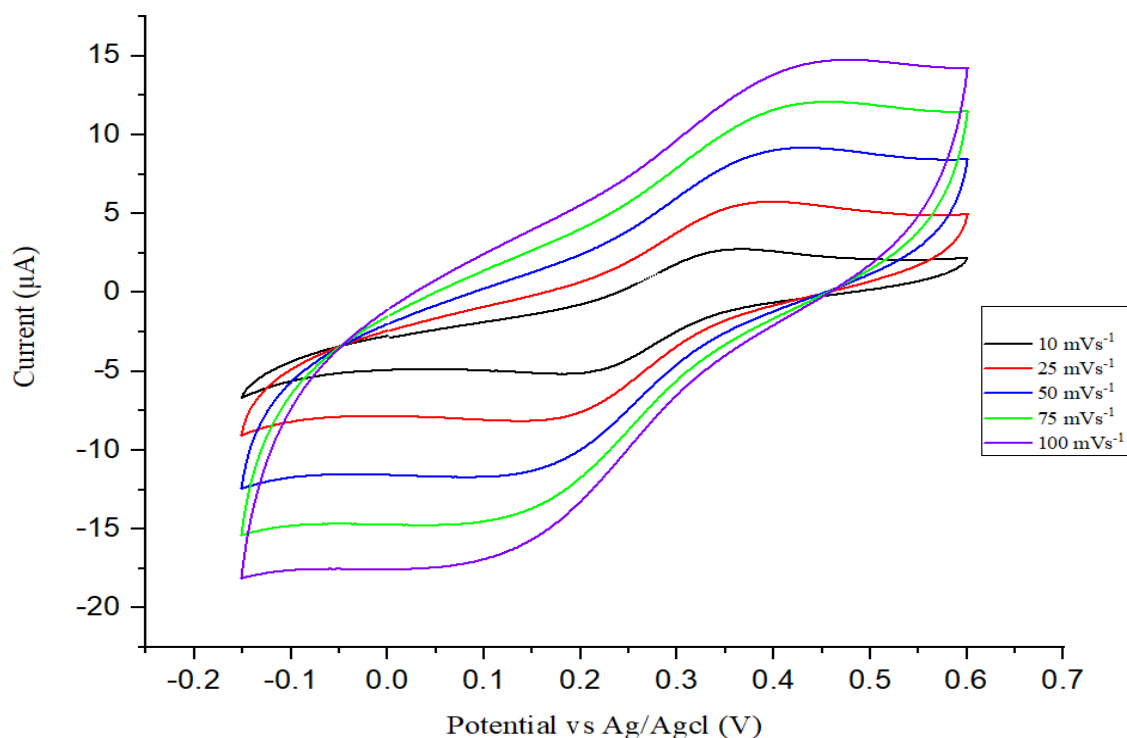


Figure 5-5. Cyclic voltammograms of LSG_{uvc} electrode at different scan rates in potassium ferricyanide redox species.

Similarly, as seen in table 5-2, the anodic peak potential (E_{pa}) of 0.4744 V at 100 mVs^{-1} was observed to be the highest peak potential compared to those at other scan rates tested. The cathodic peak potential (E_{pc}) with a value of 0.068 V at the same scan rate was also recorded as the highest peak potential. Additionally, the readings for the oxidation and reduction peak currents of $14.74 \mu\text{A}$ and $-17.303 \mu\text{A}$ respectively were found to be the highest values, indicating that the electrode is porous.

5.4.3 CV of LSG_{N_2} Electrode

The CV of the LSG_{N_2} electrode has also been tested using multiple scan rates in order to investigate its electrochemical behaviour and its suitability for electrochemical-dependent applications. The same trend that has been observed when testing the LSG_{air} and LSG_{uvc} electrodes has also been found in this case. It was observed that, as the scan rate increases from 10 mVs^{-1} to 100 mVs^{-1} , there were a gradual increase in the anodic and cathodic currents and potential peaks, as seen in figure 5-6 and table 5-2. The peak current and potential at a scan rate of 100 mVs^{-1} are also the highest detected compared with other scan rates tested. These results indicate that the lower the applied scan rate, the higher the electrochemical activity of the electrode, and therefore the application of 10 mVs^{-1} as the optimal scan rate is recommended. The results from the CV can give a good idea of the electrode's behaviour and its quality when prepared under specific conditions, and hence this would lead to the most suitable application of such an electrode according to the level of its electrochemical activity [190].

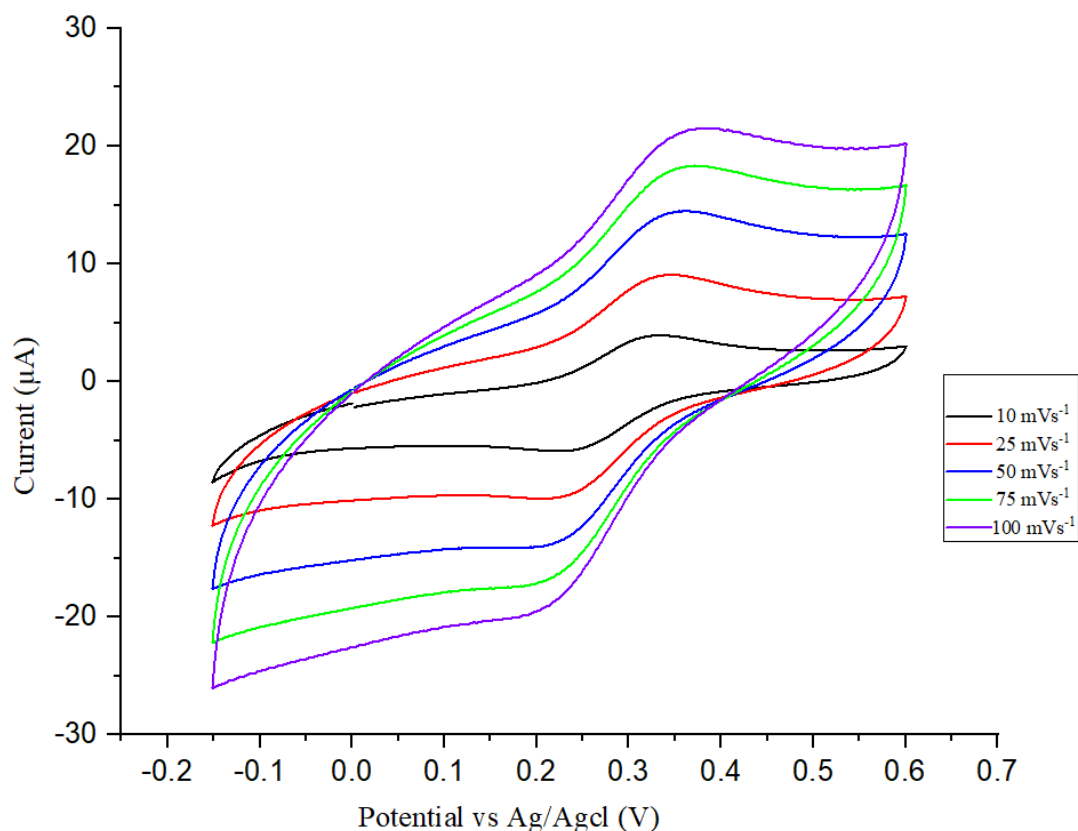


Figure 5-6. Cyclic voltammograms of LSG_{N_2} electrode at different scan rates in potassium ferricyanide redox species.

5.4.4 CV of LSG_{Ar} Electrode

The data presented in figure 5-7 show the same trend observed for both the LSG_{uvc} and LSG_{N_2} electrodes. The gradual increase in the scan rate applied also resulted in increased current and potential peak values. It is shown that the values of $23.90 \mu A$ and $-24.02 \mu A$ were recorded for the anodic and cathodic peak currents respectively, suggesting a porous electrode with more electrochemical activity compared with other electrodes tested.

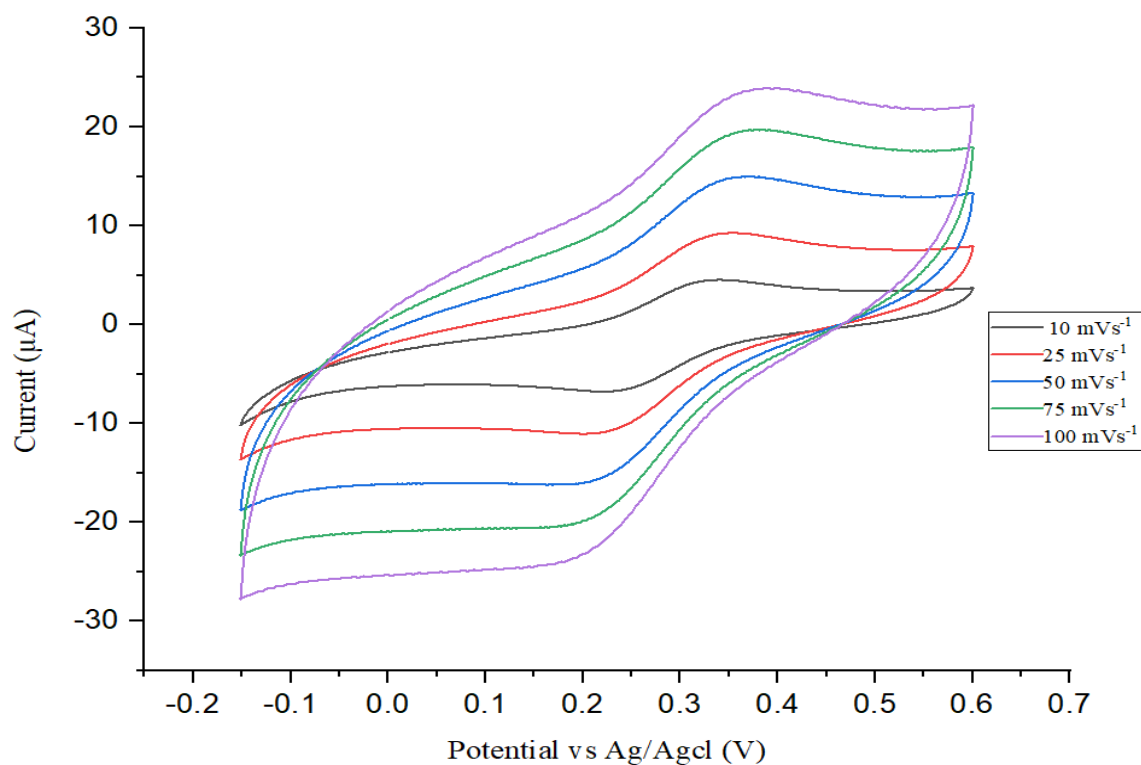


Figure 5-7. Cyclic voltammograms of LSG_{Ar} electrode at different scan rates in potassium ferricyanide redox species.

Table 5-2. Electrochemical response results for all GO₂ electrodes (LSG_{air}, LSG_{uvc}, LSG_{N₂}, and LSG_{Ar}) in potassium ferricyanide redox species.

Redox Species	Electrode Type	Scan Rate (mVs ⁻¹)	E _{pa} (V)	E _{pc} (V)	I _{pa} (µA)	I _{pc} (µA)
Potassium Ferricyanide	LSG _{air}	10	0.364	0.1904	5.11	-5.29
		25	0.3955	0.1489	9.344	-11.35
		50	0.4321	0.1155	14.575	-16.04
		75	0.4736	0.0708	18.67	-19.76
		100	0.437	0.1091	15.17	-15.23
	LSG _{uvc}	10	0.3613	0.1782	2.744	-5.17
		25	0.3931	0.1465	5.749	-8.14
		50	0.4248	0.1025	9.164	-11.67
		75	0.4419	0.1	12.05	-14.65
		100	0.474	0.068	14.74	-17.30
	LSG _{N₂}	10	0.3345	0.2271	3.915	-5.91
		25	0.3442	0.2124	9.048	-9.95
		50	0.3564	0.2051	14.44	-13.998
		75	0.366	0.1977	18.27	-17.23
		100	0.3833	0.2124	21.49	-19.09
	LSG _{Ar}	10	0.3393	0.2246	4.540	-6.7505
		25	0.3540	0.2002	9.280	-11.01
		50	0.3662	0.1855	14.94	-16.19
		75	0.380	0.17	19.671	-18.29
		100	0.3857	0.1758	23.90	-24.02

All measurements are average values from 3 samples.

5.5 CV of GO2 Electrodes in 1,1'-ferrocene Dimethanol Redox Species

Using CV, the four GO2 electrodes prepared under the previously mentioned conditions in the 1,1'-ferrocene dimethanol have also been tested as an outer-sphere redox species [191]. This section compares the electrochemical activity of these electrodes at different scan rates.

5.5.1 CVs of LSG_{air}, LSG_{uvc}, LSG_{N₂}, and LSG_{Ar} Electrodes

The electrochemical activity of the four GO2 electrodes prepared under air, vacuum, nitrogen gas, and argon gas conditions (LSG_{air}, LSG_{uvc}, LSG_{N₂}, and LSG_{Ar}) with the 1,1'-ferrocene dimethanol redox species have been investigated using CV. CV scan rates ranging from 10 to 100 mVs⁻¹ were employed in order to explore the response of the electrodes tested in terms of the potential and current peak values detected. In all of these electrodes, increases in the anodic and cathodic potential and current peak values matched the gradual elevation of scan rate. As demonstrated in figure 5-8 and table 5-3, the LSG_{air} electrode exhibited an E_{pc} value of 0.1731 V and an E_{pa} value of 0.3514 V as the highest values recorded using a scan rate of 100 mVs⁻¹. This electrode also gave the highest values of anodic peak current at 28.06 μA and cathodic peak current value at -27.16 μA, indicating that the electrode is porous and electroactive.

In addition, the testing of the LSG_{uvc} electrode using the same scan rate of 100 mVs⁻¹ resulted in the highest an E_{pa} and the lowest E_{pc} values of 0.3318 and 0.1853 V respectively, while the maximum anodic and cathodic peak currents were recorded as 24.2 and -23.93 μA respectively, as shown in figure 5-9 and table 5-3 with an E_{pc} of 0.27 V.

Moreover, as shown in figure 5-10 and table 5-3, the maximum values of E_{pa}, E_{pc}, I_{pa}, and I_{pc} for the LSG_{N₂} electrode at a scan rate of 100 mVs⁻¹ were recorded as 0.314 V, 0.207 V, 34.95 μA, and -33.75 μA respectively.

Finally, figure 5-11 and table 5-3 demonstrate that the maximum E_{pa}, E_{pc}, I_{pa}, and I_{pc} values of the LSG_{Ar} electrode occurred at the highest scan rate applied of 100 mVs⁻¹, which were recorded as 0.3299 V, 0.217 V, 35.549 μA, and -34.048 μA respectively.

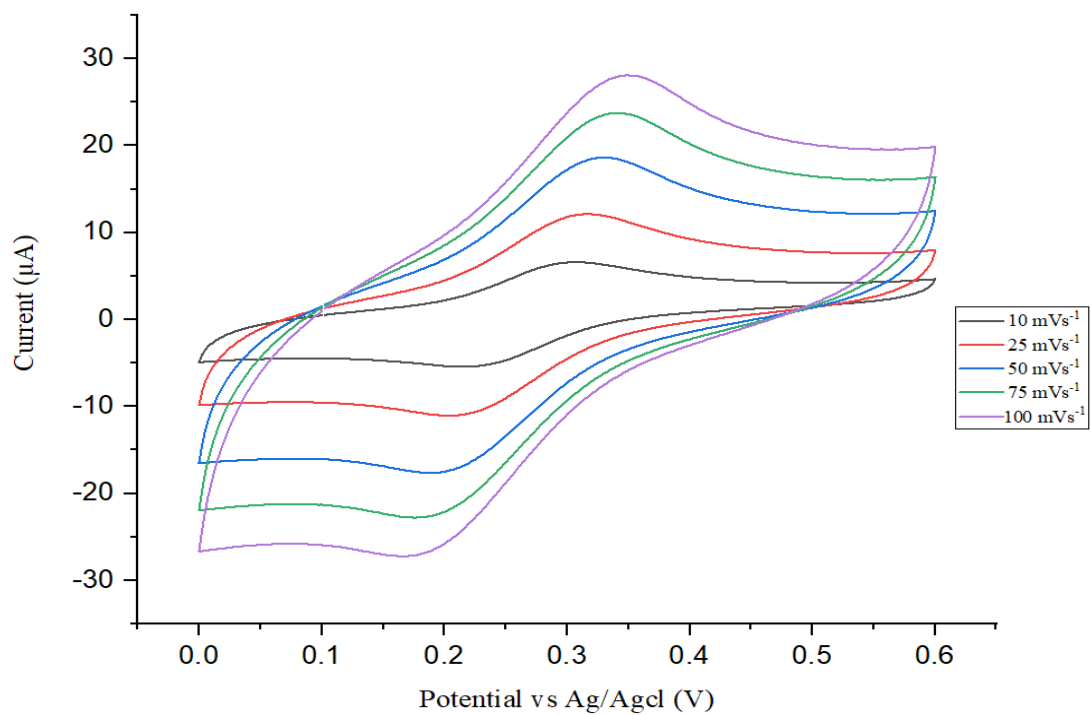


Figure 5-8. Cyclic voltammograms for LSG_{air} at different scan rates in 1,1'-ferrocene dimethanol redox species.

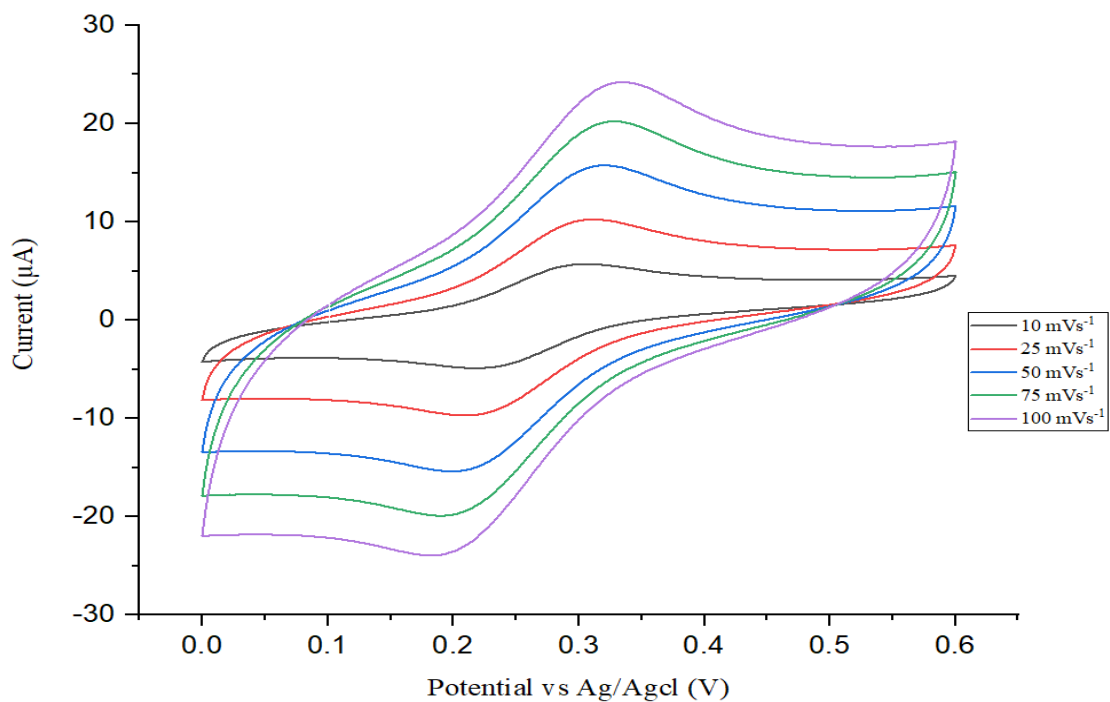


Figure 5-9. Cyclic voltammograms for LSG_{uvc} at different scan rates in 1,1'-ferrocene dimethanol redox species.

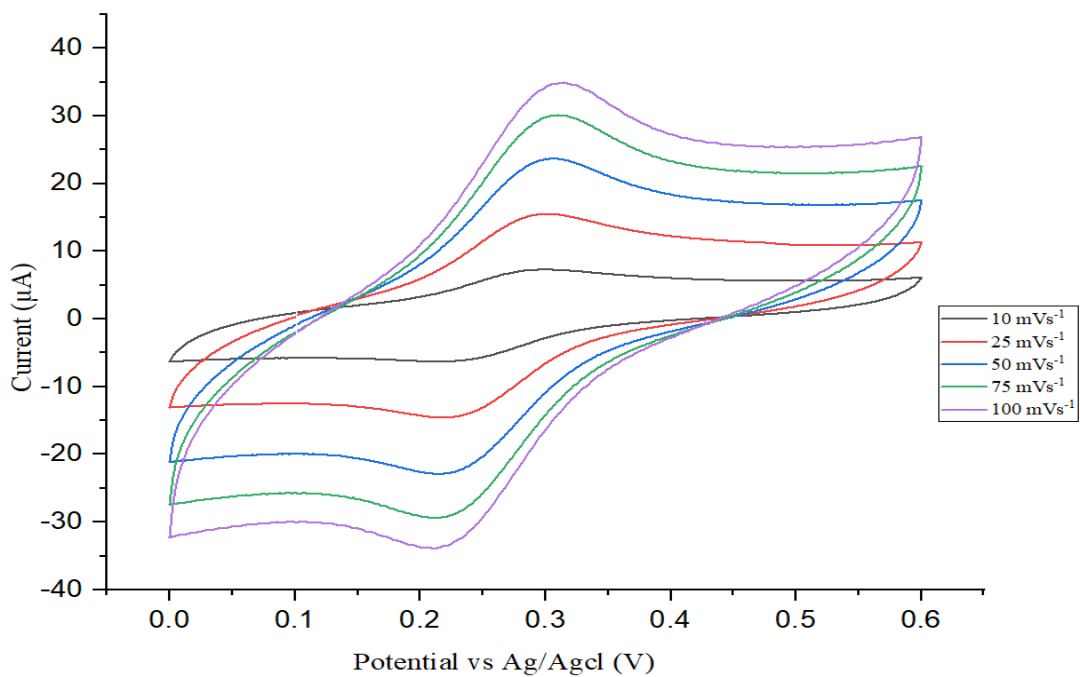


Figure 5-10. Cyclic voltammograms for LSG_{N2} at different scan rates in 1,1'-ferrocene dimethanol redox species.

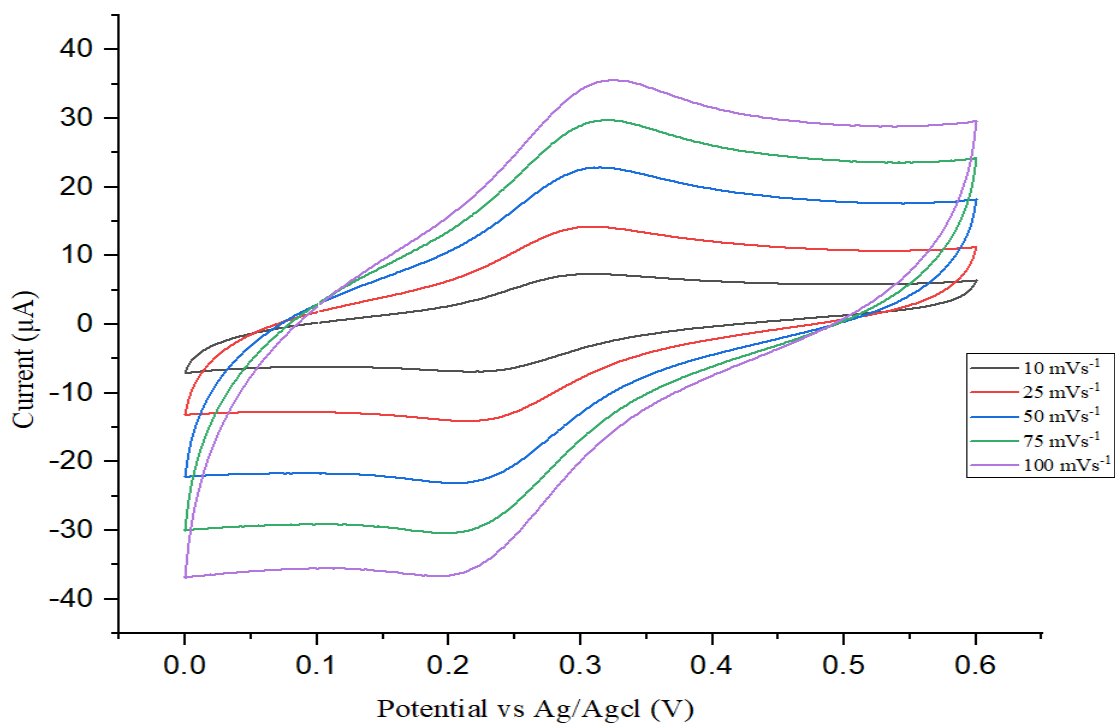


Figure 5-11. Cyclic voltammograms for LSG_{Ar} at different scan rates in 1,1'-ferrocene dimethanol redox species.

Table 5-3 Recorded results of electrochemical responses for all GO2 electrodes (LSG_{air}, LSG_{uvc}, LSG_{N₂}, and LSG_{Ar}) in 1,1'-ferrocene dimethanol redox species

Redox Species	Electrode Type	Scan Rate (mVs ⁻¹)	E _{pa} (V)	E _{pc} (V)	I _{pa} (μA)	I _{pc} (μA)
1,1'-ferrocene dimethanol	LSG _{air}	10	0.351	0.1805	7.736	-6.80
		25	0.3172	0.2049	13.718	-12.90
		50	0.3294	0.2024	18.627	-17.43
		75	0.3367	0.1878	23.730	-22.641
		100	0.3514	0.1731	28.064	-27.17
	LSG _{uvc}	10	0.3075	0.2196	5.695	-4.903
		25	0.3123	0.2098	10.245	-9.71
		50	0.3196	0.2049	15.750	-15.36
		75	0.3245	0.1878	20.20	-19.93
		100	0.3318	0.1853	24.200	-23.93
	LSG _{N₂}	10	0.3001	0.224	5.5023	-5.30
		25	0.3026	0.2220	15.524	-14.51
		50	0.3025	0.2195	23.629	22.74
		75	0.3025	0.2073	29.93	-29.35
		100	0.3147	0.2073	34.95	-33.75
	LSG _{Ar}	10	0.3075	0.219	7.321	-6.88
		25	0.3099	0.2147	14.212	-14.08
		50	0.307	0.21	22.74	-22.93
		75	0.3148	0.2098	29.66	-23.25
		100	0.3299	0.2171	35.54	-34.05

5.6 Conclusion

This chapter presents the preliminary results of experiments on the electrochemical responses shown in the cyclic voltammograms of the electrode devices in both the outer and inner redox species. As a general trend, and as observed from the cyclic voltammograms, the peak potentials (peak anodic and cathodic current) increasing proportionally when the scan rate was gradually elevated. Unlikely, the electrochemical activity of the four tested electrodes decreased with increasing scan rate from 10 mVs⁻¹ to 100 mVs⁻¹. The cyclic voltammograms from each redox species also give an indication of the nature of the electrode material and the efficiency of the manufacturing techniques used and hence give useful information about the appropriate application of the electrode devices produced with respect to their electrochemical sensing capability.

From the analysis of data, it is concluded that the electrochemical responses of the four electrodes (LSG_{air}, LSG_{uvc}, LSG_{N₂}, and LSG_{Ar}) were much weaker in the potassium ferricyanide than in the 1,1'-ferrocene dimethanol. However, the significant differences in their values as recorded in tables 5-2 and 5.3 indicate that the responses of the electrodes differ from each other since each type was manufactured using different fabrication techniques [162].

Chapter 6. Discussion of Results

6.1 Introduction

This chapter follows up on the work described in chapter 5, focusing on a further examination of the results of the electrochemical experiments carried out with the two redox species tested. The evaluation of the influence of different scan rates in affecting the characteristics of the manufactured electrode devices as well as their other properties is considered along with subsequent discussions in relation to other electrodes reported in the literature. To study the results in depth, the effect of the manufacturing technique used is also be evaluated with respect to scan rate. The investigation begins with the results for potassium ferricyanide followed by those for the 1,1'-ferrocene dimethanol.

6.2 Electrochemical Performance of Each Electrode in Potassium Ferricyanide

The results presented in this section focus on the responses associated with the various scan rates used in this electrochemical examination of each electrode material. From these results, the manufactured materials can be interpreted so that their characteristics can be compared in order to select a suitable scan rate that can be used to as an optimal parameter for electrode performance.

6.2.1 Electrochemical Characteristics of the Prepared Electrodes

For the redox probe of potassium ferricyanide with 1 M KCl as a supporting redox species, it is important to look at the effect of scan rate on the response characteristics of the manufactured electrodes, which will be used to determine the system's performance. These results can also give insights into the electrochemical behaviour of devices manufactured under different conditions. CV was used to measure two parameters which taken together can be used to determine if a reaction is reversible, quasi-reversible or irreversible for a given scan rate, according to differences in the observed peak separation potential of the anodic peak current and the cathodic peak current shown in the cyclic voltammogram, and the intensity of the anodic (I_{pa}) and cathodic (I_{pc}) peak currents relative to the baseline on the cyclic voltammogram [47]. This section initially focuses on the effect of a scan rate of 10 mVs^{-1} on the manufactured electrode material and its response characteristics, as this was shown to be the best scan rate to be applied compared to the other values tested.

One of the indications that an electrochemical process is reversible, quasi-reversible or irreversible is given by the ratio of I_{pa} to I_{pc} [47], and the results for the electrodes are presented in table 6-1. In the case of reversibility, the peak current ratio should be equal to one [47, 51]. It can be seen from the I_{pa}/I_{pc} data in table 6-1 that the ratios for all of the electrodes are below unity, which indicate that this process at a scan rate of 10 mVs^{-1} does not exhibit the behaviour associated with reversibility. table 6-1 also illustrates that the electrochemical activity of all of the electrodes, as indicated by their response in terms of the rate at which they reach their individual peak currents, suggests that they possess multiple layers. These results closely match those of Randviir [53], who concluded that the peak-to-peak separation potential (ΔE_p) in voltametric waves increases as the number of graphene layer decreases, representing a decrease in the heterogeneous electron transfer rate and therefore slower electrochemical performance. However, for an ideal Nernstian one electron transfer process, the value of ΔE_p would be 59 mV [47, 48]. From the results shown in table 6-1 at a scan rate of 10 mVs^{-1} , the data for peak separation potential obtained using Equation 2-1 indicate that the LSG_{N2} electrode possesses the lowest value of 107.4 mV. This is the value closest to the ideal value of 59 mV, and hence this electrode exhibits the fastest rate of electron transfer compared to that of the LSG_{uvc} which exhibits the slowest electron transfer rate.

To further indicate the electrochemical responses of each electrode and the reversibility, quasi-reversibility or irreversibility of the system, it is important to determine the heterogeneous electron transfer, or electron transfer rate, at the electrode surface (k^0) [48, 50]. As mentioned in chapter 2, when the value of k^0 ranges from 10^{-5} to 0.05 cms^{-1} ($0.05 > k^0 > 10^{-5} \text{ cms}^{-1}$), the electron transfer reaction is called a quasi-reversible process [50]. From the data in table 6-1, the value of k^0 for all of the electrodes (LSG_{air} , LSG_{uvc} , LSG_{N2} , and LSG_{Ar}) was estimated to be 0.0016 cms^{-1} with a standard deviation of 10^{-5} at the scan rate of 10 mVs^{-1} . The dimensionless kinetic parameter Ψ in Equation 2.2 is also important in determining the system performance. If $\Psi > 10$, this indicates the electrochemical reversibility of the system, whereas if $10 > \Psi > 10^2$ the system is considered to be quasi-reversible, and if $\Psi < 10^2$, the system is an irreversible one [47, 53]. From this, it can be concluded that all of the manufactured electrodes exhibit quasi-reversibility at a scan rate of 10 mVs^{-1} since their Ψ values are approximately 0.6.

The mass transport in these electrodes is also another parameter that can describe the performance characteristics of the electrode system, which can be derived using Equation 2.6. As reported elsewhere [47], the slowest process involved determines electrochemical performance in every case if:

$K^0 \gg M_{\text{trans}}$, where the electrode process is termed reversible and controlled by diffusion.

$K^0 \approx M_{\text{trans}}$, where both diffusion and electron transfer are of the same order and the process is called quasi-reversible; and

$K^0 \ll M_{\text{trans}}$, where electron transfer is termed irreversible because the process will be rate-determined when the mass transport is faster than the electron transfer rate.

Thus, at a scan rate of 10 mVs^{-1} , the value of M_{trans} for all of the electrodes is 0.00257 cms^{-1} , which is close to that of K^0 and can be approximately equal, confirming the quasi-reversible behaviour of all of the electrodes, as shown in table 6-1.

Using the same analysis, equations, and results from table 6-1, it can be deduced that, with scan rates of 25 mVs^{-1} , 50 mVs^{-1} , 75 mVs^{-1} , and 100 mVs^{-1} , the electrochemical behaviour of all of the manufactured electrodes is also quasi-reversible.

Table 6-1. Response characteristics of the LSG_{air}, LSG_{uvc}, LSG_{N₂}, and LSG_{Ar} electrodes in potassium ferricyanide redox species.

Redox Species	Electrode Type	Scan Rate (mVs⁻¹)	I_{pa}/I_{pc}	ΔE_p (mV)	Ψ	K⁰	M_{trans}
Potassium Ferricyanide	LSG_{air}	10	-0.97	173.6	0.6303	0.0016	0.00257
		25	-0.82	246.6	0.631	0.00256	0.00406
		50	-0.91	316.6	0.6315	0.00362	0.00575
		75	-0.94	402.8	0.632	0.00444	0.00704
		100	-1.00	327.9	0.6316	0.00512	0.00813
	LSG_{uvc}	10	-0.53	183.1	0.631	0.00162	0.00257
		25	-0.71	246.6	0.6315	0.00256	0.00406
		50	-0.79	322.3	0.6321	0.00363	0.00575
		75	-0.82	341.9	0.6323	0.00445	0.00704
		100	-0.85	406	0.6323	0.00514	0.00813
	LSG_{N₂}	10	-0.66	107.4	0.6297	0.00162	0.00257
		25	-0.91	122.1	0.6299	0.00256	0.00406
		50	-1.03	151.3	0.6302	0.00362	0.00575
		75	-1.06	168.3	0.6303	0.00444	0.00704
		100	-1.13	170.9	0.6304	0.00512	0.00813
	LSG_{Ar}	10	-0.67	114.7	0.6298	0.00162	0.00257
		25	-0.84	153.8	0.6301	0.00256	0.00406
		50	-0.92	180.7	0.6304	0.00362	0.00575
		75	-1.08	210	0.6305	0.00444	0.00704
		100	-0.98	214.2	0.6306	0.00513	0.00813

6.3 Electrochemical Performance of Each Electrode in 1,1'-ferrocene Dimethanol Redox Species

This section presents an analysis of the response characteristics of the manufactured electrodes at a scan rate of 10 mVs^{-1} by examining their individual electrochemical responses. The results of this analysis will then be used to suggest which of the tested electrode materials has the most suitable electrochemical response characteristics that would indicate its choice for use in the intended application.

6.3.1 Electrochemical Characteristics of the Prepared Electrodes

In the same manner as for the potassium ferricyanide redox species, the electrochemical details of the device manufactured under different conditions in the 1,1'-ferrocene dimethanol redox species are also analysed here. This section initially focuses on the effect of the scan rate of 10 mVs^{-1} on the performance of the manufactured electrode materials. In order to determine the nature of the electrochemical process, the same analysis of parameters was also employed to determine which of the electrode systems and at which scan rates they possess the features of reversibility, quasi-reversibility or irreversibility. Firstly, as demonstrated in table 6-2, the ratio of I_{pa} to I_{pc} for the LSG_{UVC} electrode at a scan rate of 10 mVs^{-1} is reported as 1.16, which is slightly above the value of unity that is required for a system to be termed reversible. However, if this ratio is close to one, as in this case, it indicates the existence of a quasi-reversible electron transfer reaction [50]. Considering all the scan rates from 10 mVs^{-1} to 100 mVs^{-1} for the LSG_{air} electrode, a mean value of this ratio is found of 1.07 with a standard deviation of 0.04, which also indicates a quasi-reversible system. The same trend was also observed with the other electrodes, where for LSG_{UVC} the mean value of the peak current ratio is 1.05 with a standard deviation of 0.05, which again indicates a quasi-reversible system. Meanwhile, for the LSG_{N_2} electrode, the mean of the ratio is 1.04 with a standard deviation of 0.08, and so this electrode falls within the range of both reversible and quasi-reversible systems. However, for all of the scan rates, this ratio for the LSG_{Ar} has a mean value of 1.04 and a standard deviation of 0.04, thus indicating a quasi-reversible system.

Furthermore, the results from table 6-2 for all scan rates for the electrodes show that the average value of Ψ is 0.63 falls within the set of values which indicate that the system's behaviour is quasi-reversible. Additionally, analysis of the parameters recorded in table 6-2 reveals that the average value of K^0 for these electrodes at 10 mVs^{-1} is 0.0018 cms^{-1} which again is found in

the range of values that indicate quasi-reversible systems. The K^0 values also compares closely with values of M_{trans} for the electrodes concerned, giving a mean value of 0.0029 cm s^{-1} . This similarity in the values of K^0 and M_{trans} is also a reason to conclude that these electrodes exhibit quasi-reversibility in their electrochemical responses. The same reasoning is applicable for the remaining scan rates from 25 mVs^{-1} to 100 mVs^{-1} with the 1,1'-ferrocene dimethanol, thus indicating that the electrode systems with this redox species exhibit quasi-reversible reactions in their electrochemistry.

Table 6-2. Response characteristics of the LSG_{air}, LSG_{uvc}, LSG_{N₂}, and LSG_{Ar} electrodes in 1,1'-ferrocene dimethanol redox species.

Redox Species	Electrode Type	Scan Rate (mVs ⁻¹)	I _{pa} /I _{pc}	ΔE _p (mV)	Ψ	K ⁰	M _{trans}
1,1'-ferrocene dimethanol	LSG _{air}	10	-1.14	90.3	0.629577	0.001869	0.002968
		25	-1.06	112.1	0.629766	0.002955	0.004693
		50	-1.07	127	0.629893	0.00418	0.006637
		75	-1.05	148.9	0.630082	0.005122	0.008128
		100	-1.03	176.9	0.630336	0.005916	0.009386
	LSG _{uvc}	10	-1.16	87.9	0.629556	0.001869	0.002968
		25	-1.06	102.5	0.629682	0.002955	0.004693
		50	-1.03	114.7	0.629787	0.00418	0.006637
		75	-1.01	136.7	0.629977	0.005121	0.008128
		100	-1.01	146.5	0.630062	0.005914	0.009386
	LSG _{N₂}	10	-1.03	76.1	0.629451	0.001869	0.002968
		25	-1.07	80.6	0.629493	0.002954	0.004693
		50	1.04	83	0.629514	0.004178	0.006637
		75	-1.02	95.2	0.629619	0.005118	0.008128
		100	-1.04	107.4	0.629724	0.00591	0.009386
	LSG _{Ar}	10	-1.06	88.5	0.629556	0.001869	0.002968
		25	-1.01	95.2	0.629619	0.002955	0.004693
		50	-0.99	97	0.629556	0.004178	0.006637
		75	-1.11	105	0.629709	0.005119	0.008128
		100	-1.04	112.8	0.629619	0.00591	0.009386

6.4 Supporting Electrochemical Analysis of the Prepared Electrodes in Potassium Ferricyanide Redox Species

In the current work, the laser scribing technique was used to convert GO into rGO, and other studies have demonstrated that the threshold laser power that is required for the conversion of GO into laser induced graphene (LIG) is dependent upon the write speed of the CO₂ laser cutting machine [162, 192]. The composition of the LIG material and its sheet resistance and thickness and specific area capacitance can be changed according to the laser power used [192]. In the current chapter, the cyclic voltammetry data obtained from our electrodes prepared using the four conditions (LSG_{air}, LSG_{uvc}, LSG_{N₂}, and LSG_{Ar}) were compared with the results of other studies which have used the LIG technique to produce rGO. Nevertheless, this work has focused on the electrochemical behaviour of the electrodes produced in potassium ferricyanide as the selected redox species.

Firstly, the electrodes were examined using CV with potassium ferricyanide redox species along with 1 M KCl as supporting redox species over a range of scan rates from 10-100 mVs⁻¹. The mean values of peak-peak potential separation (ΔE_p) for each electrode at these scan rates are recorded in table 6-1 and plotted as shown in figure 6-1. From the figure it can be observed that, for a backward forecast, at a scan rate of 0, the value of ΔE_p for LSG_{N₂} is 90 mV and this increased at a rate of 1.74 mV for every 1mVs⁻¹ to reach a value of 107.4 mV at 10 mVs⁻¹, while for LSG_{Ar} the ΔE_p was 95 mV at a scan rate of 0 mVs⁻¹ rising by 1.97 mV for each 1mVs⁻¹ to a value of 114.7 mV at 10 mVs⁻¹ scan rate. For LSG_{air} the corresponding values were 98 mV at 0 mVs⁻¹ increasing by 7.6 mV for every 1mVs⁻¹ to reach 173.6mV at 10 mVs⁻¹; whereas those for LSG_{uvc} were recorded as 154 mV at a scan rate of 0 mVs⁻¹ increasing by 2.91mV for every 1mVs⁻¹ to reach a value of 183.1mV at 10 mVs⁻¹. As a general trend, the values of ΔE_p for each electrode increased to the final levels shown in figure 6-1. This means that, the electrodes kinetics was able to maintain a maximum response to faster scan rates, indicating irreversible behaviour in the CV tests [193]. But some electrodes did not fully comply with this trend, instead exhibiting quasi-reversible behaviour [142]. From the results in figure 6-1, it can be observed that the maximum ΔE_p of the electrodes occurs at 406 mV, which is considerably higher than the ideal value of 59 mV, or in some cases 57 mV [48], which is the expected value of an ideal Nernstian diffusional process involving the transfer of one electron, which would indicate a ‘thin layer’ response [162, 194]. The effect of adsorption of the redox species which resulted from their entrapment inside the porous structure is likely

responsible to lower the value of the peak-to-peak separation in the LSG electrodes [142]. But, from the CV data of our electrodes with potassium ferricyanide redox species, the ΔE_p values were observed to be higher than 59 mV. The sponginess present due to the size and position of the pores changes the electrochemistry of an electrode used in this redox species. For the LSG_{N2} electrode, values of ΔE_p in potassium ferricyanide were recorded as low as 107.4 mV at a scan rate of 10 mVs⁻¹, which indicates that this electrode is the closest one to the ideal value compared with the other electrodes examined at the same scan rate.

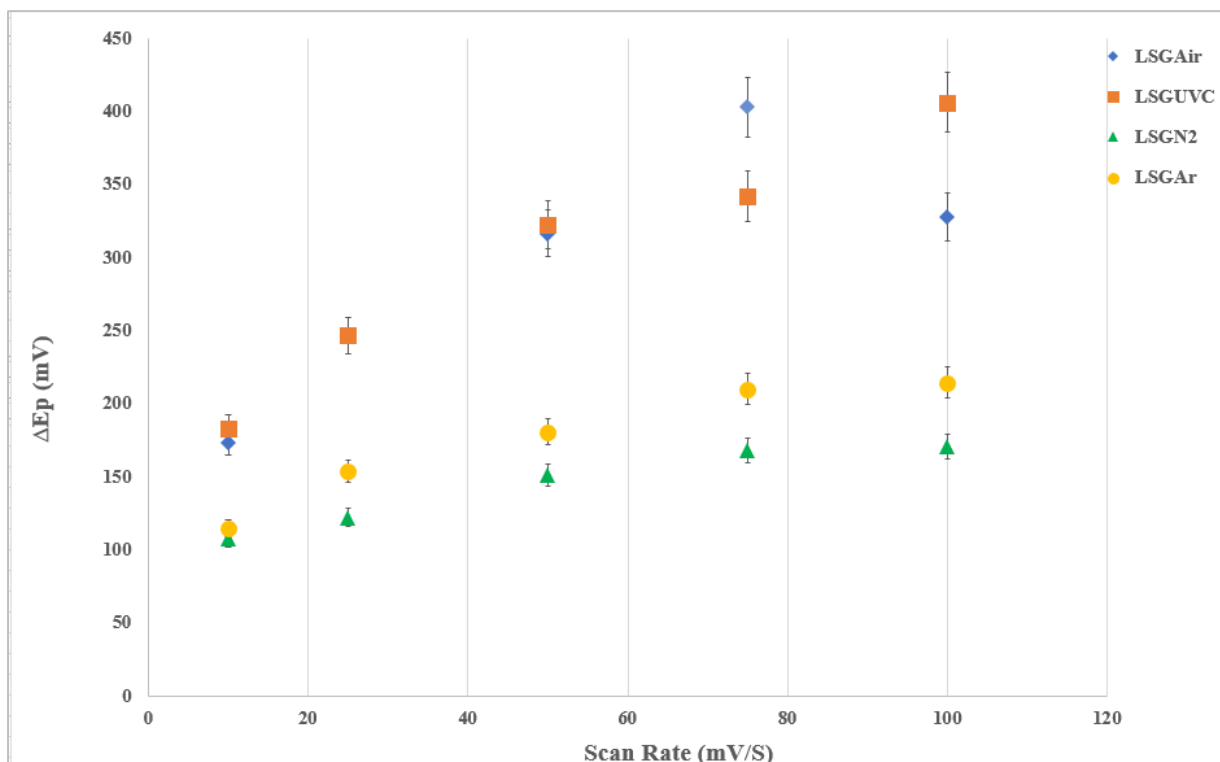


Figure 6-1. Plot of peak-peak potential separation against scan rate for the electrodes prepared using four different conditions (LSG_{air}, LSG_{uvc}, LSG_{N2}, and LSG_{Ar}) in potassium ferricyanide redox species.

More results of the CV for the manufactured electrodes are presented in figures 6-2 and 6-3 which show the plot of the peak current against scan rate and the square root of scan rate for all electrodes. The result shows a linear trend for all the electrodes where the current responses is proportional to the square root of the scan rate, thus indicating diffusion controlled voltametric process [162, 195-197]. However, to gain a better understanding of electrode performance, the R^2 values for all electrodes were found to be very similar, as shown in figures 6-2 and 6-3 and table 6-3. Moreover, R^2 values of the LSG_{air} electrode in both figures indicate a porous electrode that possesses favourable electroactivity due to the summative effect of diffusion and thin-layer behaviour. However, from the R^2 value for the remaining electrodes, it could be suggested that their levels of electroactivity are mainly due to diffusional behaviour.

Moreover, figures 6-2 and 6-3 suggest that all of the electrodes exhibit diffusional behaviour, which is a crucial requirement for electrochemical biosensor applications [198]. Overall, the results obtained show that the LSG_{N2} electrode has the most desirable electrochemical characteristics, making it the preferred choice to be used with this redox specie.

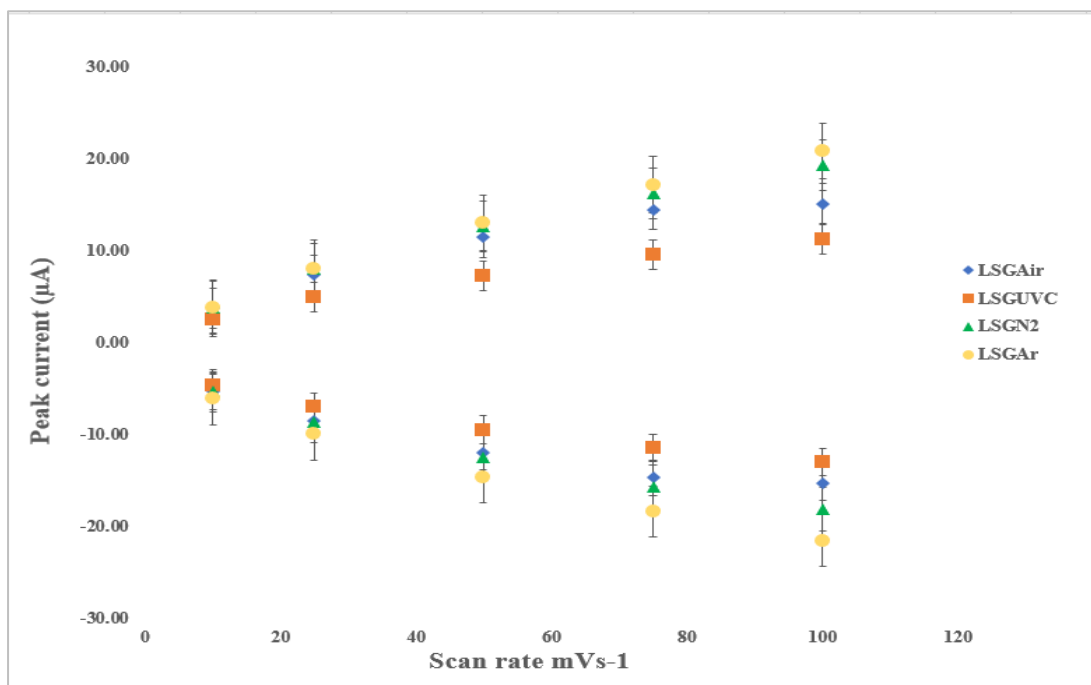


Figure 6-2. Plot of peak current against scan rate for the electrodes prepared using four different conditions (LSG_{air}, LSG_{uvc}, LSG_{N2}, and LSG_{Ar}) in potassium ferricyanide redox species.

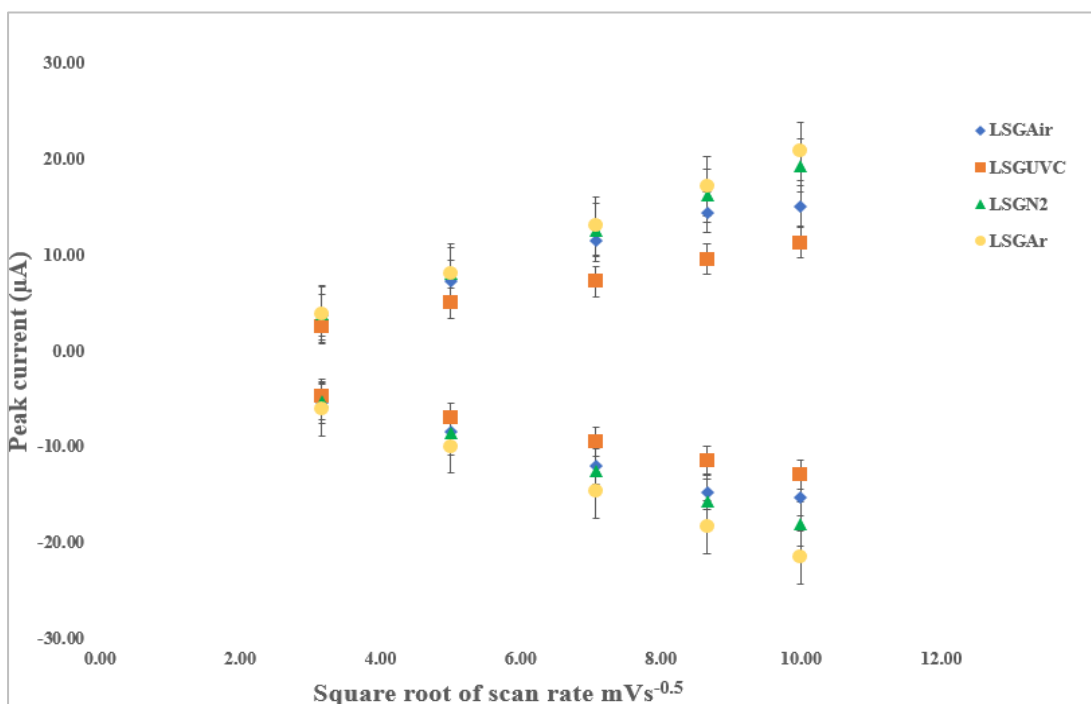


Figure 6-3. Plot of peak current against square root of scan rate for the electrodes prepared using four different conditions (LSG_{air}, LSG_{uvc}, LSG_{N2}, and LSG_{Ar}) in potassium ferricyanide redox species.

Table 6-3. R^2 values for the four manufactured electrodes (LSG_{air}, LSG_{uvc}, LSG_{N2}, and LSG_{Ar}) in potassium ferricyanide redox species.

Square root of scan rate			
Redox species	Electrode type	R^2_{Ipa}	R^2_{Ipc}
Potassium ferricyanide	LSGair	0.9805	0.9817
	LSGuvc	0.9984	0.9998
	LSGN2	0.9999	0.9997
	LSGAR	0.999	0.9995
Scan rate			
Potassium ferricyanide	LSGair	0.9278	0.931
	LSGuvc	0.9807	0.9759
	LSGN2	0.9804	0.9812
	LSGAR	0.987	0.9848

6.5 Supporting Electrochemical analysis of the Prepared Electrodes in 1,1'-ferrocene Dimethanol Redox Species

In this section, the CV results are used to assess the electrochemical performance of the manufactured electrodes with 1,1'-ferrocene dimethanol as the second selected redox type. The electrode devices in this case were the same electrodes made of LSG material under the various fabrication conditions as mentioned earlier. The values of ΔE_p for each electrode are plotted against the range of scan rates applied from 10 to 100 mVs^{-1} as shown in figure 6-4. It can be noted that, if viewed in reverse towards the initial scan rate of 0 mVs^{-1} , the value of ΔE_p for LSG_{air} is 84 mV and which then rises at a rate of 0.63 mV for each increase in rate of 1 mV s^{-1} to reach a value of 90.3 mV at 10 mV s^{-1} . Meanwhile, for LSG_{uvc}, its value is initially 84 mV and then rises by 0.39 mV for every 1 mV s^{-1} to reach a value of 87.9 mV at 10 mV s^{-1} , whereas the ΔE_p of LSG_{Ar} was initially 86 mV at a scan rate of 0 mVs^{-1} before surging at a rate of 0.25 mV for every 1 mV s^{-1} to a value of 88.5 mV at 10 mV s^{-1} . Finally, the initial value for LSG_{N2} of 71 mV increased by 0.51 mV for every 1 mV s^{-1} to a value 76.1 mV at a scan rate of 10 mV s^{-1} . This behaviour shows that the kinetics of all electrodes were maintained at their maximum response to faster scan rates, indicating unique response behaviour for each electrode.

It can also be noted that there is a mixed trend of both a fairly stable and an increase in the value of ΔE_p as scan rate increases, which is a common trend among all of the electrodes. This suggests that the kinetics of these electrodes do not fully maintain the maximum possible response to faster scan rates [142]. From the results shown in figure 6-4, it can be seen that the maximum value of ΔE_p for the electrodes occurs at 176.9 mV, which is larger than the ideal ΔE_p value [162, 194]. This large value of ΔE_p does not indicate the entrapment of the redox species inside the porous structure of the LSG electrodes, because porosity in the LSG electrodes in terms of the number, size and location of the pores would change their electrochemistry. In the results of this experiment, the LSG_{N₂} electrode in 1,1'-ferrocene dimethanol at the scan rates mentioned clearly exhibited the lowest ΔE_p value of 76.1 mV, while the highest value of 176.9 mV was observed for electrodes produced under atmospheric conditions as presented in figure 6-4.

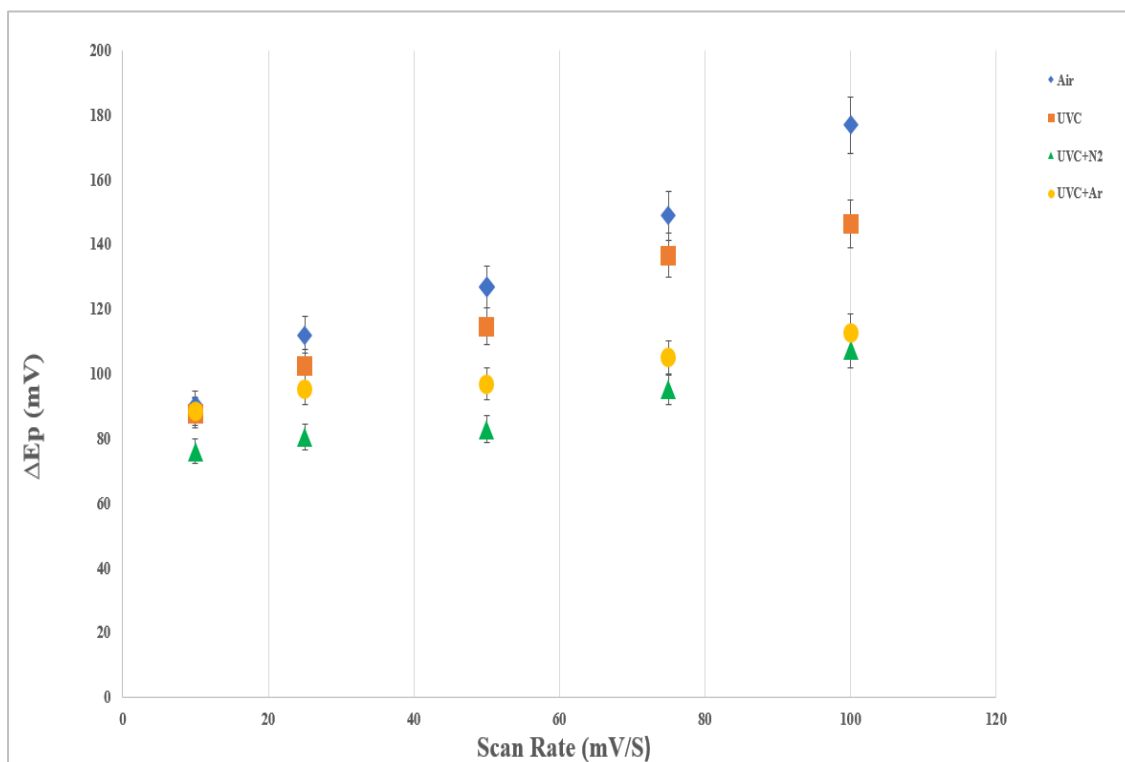


Figure 6-4. Plot of ΔE_p against scan rate for the electrodes produced under different conditions (LSG_{air}, LSG_{uvc}, LSG_{N₂}, and LSG_{Ar}) in 1,1'-ferrocene dimethanol redox species.

Employing the same analysis as mentioned above, the performance results of the electrodes are presented in table 6-4 and figures 6-5 and 6-6. It can be noticed that the results of all of the electrodes tested show a linear trend indicating a proportional relationship between peak current and scan rate as well as peak current and the square root of scan rate, hence illustrating an electrochemical response controlled by diffusion [162, 195-197]. From a comparison of the

R^2 values in table 6.4 for all electrodes, it is deduced that their electrochemical activity is principally due to diffusion behaviour, and that means that these electrodes are suitable for electrochemical biosensor applications, as in the case of the redox species potassium ferricyanide. Also, from these results, it can be concluded that, since the LSG_{N_2} electrode has the lowest value of ΔE_p , it therefore exhibits the best electrochemical response. Therefore, it is the most favoured of the electrodes for use with the 1,1'-ferrocene dimethanol.

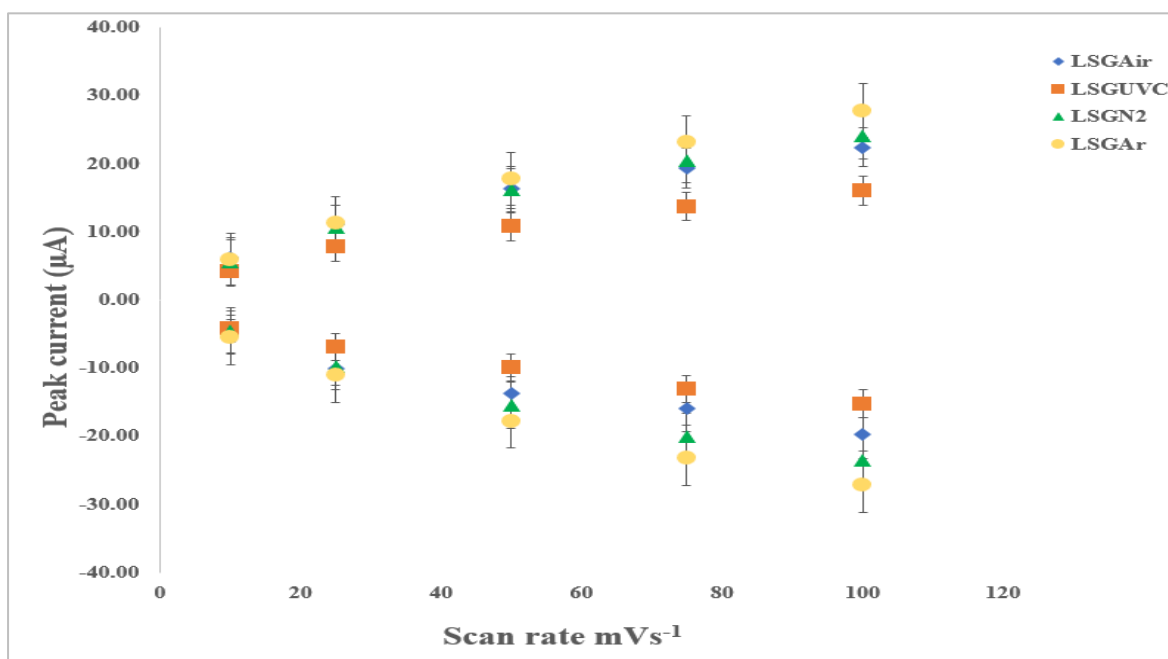


Figure 6-5. Plot of peak current against scan rate for the electrodes produced under the different conditions (LSG_{air} , LSG_{uvc} , LSG_{N_2} , and LSG_{Ar}) in 1,1'-ferrocene dimethanol redox species.

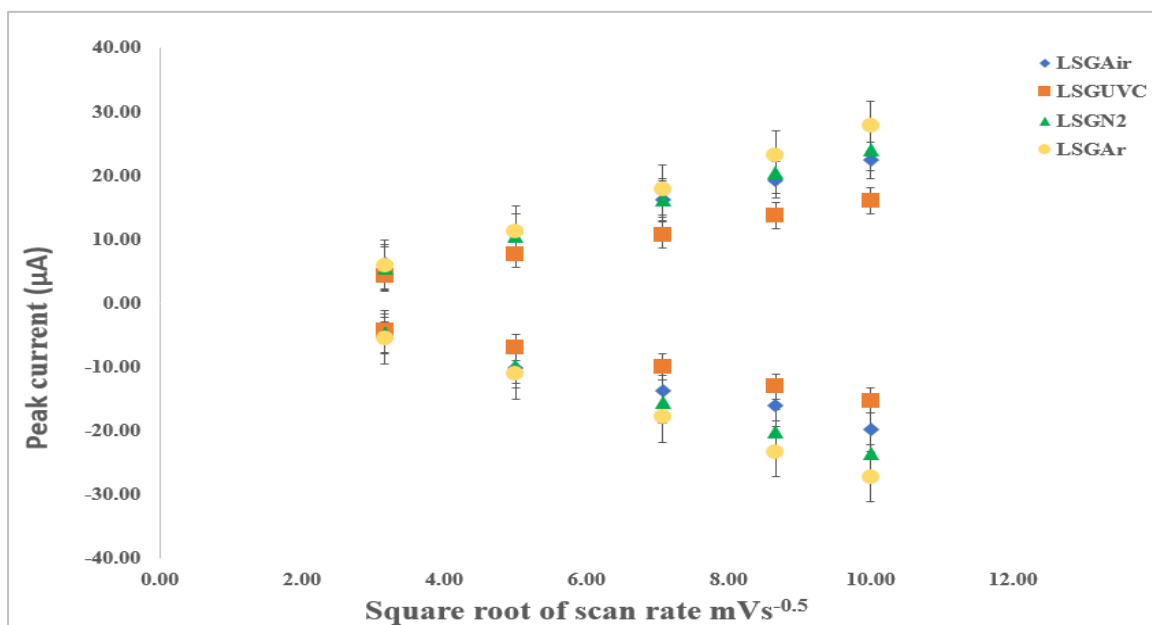


Figure 6-6. Plot of peak current against the square root of scan rate for the electrodes produced under the different conditions (LSG_{air} , LSG_{uvc} , LSG_{N_2} , and LSG_{Ar}) in 1,1'-ferrocene dimethanol redox species.

Table 6-4. R^2 values for the manufactured electrodes (LSG_{air}, LSG_{uvc}, LSG_{N2}, and LSG_{Ar}) in 1,1'-ferrocene dimethanol redox species.

Square root of scan rate			
Redox species	Electrode type	R^2_{Ipa}	R^2_{Ipc}
1,1'-ferrocene dimethanol	LSG_{air}	0.997	0.9619
	LSG_{uvc}	0.985	0.9968
	LSG_{N2}	1	0.9995
	LSG_{Ar}	0.999	0.9996
Scan rate			
1,1'-ferrocene dimethanol	LSG_{air}	0.9619	0.9619
	LSG_{uvc}	0.9776	0.9896
	LSG_{N2}	0.9774	0.9761
	LSG_{Ar}	0.9871	0.9803

6.6 Electrochemical Performance

In this section, the findings obtained in the current work are compared with those reported by other researchers in relevant studies. Table 6-5 gives comprehensive details of the comparison of the current study's results and those of previous work using cyclic voltammetry and Raman spectroscopy in addition to XPS and SEM observations. Cyclic voltammetry is used to compare the peak separation potential of the different electrode devices, and the results in the table indicate that the value of ΔE_p for the manufactured graphene electrode for the inner-sphere redox species potassium ferricyanide are generally higher than those of the outer-sphere redox species 1,1'-ferrocene dimethanol in the present study. This indicates that the electrochemical response is faster in the outer-sphere redox than the inner-sphere redox species. Another significant point is that the electrochemical response of the manufactured LSG_{N₂} electrode is faster than those of SLG, EPPG, and BPPG, making it more suitable for electrochemical applications than its single layer graphene (SLG), edge-plane pyrolytic graphite (EPPG), and basal-plane pyrolytic graphite (BPPG) counterparts.

Moreover, the Raman spectroscopy results show that the D and G band wavenumbers of the GO2 sample are extremely close to that of SLG. These data closely match those from the cyclic voltammetry of GO2 for the LSG_{N₂} sample, which proves that the electrochemical behaviour of this electrode is closest to the ideal value of 59 mV. In addition, the XPS data showed that the percentage oxygen content for all electrodes after treatment using the laser scribe technique was reduced to the range between 4.95 under nitrogen gas and 10.04 under vacuum conditions. These observations are also supported by the SEM micrographs which showed more crumpled and wrinkled thin layers indicating higher electrochemical activity in the prepared electrodes which closely matches the CV and Raman results in suggesting that the application of nitrogen gas during the manufacturing process would be the optimal and preferred condition for the production of electrochemically active graphene electrodes.

Eventually, it could be concluded that the characterisation results from the SEM indicates that the LSG_{N₂} and LSG_{Ar} have more crumple than their LSG_{uvc} and LSG_{air} counterparts. This property supported by the Raman spectroscopy of both materials which showed better Id/Ig ratio and means that they possess characteristics that make them more conductive and more reactive. Further proof of this was also found in the XPS characteristics of these material (LSG_{N₂} and LSG_{Ar}), where their oxygen content tends to be the lowest among the other electrodes making them suitable for electrochemical activities. All these data are strongly

matched with the favourable results observed for their cyclic voltammetry analysis, where their ΔE_p measurements make them desired materials for electrochemical applications.

Furthermore, it is important to state that the LightScribe DVD drive used in the manufacture of the LSG_{N_2} electrode in the current work has a laser power of 5mW, while the CO_2 laser power used for the manufacture of the LIG has a laser power of 12W [142]. Hence a comparison of the values of ΔE_p achieved according to the power levels used in manufacturing indicates that the electrode LSG_{N_2} shows a more favourable electrochemical response when compared to the LIG electrode.

Table 6-5. Tested parameters of the optimum electrode devices compared with other published work.

Parameter of GO2	Data analysis					
Cyclic Voltammetry	Redox Species	Electrode type	ΔE_p (mV)	Ref.		
	Potassium Ferricyanide	LSG _{air}	173.6	This work		
		LSG _{uvc}	183.1	This work		
		LSG _{N2}	107.4	This work		
		LSG _{Ar}	114.7	This work		
		SLG	1242.7	[199]		
		LIG	53	[162]		
		BPPG	242	[200]		
		EPPG	97.7	[199]		
	1,1'-ferrocene dimethanol	LSG _{air}	90.3	This work		
		LSG _{uvc}	87.9	This work		
		LSG _{N2}	76.1	This work		
		LSG _{Ar}	88.5	This work		
		SLG	79	[142]		
		LIG	45	[162]		
		BPPG	59	[142, 162]		
EPPG		58	[162]			
Raman Spectroscopy	Electrode	D Band cm ⁻¹	G Band cm ⁻¹	2D Band cm ⁻¹	I _d /I _g	Ref
	SLG	1350	1580	2670	-	[147, 148, 169, 177, 178]
	MLG	1355	1583	2710	0.58824	[183]
	rGO	1339.2	1587.3	2663.3	1.66667	[184]
	LSG _{air}	1343.51	1578.83	2677.2	0.94715	This work
	LSG _{uvc}	1345.92	1575.07	2677.2	0.95235	This work
	LSG _{Ar}	1341.1	1576.95	2680.42	0.99873	This work
	LSG _{N2}	1348.42	1578.83	2690.1	1.02583	This work
SEM	LSG _{air}	crumpled thin sheets				
	LSG _{uvc}	crumpled thin sheets				
	LSG _{Ar}	More crumpled thin sheets				
	LSG _{N2}	More crumpled thin sheets				
XPS	Electrode preparation condition	GO		rGO		
		Carbon%	Oxygen%	Carbon%	Oxygen%	
	Air	69.87	30.13	90.73	9.27	
	Vacuum			89.96	10.04	
	N ₂			95.05	4.95	
	Ar			94.12	5.88	

6.7 Conclusion

An examination of the previously mentioned results shows that, as a general trend, the peak currents in the electrochemistry for both the inner and outer redox species indicate an increase as the manufacturing conditions become more controlled. Similar progressive increases were also observed as the scan rate was increased from 10 to 100 mVs^{-1} . The peak current ratio in the potassium ferricyanide results also increased in value towards unity as the scan rate increased to the maximum value applied. The LSG_{N_2} electrode exhibited the optimal values at all scan rates, which suggests that, as scan rate increases, the electrochemistry of the system tends to behave as a reversible system in this redox species. Likewise, the peak current ratios for the 1,1'-ferrocene dimethanol indicate a fairly stable ratio of approximately one, regardless of the scan rate used. This result suggests that the electrode system with 1,1'-ferrocene dimethanol is a reversible system if only the peak current ratio is considered.

However, the values of ΔE_p for both redox species overall are higher than the ideal Nernstian value of 59 mV for one electron transfer, with those recorded for potassium ferricyanide being significantly higher than those for the 1,1'-ferrocene dimethanol. This implies that the system is not purely reversible for either redox species. Furthermore, it can be suggested that the systems are exhibiting quasi-reversibility since for the potassium ferricyanide the values of the parameter Ψ were found to be between 0.6297 and 0.6323, while they were between 0.6294 to 0.6311 for the 1,1'-ferrocene dimethanol for all scan rates applied. This range falls of Ψ indicates a system which is quasi-reversible. The variable k^0 was also used to confirm the electrochemical response exhibited by these redox species, and for potassium ferricyanide its average value for all of the scan rates ranged from 0.00162 cms^{-1} to 0.00513 cms^{-1} with an increment of about 0.001 for each increase in scan rate. Similarly, for the 1,1'-ferrocene dimethanol the value of k^0 ranged from 0.00187 cms^{-1} to 0.00591 cms^{-1} with the same increment of about 0.001 for each scan rate increase. These results suggest the quasi-reversibility of the systems. The obtained results are highly matched with the favourable values of k^0 for EPPG at 0.002601 cms^{-1} and glassy carbon at 0.0013 cms^{-1} as reported by [142]. The values of M_{trans} for both redox species indicate levels closer to their individual k^0 values, thus confirming that the electrochemical response for both redox species reflects that of a quasi-reversible system.

However, the values of R^2 for the electrodes with respect to the scan rate and square root of scan rate indicate that all of the electrodes exhibit diffusional rather than thin-layer behaviour. From these results it is shown that the LSG_{N2} electrode exhibits the most desirable electrochemical characteristics, making it the preferred choice of electrode to be used with either redox species.

Chapter 7. Conclusion and Future Work

7.1 Conclusion

The present study has involved the manufacture of highly conductive materials such as GO for the development of electrochemical biosensors. These sensors are known to be dependent on transduction, and the use of graphene oxide rather than pristine graphene has been identified as promising in terms of biosensor efficiency. The main reason for an exploration of potential manufacturing methods is to establish a method and technique with improved, more cost effective, and repeatable rGO material. The current study started with an attempt to fabricate and customise LSG electrodes fabricated from two kinds of GO (GO1 and GO2) as sensors for use as superior electrochemical biosensors.

The sensors fabricated have been characterised using various instrumental analyses. The characterisation results in SEM micrographs showed that the GO2 electrode material possesses more folds and wrinkles than GO1. These folds could enhance both the chemical activity and thermal conductivity of the electrode, thus suggesting its greater potential for use as an electrochemical biosensor compared with GO1. Raman spectroscopy of the LSG_{N2} electrodes made from both GO1 and GO2 showed approximately similar values, as reported in table 4-2. In addition, XPS data showed that the oxygen levels in all of the materials prepared was minimised after treatment using the laser scribe technique where the lowest oxygen percentage of 4.95 was recorded under nitrogen gas conditions. Moreover, cyclic voltammograms of the materials showed more distinct oxidation and reduction peaks for GO2 as compared with the GO1 electrode, as represented by increases in the values of E_{pa} and E_{pc} with scan rates from 10 mVs^{-1} to 100 mVs^{-1} . From these results, the further use of GO2 throughout the rest of the study was recommended as it is clearly the most promising material. However, the electrochemical behaviour of one of the four GO1 electrodes (LSG_{uvc}) tested in potassium ferricyanide included a single oxidation/reduction peak, while in the case of 1,1'-ferrocene dimethanol each of LSG_{uvc} and LSG_{Ar} showed one oxidation/reduction peak.

The selected GO2 electrode was manufactured under different conditions of air, vacuum, and argon and nitrogen gases. The values obtained of ΔE_p , k^0 , M_{trans} , and R^2 value reveal that LSG_{N2} was the best electrode tested, and hence it was selected for the further experiments. The cyclic voltammetry results for the use of LSG_{N2} in the potassium ferricyanide solution showed that its peak current ratio (I_{pa} and I_{pc}) increased in value as the scan rate applied increased to its

maximum value, which shows that the electrochemistry of the system behaves like a reversible system. Similarly, the peak current ratio for the results with the 1,1'-ferrocene dimethanol redox species indicate a fairly stable ratio of unity regardless of the scan rate used, which suggest that the electrode material with 1,1'-ferrocene dimethanol yields a reversible system if the peak current ratio only is considered.

The values of ΔE_p for both redox species of potassium ferricyanide and 1,1'-ferrocene dimethanol are all higher than the ideal Nernstian value of 59 mV for one electron transfer. The values of Ψ for potassium ferricyanide were noted to be between 0.6297 and 0.632, while those for the 1,1'-ferrocene dimethanol redox species were between 0.6295 to 0.6299 for all scan rates. These levels all fall well within the range of Ψ associated with quasi-reversible systems.

For confirmation of this conclusion, the values of k^0 were also determined so as to investigate the electrochemical response exhibited by these redox species. Its average values for potassium ferricyanide and 1,1'-ferrocene dimethanol shows increments of about 0.001 with each increase in scan rate, which suggests the quasi-reversibility of the systems. Moreover, values of M_{trans} for both redox species were close to their individual k^0 values, confirming that the electrochemical responses for both redox species are those of a quasi-reversible system.

However, the R^2 values of all of the electrodes with potassium ferricyanide when considering the square root of scan rate were very similar, with a standard deviation of 0.0006, whereas a standard deviation of 0.009 was found when considering scan rate. This indicates that all of the electrodes exhibited diffusional behaviour. Similarly, when considering the square root of scan rate for the 1,1'-ferrocene dimethanol redox species, the R^2 values of all the electrodes are similar with a standard deviation as 0.003 compared to a standard deviation of 0.016 when considering scan rate. These results also show that the electrodes demonstrate diffusional rather than thin-layer behaviour in their electrochemical response.

It could be concluded that the GO2 electrode prepared under nitrogen gas conditions (LSG_{N2}) is the optimal device when used with the 1,1'-ferrocene dimethanol redox species and it is able to yield a quasi-reversible system which exhibits an electrochemistry process characterised by diffusional behaviour.

The cyclic voltammetry analysis of the devices has provided valuable information on their electrochemical performance. The evidence from the results obtained by other characterisations of the manufactured materials provides useful information on the material that exhibits the most suitable electrochemical response for the intended applications. Moreover, the

characterisation results from SEM presented in chapter 4 indicate that the LSG_{uvc} and LSG_{air} materials have crumpled surfaces; however, LSG_{N₂} and LSG_{Ar} were observed to have even more crumpling. This indicates the presence of more defects, which would make them more conductive and electrochemically active. This property can explain why these materials were found in the Raman spectroscopy analysis to have better Id/Ig ratios closer in value to that of SLG, which means that they possess characteristics that make them more conductive and more reactive. Further highlighting their performance, the XPS characterisation of the LSG_{N₂} and LSG_{Ar} materials showed that their percentage oxygen content tended to be the lowest, making them suitable for electrochemical activity. hence the favourable results illustrated by their CV analysis illustrating ΔE_p results that make them desired materials for electrochemical biosensor applications. Overall, the LSG_{N₂} can be highly recommended as an electrode/biosensor for electrochemical applications.

7.2 Recommendations and Future Work

For the purpose of obtaining improved electrode devices, effort must be devoted to using an appropriate concentration of GO when mixed with water in order to ensure the optimal ratio. It is also imperative to fabricate the electrode with a laser system that possesses more power than 5mW, which could result in the formation of more electrically conductive and chemically stable electrodes. Moreover, the vacuum pressure could be maintained at 0.5 mbar for optimum electrode manufacture, but the effect of variation in this parameter might be investigated. One other proposition is to explore the utilisation of higher CV scan rates to determine their efficacy.

The future holds great promise for LSG applications, not only in electrochemical biosensing but also in other areas where the quality of the material used is of immense importance. One factor that may assist in obtaining of higher material quality is the intensity of the power of the laser applied. The use of a CO₂ laser scan offers better controllable conditions of the power intensity of the laser and would be preferred over a DVD laser scribe. In addition, it is more reproducible system that can be used effectively in multiple times rather than DVD laser scribes that became uncommon and are not currently manufactured.

7.3 Contribution to knowledge

- ❖ As graphene compound is the most preferable effective and cheap material for biosensors; our research objective was to prepare another form of carbonaceous materials that has close properties and much cheaper compared with graphene. For this work the contribution to the body of research are:
 - The use of different manufacturing techniques to produce electrodes for graphene oxide-based electrochemical applications.
 - The electrodes performance was compared to determine the optimum electrode for intended applications.
 - The electrodes were prepared with a novel technology that guarantee its repeatability and reproducibility.

References

- [1] B. Jurado-Sánchez, Nanoscale biosensors based on self-propelled objects, *Biosensors*, 8 (2018) 59.
- [2] A. Haleem, M. Javaid, R.P. Singh, R. Suman, S. Rab, Biosensors applications in medical field: A brief review, *Sensors International*, (2021) 100100.
- [3] P. Mehrotra, Biosensors and their applications—A review, *Journal of oral biology and craniofacial research*, 6 (2016) 153-159.
- [4] A. Faqih, J. Hedley, Developing Manufacturing Process for the Graphene Sensors, *International Journal of Industrial and Manufacturing Engineering*, 15 (2021) 171-174.
- [5] Y.C. Reyes R, T.B. Rouf, O.E. Torres, E.E. González, Fluorescent Molecular Sensor for the Detection of Cadmium in Basil Roots, *ACS Agricultural Science & Technology*, (2022).
- [6] R. Tarcan, O. Todor-Boer, I. Petrovai, C. Leordean, S. Astilean, I. Botiz, Reduced graphene oxide today, *Journal of Materials Chemistry C*, 8 (2020) 1198-1224.
- [7] B. Jalali, S. Fathpour, Silicon photonics, *Journal of lightwave technology*, 24 (2006) 4600-4615.
- [8] X. Li, J. Yu, S. Wageh, A.A. Al-Ghamdi, J. Xie, Graphene in photocatalysis: a review, *Small*, 12 (2016) 6640-6696.
- [9] A. St John, C.P. Price, Existing and emerging technologies for point-of-care testing, *The Clinical Biochemist Reviews*, 35 (2014) 155.
- [10] J. Tsao, S. Chowdhury, M. Hollis, D. Jena, N. Johnson, K. Jones, R. Kaplar, S. Rajan, C. Van de Walle, E. Bellotti, Ultrawide-bandgap semiconductors: research opportunities and challenges, *Advanced Electronic Materials*, 4 (2018) 1600501.
- [11] M.J. Allen, V.C. Tung, R.B. Kaner, Honeycomb carbon: a review of graphene, *Chemical reviews*, 110 (2010) 132-145.
- [12] D.R. Cooper, B. D'Anjou, N. Ghattamaneni, B. Harack, M. Hilke, A. Horth, N. Majlis, M. Massicotte, L. Vandsburger, E. Whiteway, Experimental review of graphene, *International Scholarly Research Notices*, 2012 (2012).
- [13] W. Gao, L.B. Alemany, L. Ci, P.M. Ajayan, New insights into the structure and reduction of graphite oxide, *Nature chemistry*, 1 (2009) 403-408.
- [14] S. Pei, H.-M. Cheng, The reduction of graphene oxide, *Carbon*, 50 (2012) 3210-3228.
- [15] F. Iskandar, U. Hikmah, E. Stavila, A.H. Aimon, Microwave-assisted reduction method under nitrogen atmosphere for synthesis and electrical conductivity improvement of reduced graphene oxide (rGO), *RSC advances*, 7 (2017) 52391-52397.
- [16] R. Ma, V.V. Tsukruk, Serigraphy-guided reduction of graphene oxide biopapers for wearable sensory electronics, *Advanced functional materials*, 27 (2017) 1604802.
- [17] M. Mohandoss, S.S. Gupta, A. Nelleri, T. Pradeep, S.M. Maliyekkal, Solar mediated reduction of graphene oxide, *RSC advances*, 7 (2017) 957-963.
- [18] C. Zhu, G. Yang, H. Li, D. Du, Y. Lin, Electrochemical sensors and biosensors based on nanomaterials and nanostructures, *Analytical chemistry*, 87 (2015) 230-249.
- [19] E. Bakker, M. Telting-Diaz, Electrochemical sensors, *Analytical chemistry*, 74 (2002) 2781-2800.
- [20] L. Pujol, D. Evrard, K. Groenen-Serrano, M. Freyssinier, A. Ruffien-Cizsak, P. Gros, Electrochemical sensors and devices for heavy metals assay in water: the French groups' contribution, *Frontiers in chemistry*, 2 (2014) 19.
- [21] A.S. Campbell, J. Kim, J. Wang, Wearable electrochemical alcohol biosensors, *Current opinion in electrochemistry*, 10 (2018) 126-135.
- [22] A.K. Kaushik, J.S. Dhau, H. Gohel, Y.K. Mishra, B. Kateb, N.-Y. Kim, D.Y. Goswami, Electrochemical SARS-CoV-2 sensing at point-of-care and artificial intelligence for intelligent COVID-19 management, *ACS Applied Bio Materials*, 3 (2020) 7306-7325.
- [23] L.C. Lopes, A. Santos, P.R. Bueno, An outlook on electrochemical approaches for molecular diagnostics assays and discussions on the limitations of miniaturized technologies for point-of-care devices, *Sensors and Actuators Reports*, (2022) 100087.

- [24] E.B. Bahadır, M.K. Sezgintürk, Applications of commercial biosensors in clinical, food, environmental, and biothreat/biowarfare analyses, *Analytical biochemistry*, 478 (2015) 107-120.
- [25] H. Huang, S. Su, N. Wu, H. Wan, S. Wan, H. Bi, L. Sun, Graphene-based sensors for human health monitoring, *Frontiers in chemistry*, 7 (2019) 399.
- [26] B. Nikhil, J. Pawan, F. Nello, E. Pedro, Introduction to biosensors, *Essays Biochem*, 60 (2016) 1-8.
- [27] V. Naresh, N. Lee, A Review on Biosensors and Recent Development of Nanostructured Materials-Enabled Biosensors, *Sensors*, 21 (2021) 1109.
- [28] N.J. Ronkainen, H.B. Halsall, W.R. Heineman, Electrochemical biosensors, *Chemical Society Reviews*, 39 (2010) 1747-1763.
- [29] P. Tetyana, P.M. Shumbula, Z. Njengele-Tetyana, *Biosensors: Design, Development and Applications*, (2021).
- [30] N.A. Mohd Said, *Electrochemical biosensor based on microfabricated electrode arrays for life sciences applications*, University College Cork, 2014.
- [31] P. Damborský, J. Švitel, J. Katrlík, Optical biosensors, *Essays in biochemistry*, 60 (2016) 91-100.
- [32] S.M. Borisov, O.S. Wolfbeis, Optical biosensors, *Chemical reviews*, 108 (2008) 423-461.
- [33] D. Dey, T. Goswami, Optical biosensors: a revolution towards quantum nanoscale electronics device fabrication, *Journal of Biomedicine and Biotechnology*, 2011 (2011).
- [34] V. Garzón, D.G. Pinacho, R.-H. Bustos, G. Garzón, S. Bustamante, Optical biosensors for therapeutic drug monitoring, *Biosensors*, 9 (2019) 132.
- [35] Y. Yanase, T. Hiragun, K. Ishii, T. Kawaguchi, T. Yanase, M. Kawai, K. Sakamoto, M. Hide, Surface plasmon resonance for cell-based clinical diagnosis, *Sensors*, 14 (2014) 4948-4959.
- [36] B. Špačková, P. Wrobel, M. Bocková, J. Homola, Optical biosensors based on plasmonic nanostructures: a review, *Proceedings of the IEEE*, 104 (2016) 2380-2408.
- [37] S.J. Hendel, E.R. Young, Introduction to electrochemistry and the use of electrochemistry to synthesize and evaluate catalysts for water oxidation and reduction, *Journal of Chemical Education*, 93 (2016) 1951-1956.
- [38] C. Zhang, X. Du, Electrochemical sensors based on carbon nanomaterial used in diagnosing metabolic disease, *Frontiers in Chemistry*, 8 (2020) 651.
- [39] K. Chen, W. Gao, S. Emaminejad, D. Kiriya, H. Ota, H.Y.Y. Nyein, K. Takei, A. Javey, Carbon Nanotubes: Printed Carbon Nanotube Electronics and Sensor Systems (*Adv. Mater.* 22/2016), *Advanced materials (Deerfield Beach, Fla.)*, 28 (2016) 4396.
- [40] Q. Ren, A new species and new records of the lichen genus *Pertusaria* from China, *Mycotaxon*, 130 (2015) 689-693.
- [41] X. Ding, Y. Niu, G. Zhang, Y. Xu, J. Li, Electrochemistry in carbon-based quantum dots, *Chemistry—An Asian Journal*, 15 (2020) 1214-1224.
- [42] S. Zhang, F. Xu, Z.-Q. Liu, Y.-S. Chen, Y.-L. Luo, Novel electrochemical sensors from poly [N-(ferrocenyl formacyl) pyrrole]@ multi-walled carbon nanotubes nanocomposites for simultaneous determination of ascorbic acid, dopamine and uric acid, *Nanotechnology*, 31 (2019) 085503.
- [43] J.H. Rombout, G. Yang, V. Kiron, Adaptive immune responses at mucosal surfaces of teleost fish, *Fish & Shellfish Immunology*, 40 (2014) 634-643.
- [44] M. Thangamuthu, K.Y. Hsieh, P.V. Kumar, G.-Y. Chen, Graphene-and graphene oxide-based nanocomposite platforms for electrochemical biosensing applications, *International journal of molecular sciences*, 20 (2019) 2975.
- [45] D.W. Kimmel, G. LeBlanc, M.E. Meschievitz, D.E. Cliffel, Electrochemical sensors and biosensors, *Analytical chemistry*, 84 (2012) 685-707.
- [46] C.-M. Tîlmaciu, M.C. Morris, Carbon nanotube biosensors, *Frontiers in chemistry*, 3 (2015) 59.
- [47] N. Aristov, A. Habekost, Cyclic voltammetry-A versatile electrochemical method investigating electron transfer processes, *World J. Chem. Educ*, 3 (2015) 115-119.
- [48] N. Elgrishi, K.J. Rountree, B.D. McCarthy, E.S. Rountree, T.T. Eisenhart, J.L. Dempsey, A practical beginner's guide to cyclic voltammetry, *Journal of chemical education*, 95 (2018) 197-206.

- [49] P. Joshi, D. Sutrave, A brief study of cyclic voltammetry and electrochemical analysis, *International Journal of ChemTech Research*, 11 (2018) 77.
- [50] L. Khalafi, M. Rafiee, *Cyclic Voltammetry*, Wiley: Hoboken, NJ, 2017, pp. 3437-3478.
- [51] M. de Rooij, *Electrochemical methods: fundamentals and applications*, *Anti-Corrosion Methods and Materials*, (2003).
- [52] I. Lavagnini, R. Antiochia, F. Magno, An extended method for the practical evaluation of the standard rate constant from cyclic voltammetric data, *Electroanalysis: An International Journal Devoted to Fundamental and Practical Aspects of Electroanalysis*, 16 (2004) 505-506.
- [53] E.P. Randviir, A cross examination of electron transfer rate constants for carbon screen-printed electrodes using Electrochemical Impedance Spectroscopy and cyclic voltammetry, *Electrochimica Acta*, 286 (2018) 179-186.
- [54] R.S. Nicholson, Theory and application of cyclic voltammetry for measurement of electrode reaction kinetics, *Analytical chemistry*, 37 (1965) 1351-1355.
- [55] D.A. Brownson, D.K. Kampouris, C.E. Banks, Graphene electrochemistry: fundamental concepts through to prominent applications, *Chemical Society Reviews*, 41 (2012) 6944-6976.
- [56] A.T. Valota, I.A. Kinloch, K.S. Novoselov, C. Casiraghi, A. Eckmann, E.W. Hill, R.A. Dryfe, Electrochemical behavior of monolayer and bilayer graphene, *ACS nano*, 5 (2011) 8809-8815.
- [57] D. Plana, F.G. Jones, R.A. Dryfe, The voltammetric response of bipolar cells: Reversible electron transfer, *Journal of Electroanalytical Chemistry*, 646 (2010) 107-113.
- [58] R.H. Sato, P.M. Kosaka, Á.T. Otori, E.A. Ferreira, D.F. Petri, Ó. Malvar, C.M. Domínguez, V. Pini, Ó. Ahumada, J. Tamayo, Development of a methodology for reversible chemical modification of silicon surfaces with application in nanomechanical biosensors, *Biosensors and Bioelectronics*, 137 (2019) 287-293.
- [59] L. Cui, J. Hu, C.-c. Li, C.-m. Wang, C.-y. Zhang, An electrochemical biosensor based on the enhanced quasi-reversible redox signal of prussian blue generated by self-sacrificial label of iron metal-organic framework, *Biosensors and Bioelectronics*, 122 (2018) 168-174.
- [60] Q. Hu, J. Kong, D. Han, L. Niu, X. Zhang, Electrochemical DNA biosensing via electrochemically controlled reversible addition–fragmentation chain transfer polymerization, *ACS sensors*, 4 (2019) 235-241.
- [61] V. Evtugyn, A. Ivanov, R. Davletshina, G. Evtugyn, R. Shamagsumova, Electrochemical Biosensor Based on Polyelectrolyte Complexes with Dendrimer for the Determination of Reversible Inhibitors of Acetylcholinesterase.
- [62] T. Chalklen, Q. Jing, S. Kar-Narayan, Biosensors Based on Mechanical and electrical detection techniques, *Sensors*, 20 (2020) 5605.
- [63] J. Arlett, E. Myers, M. Roukes, Comparative advantages of mechanical biosensors, *Nature nanotechnology*, 6 (2011) 203-215.
- [64] H.C. Lee, W.-W. Liu, S.-P. Chai, A.R. Mohamed, A. Aziz, C.-S. Khe, N.M. Hidayah, U. Hashim, Review of the synthesis, transfer, characterization and growth mechanisms of single and multilayer graphene, *RSC advances*, 7 (2017) 15644-15693.
- [65] P.T. Yin, S. Shah, M. Chhowalla, K.-B. Lee, Design, synthesis, and characterization of graphene–nanoparticle hybrid materials for bioapplications, *Chemical reviews*, 115 (2015) 2483-2531.
- [66] T.M. Radadiya, A properties of graphene, *European Journal of Material Sciences*, 2 (2015) 6-18.
- [67] Y. Zhu, H. Ji, H.-M. Cheng, R.S. Ruoff, Mass production and industrial applications of graphene materials, *National Science Review*, 5 (2018) 90-101.
- [68] M. Roberts, C. Clemons, J. Wilber, G. Young, A. Buldum, D. Quinn, Continuum plate theory and atomistic modeling to find the flexural rigidity of a graphene sheet interacting with a substrate, *Journal of Nanotechnology*, 2010 (2010).
- [69] S. Ranjan, N. Dasgupta, E. Lichtfouse, *Nanoscience in food and agriculture*, Springer, 2016.
- [70] M. Sang, J. Shin, K. Kim, K.J. Yu, Electronic and thermal properties of graphene and recent advances in graphene based electronics applications, *Nanomaterials*, 9 (2019) 374.

- [71] K.Y. Rhee, Electronic and thermal properties of graphene, Multidisciplinary Digital Publishing Institute, 2020, pp. 926.
- [72] W.-K. Tse, E. Hwang, S. Das Sarma, Ballistic hot electron transport in graphene, *Applied Physics Letters*, 93 (2008) 023128.
- [73] K.Y. Rhee, Electronic and thermal properties of graphene, Multidisciplinary Digital Publishing Institute, 2020.
- [74] E. Pop, V. Varshney, A.K. Roy, Thermal properties of graphene: Fundamentals and applications, *MRS bulletin*, 37 (2012) 1273-1281.
- [75] X. Wang, Graphene Characterization and Device Fabrication: Doping Analysis, Strain Engineering towards Terahertz Radiation, Boston University, 2017.
- [76] D.G. Papageorgiou, I.A. Kinloch, R.J. Young, Mechanical properties of graphene and graphene-based nanocomposites, *Progress in Materials Science*, 90 (2017) 75-127.
- [77] K.S. Novoselov, V. Fal, L. Colombo, P. Gellert, M. Schwab, K. Kim, A roadmap for graphene, *nature*, 490 (2012) 192-200.
- [78] A.T. Smith, A.M. LaChance, S. Zeng, B. Liu, L. Sun, Synthesis, properties, and applications of graphene oxide/reduced graphene oxide and their nanocomposites, *Nano Materials Science*, 1 (2019) 31-47.
- [79] V. Skrypnichuk, N. Boulanger, A. Nordenström, A. Talyzin, Aqueous activated graphene dispersions for deposition of high-surface area supercapacitor electrodes, *The journal of physical chemistry letters*, 11 (2020) 3032-3038.
- [80] T. Mahmoudi, Y. Wang, Y.-B. Hahn, Graphene and its derivatives for solar cells application, *Nano Energy*, 47 (2018) 51-65.
- [81] M. Yi, Z. Shen, A review on mechanical exfoliation for the scalable production of graphene, *Journal of Materials Chemistry A*, 3 (2015) 11700-11715.
- [82] V. Kurt, Optimization of graphene synthesis by electrochemical exfoliation of graphite, 2019.
- [83] A. O'Neill, U. Khan, P.N. Nirmalraj, J. Boland, J.N. Coleman, Graphene dispersion and exfoliation in low boiling point solvents, *The Journal of Physical Chemistry C*, 115 (2011) 5422-5428.
- [84] Y. Hernandez, V. Nicolosi, M. Lotya, F.M. Blighe, Z. Sun, S. De, I. McGovern, B. Holland, M. Byrne, Y.K. Gun'Ko, High-yield production of graphene by liquid-phase exfoliation of graphite, *Nature nanotechnology*, 3 (2008) 563-568.
- [85] K. Parvez, S. Yang, X. Feng, K. Müllen, Exfoliation of graphene via wet chemical routes, *Synthetic Metals*, 210 (2015) 123-132.
- [86] S.S. Shams, R. Zhang, J. Zhu, Graphene synthesis: a Review, *Mater. Sci. Pol.*, 33 (2015) 566-578.
- [87] J. Jobst, D. Waldmann, F. Speck, R. Hirner, D.K. Maude, T. Seyller, H.B. Weber, How graphene-like is epitaxial graphene? \quantum oscillations and quantum hall effect, *arXiv preprint arXiv:0908.1900*, (2009).
- [88] L. Sun, G. Yuan, L. Gao, J. Yang, M. Chhowalla, M.H. Gharahcheshmeh, K.K. Gleason, Y.S. Choi, B.H. Hong, Z. Liu, Chemical vapour deposition, *Nature Reviews Methods Primers*, 1 (2021) 5.
- [89] L. Lin, B. Deng, J. Sun, H. Peng, Z. Liu, Bridging the Gap between Reality and Ideal in Chemical Vapor Deposition Growth of Graphene, *Chemical Reviews*, 118 (2018) 9281-9343.
- [90] Z. Cai, B. Liu, X. Zou, H.-M. Cheng, Chemical Vapor Deposition Growth and Applications of Two-Dimensional Materials and Their Heterostructures, *Chemical Reviews*, 118 (2018) 6091-6133.
- [91] D.E. Carlson, C.R. Wronski, Amorphous silicon solar cell, *Applied Physics Letters*, 28 (1976) 671-673.
- [92] H. Sun, L. Wu, W. Wei, X. Qu, Recent advances in graphene quantum dots for sensing, *Materials today*, 16 (2013) 433-442.
- [93] M. Zhang, A. Halder, X. Cao, C. Hou, Q. Chi, Graphene-paper based electrochemical sensors, *Electrochemical Sensors Technologies*, (2017) 33-62.
- [94] X. Jin, C. Feng, D. Ponnamma, Z. Yi, J. Parameswaranpillai, S. Thomas, N.V. Salim, Review on exploration of graphene in the design and engineering of smart sensors, actuators and soft robotics, *Chemical Engineering Journal Advances*, 4 (2020) 100034.

- [95] F. Perreault, A.F. De Faria, M. Elimelech, Environmental applications of graphene-based nanomaterials, *Chemical Society Reviews*, 44 (2015) 5861-5896.
- [96] K.A. Madurani, S. Suprpto, N.I. Machrita, S.L. Bahar, W. Illiya, F. Kurniawan, Progress in graphene synthesis and its application: history, challenge and the future outlook for research and industry, *ECS Journal of Solid State Science and Technology*, 9 (2020) 093013.
- [97] M. Sakar, H. Chandan, R. Shwetharani, Graphene Paper-Based Electrochemical Sensors for Biomolecules, *Graphene-Based Electrochemical Sensors for Biomolecules*, Elsevier, 2019, pp. 297-320.
- [98] J. Liu, M. Liu, Y. Bai, J. Zhang, H. Liu, W. Zhu, Recent progress in flexible wearable sensors for vital sign monitoring, *Sensors*, 20 (2020) 4009.
- [99] M. Xu, D. Obodo, V.K. Yadavalli, The design, fabrication, and applications of flexible biosensing devices, *Biosensors and Bioelectronics*, 124 (2019) 96-114.
- [100] I. Jeerapan, S. Poorahong, flexible and stretchable electrochemical sensing systems: materials, energy sources, and integrations, *Journal of The Electrochemical Society*, 167 (2020) 037573.
- [101] L. Dong, C. Xu, Y. Li, Z.-H. Huang, F. Kang, Q.-H. Yang, X. Zhao, Flexible electrodes and supercapacitors for wearable energy storage: a review by category, *Journal of Materials Chemistry A*, 4 (2016) 4659-4685.
- [102] A. Aqel, K.M. Abou El-Nour, R.A. Ammar, A. Al-Warthan, Carbon nanotubes, science and technology part (I) structure, synthesis and characterisation, *Arabian Journal of Chemistry*, 5 (2012) 1-23.
- [103] A. Ahammad, J.-J. Lee, M. Rahman, Electrochemical sensors based on carbon nanotubes, *sensors*, 9 (2009) 2289-2319.
- [104] T. Kim, M. Cho, K.J. Yu, Flexible and stretchable bio-integrated electronics based on carbon nanotube and graphene, *Materials*, 11 (2018) 1163.
- [105] A.N. Banerjee, Graphene and its derivatives as biomedical materials: future prospects and challenges, *Interface Focus*, 8 (2018) 20170056.
- [106] B.L. Dasari, J.M. Nouri, D. Brabazon, S. Naher, Graphene and derivatives—Synthesis techniques, properties and their energy applications, *Energy*, 140 (2017) 766-778.
- [107] Q. Ke, J. Wang, Graphene-based materials for supercapacitor electrodes—A review, *Journal of Materiomics*, 2 (2016) 37-54.
- [108] A.M. Al-Dhahebi, S.C.B. Gopinath, M.S.M. Saheed, Graphene impregnated electrospun nanofiber sensing materials: A comprehensive overview on bridging laboratory set-up to industry, *Nano convergence*, 7 (2020) 1-23.
- [109] K. Chen, W. Chou, L. Liu, Y. Cui, P. Xue, M. Jia, Electrochemical Sensors Fabricated by Electrospinning Technology: An Overview, *Sensors*, 19 (2019) 3676.
- [110] A.F. Carvalho, B. Kulyk, A.J. Fernandes, E. Fortunato, F.M. Costa, A Review on the Applications of Graphene in Mechanical Transduction, *Advanced Materials*, (2021) 2101326.
- [111] O. Moldovan, B. Iñiguez, M.J. Deen, L.F. Marsal, Graphene electronic sensors—review of recent developments and future challenges, *IET Circuits, Devices & Systems*, 9 (2015) 446-453.
- [112] H. Tian, Y. Shu, X.-F. Wang, M.A. Mohammad, Z. Bie, Q.-Y. Xie, C. Li, W.-T. Mi, Y. Yang, T.-L. Ren, A graphene-based resistive pressure sensor with record-high sensitivity in a wide pressure range, *Scientific reports*, 5 (2015) 1-6.
- [113] J.J. Park, W.J. Hyun, S.C. Mun, Y.T. Park, O.O. Park, Highly stretchable and wearable graphene strain sensors with controllable sensitivity for human motion monitoring, *ACS applied materials & interfaces*, 7 (2015) 6317-6324.
- [114] B. Cheng, S. Chang, H. Li, Y. Li, W. Shen, Y. Shang, A. Cao, Highly Stretchable and Compressible Carbon Nanofiber–Polymer Hydrogel Strain Sensor for Human Motion Detection, *Macromolecular Materials and Engineering*, 305 (2020) 1900813.
- [115] T. Yang, X. Jiang, Y. Zhong, X. Zhao, S. Lin, J. Li, X. Li, J. Xu, Z. Li, H. Zhu, A Wearable and Highly Sensitive Graphene Strain Sensor for Precise Home-Based Pulse Wave Monitoring, *ACS Sensors*, 2 (2017) 967-974.

- [116] T. Wang, Z. Ouyang, F. Wang, Y. Liu, A review on graphene strain sensors based on fiber assemblies, *SN Applied Sciences*, 2 (2020) 1-22.
- [117] E. Chehura, S.W. James, R.P. Tatam, Temperature and strain discrimination using a single tilted fibre Bragg grating, *Optics communications*, 275 (2007) 344-347.
- [118] A.D. Smith, K. Elgammal, F. Niklaus, A. Delin, A.C. Fischer, S. Vaziri, F. Forsberg, M. Rålander, H. Hugosson, L. Bergqvist, Resistive graphene humidity sensors with rapid and direct electrical readout, *Nanoscale*, 7 (2015) 19099-19109.
- [119] K. Shehzad, T. Shi, A. Qadir, X. Wan, H. Guo, A. Ali, W. Xuan, H. Xu, Z. Gu, X. Peng, Designing an efficient multimode environmental sensor based on graphene–silicon heterojunction, *Advanced Materials Technologies*, 2 (2017) 1600262.
- [120] Z. Zhen, Z. Li, X. Zhao, Y. Zhong, L. Zhang, Q. Chen, T. Yang, H. Zhu, Formation of Uniform Water Microdroplets on Wrinkled Graphene for Ultrafast Humidity Sensing, *Small*, 14 (2018) 1703848.
- [121] H. Bi, K. Yin, X. Xie, J. Ji, S. Wan, L. Sun, M. Terrones, M.S. Dresselhaus, Ultrahigh humidity sensitivity of graphene oxide, *Scientific reports*, 3 (2013) 1-7.
- [122] S. Borini, R. White, D. Wei, M. Astley, S. Haque, E. Spigone, N. Harris, J. Kivioja, T. Ryhänen, Ultrafast Graphene Oxide Humidity Sensors, *ACS Nano*, 7 (2013) 11166-11173.
- [123] L. Guo, H.-B. Jiang, R.-Q. Shao, Y.-L. Zhang, S.-Y. Xie, J.-N. Wang, X.-B. Li, F. Jiang, Q.-D. Chen, T. Zhang, Two-beam-laser interference mediated reduction, patterning and nanostructuring of graphene oxide for the production of a flexible humidity sensing device, *Carbon*, 50 (2012) 1667-1673.
- [124] D.-T. Phan, G.-S. Chung, Effects of rapid thermal annealing on humidity sensor based on graphene oxide thin films, *Sensors and Actuators B: Chemical*, 220 (2015) 1050-1055.
- [125] V. Ruiz, I. Fernández, P. Carrasco, G. Cabañero, H.J. Grande, J. Herrán, Graphene quantum dots as a novel sensing material for low-cost resistive and fast-response humidity sensors, *Sensors and Actuators B: Chemical*, 218 (2015) 73-77.
- [126] T. Purkait, G. Singh, D. Kumar, M. Singh, R.S. Dey, High-performance flexible supercapacitors based on electrochemically tailored three-dimensional reduced graphene oxide networks, *Scientific reports*, 8 (2018) 1-13.
- [127] P. Sehwat, A. Abid, S.S. Islam, A. Mauger, C.M. Julien, Nanostructured Graphene Oxide-Based Hybrids as Anodes for Lithium-Ion Batteries, *C*, 6 (2020) 81.
- [128] M. Tokur, M.Y. Jin, B.W. Sheldon, H. Akbulut, Stress bearing mechanism of reduced graphene oxide in silicon-based composite anodes for lithium ion batteries, *ACS Applied Materials & Interfaces*, 12 (2020) 33855-33869.
- [129] S.H. Huh, Thermal reduction of graphene oxide, *Physics and Applications of Graphene-Experiments*, 19 (2011) 73-90.
- [130] M. Skoda, I. Dudek, A. Jarosz, D. Szukiewicz, Graphene: one material, many possibilities—application difficulties in biological systems, *Journal of Nanomaterials*, 2014 (2014).
- [131] A. Kathalingam, H.M.S. Ajmal, S. Ramesh, H.S. Kim, S.-D. Kim, S.H. Choi, W. Yang, K.K. Kim, H.-S. Kim, Poly (methyl methacrylate)-derived graphene films on different substrates using rapid thermal process: A way to control the film properties through the substrate and polymer layer thickness, *Journal of Materials Research and Technology*, 8 (2019) 3752-3763.
- [132] X. Wang, L. Zhi, K. Müllen, Transparent, conductive graphene electrodes for dye-sensitized solar cells, *Nano letters*, 8 (2008) 323-327.
- [133] L. Huang, Y. Liu, L.-C. Ji, Y.-Q. Xie, T. Wang, W.-Z. Shi, Pulsed laser assisted reduction of graphene oxide, *Carbon*, 49 (2011) 2431-2436.
- [134] R. Rodriguez, G. Murastov, A. Lipovka, M. Fatkullin, O. Nozdrina, S. Pavlov, P. Postnikov, M. Chehimi, J.-J. Chen, E. Sheremet, High-power laser-patterning graphene oxide: A new approach to making arbitrarily-shaped self-aligned electrodes, *Carbon*, 151 (2019) 148-155.
- [135] A.T. Dideikin, A.Y. Vul, Graphene oxide and derivatives: the place in graphene family, *Frontiers in Physics*, 6 (2019) 149.

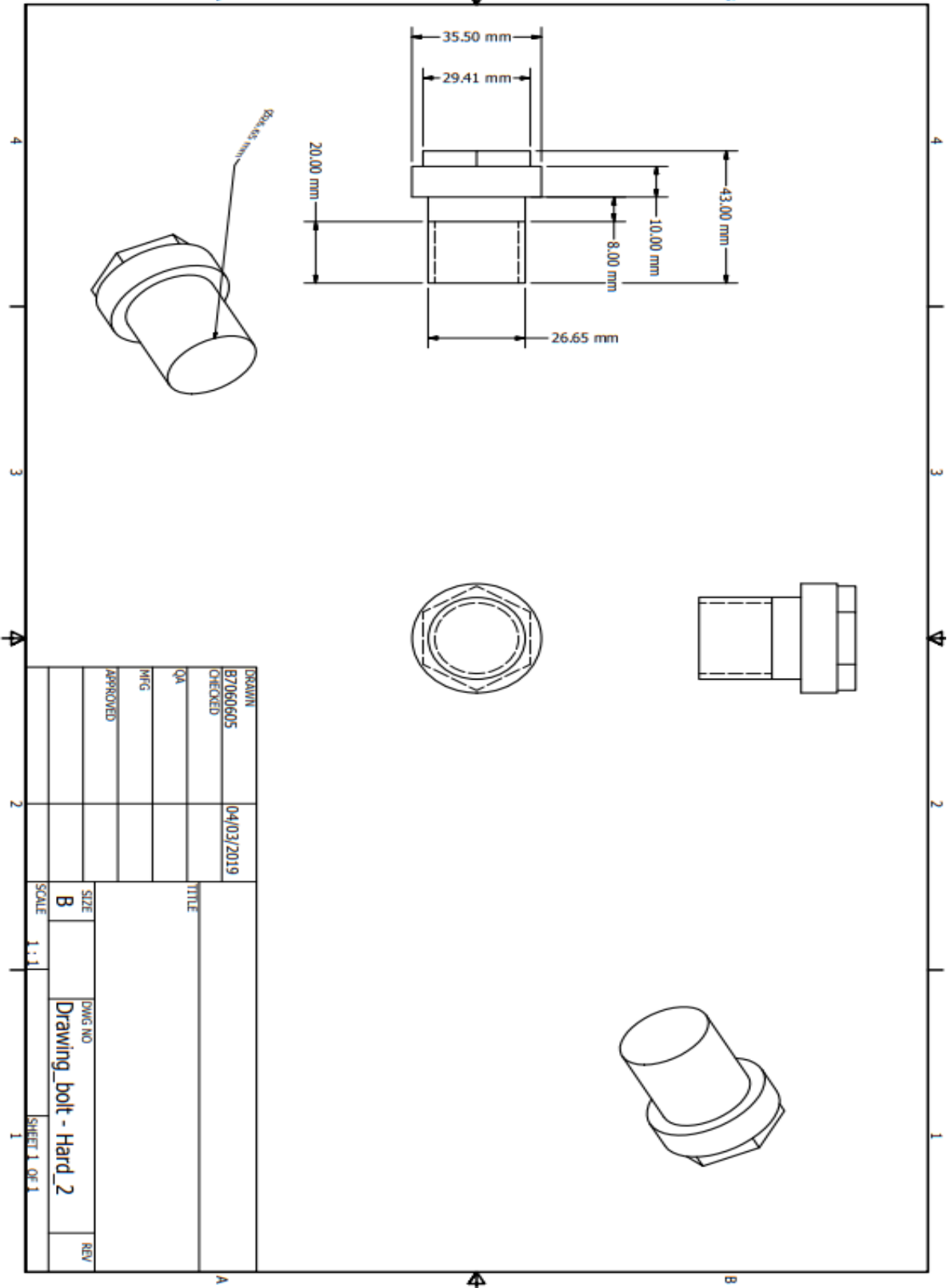
- [136] H. Wang, J.T. Robinson, X. Li, H. Dai, Solvothermal reduction of chemically exfoliated graphene sheets, *Journal of the American Chemical Society*, 131 (2009) 9910-9911.
- [137] M. Mathew, S. Radhakrishnan, A. Vaidyanathan, B. Chakraborty, C.S. Rout, Flexible and wearable electrochemical biosensors based on two-dimensional materials: Recent developments, *Analytical and Bioanalytical Chemistry*, 413 (2021) 727-762.
- [138] P. Puetz, A. Behrent, A.J. Baeumner, J. Wegener, Laser-scribed graphene (LSG) as new electrode material for impedance-based cellular assays, *Sensors and Actuators B: Chemical*, 321 (2020) 128443.
- [139] A. Ghanam, A.A. Lahcen, T. Beduk, H.N. Alshareef, A. Amine, K.N. Salama, Laser scribed graphene: A novel platform for highly sensitive detection of electroactive biomolecules, *Biosensors and Bioelectronics*, 168 (2020) 112509.
- [140] H. Tian, M.A. Mohammad, W.-T. Mi, Y. Yang, T.-L. Ren, Laser-scribing technology for wafer-scale graphene devices, *Advances in Carbon Nanostructures*, (2016) 63.
- [141] F. Perrozzi, S. Prezioso, L. Ottaviano, Graphene oxide: from fundamentals to applications, *Journal of Physics: Condensed Matter*, 27 (2014) 013002.
- [142] K. Griffiths, Characterisation of laser fabricated graphene materials and their application in electrochemical sensing, Newcastle University, 2017.
- [143] R. Panowicz, M. Konarzewski, T. Durejko, M. Szala, M. Łazińska, M. Czerwińska, P. Prasufa, Properties of polyethylene terephthalate (PET) after thermo-oxidative aging, *Materials*, 14 (2021) 3833.
- [144] K. Hon, L. Li, I. Hutchings, Direct writing technology—Advances and developments, *CIRP annals*, 57 (2008) 601-620.
- [145] A. Watanabe, G. Qin, J. Cai, Laser Direct Writing on Copper Nanoparticle Film by LightScribe Technique, *Journal of Photopolymer Science and Technology*, 28 (2015) 99-102.
- [146] A.C. Ferrari, D.M. Basko, Raman spectroscopy as a versatile tool for studying the properties of graphene, *Nature nanotechnology*, 8 (2013) 235-246.
- [147] N. Hidayah, W.-W. Liu, C.-W. Lai, N. Noriman, C.-S. Khe, U. Hashim, H.C. Lee, Comparison on graphite, graphene oxide and reduced graphene oxide: Synthesis and characterization, *AIP Conference Proceedings*, AIP Publishing LLC, 2017, pp. 150002.
- [148] M. Wall, The Raman spectroscopy of graphene and the determination of layer thickness, *Thermo Sci*, 5 (2011) 1-5.
- [149] C.N.R. Rao, A.K. Sood, *Graphene: synthesis, properties, and phenomena*, John Wiley & Sons, 2013.
- [150] A.C. Ferrari, Raman spectroscopy of graphene and graphite: Disorder, electron–phonon coupling, doping and nonadiabatic effects, *Solid state communications*, 143 (2007) 47-57.
- [151] D. Konios, M.M. Stylianakis, E. Stratakis, E. Kymakis, Dispersion behaviour of graphene oxide and reduced graphene oxide, *Journal of colloid and interface science*, 430 (2014) 108-112.
- [152] S. Aharinejad, A. Lametschwandtner, *Fundamentals of scanning electron microscopy, Microvascular corrosion casting in scanning electron microscopy*, Springer, 1992, pp. 44-51.
- [153] S. Swapp, S.E. Microscopy, University of Wyoming, *Scanning Electron Microscopy (SEM)*, [online]. [cit. 2019-04-29] Dostupné z: https://serc.carleton.edu/research_education/geochemsheets/techniques/SEM.html.
- [154] A. Ambrosi, C.K. Chua, A. Bonanni, M. Pumera, Electrochemistry of graphene and related materials, *Chemical reviews*, 114 (2014) 7150-7188.
- [155] H.-H. Huang, K.K.H. De Silva, G. Kumara, M. Yoshimura, Structural evolution of hydrothermally derived reduced graphene oxide, *Scientific reports*, 8 (2018) 1-9.
- [156] D.Q. McNerny, B. Viswanath, D. Copic, F.R. Laye, C. Prohoda, A.C. Brieland-Shoultz, E.S. Polsen, N.T. Dee, V.S. Veerasamy, A.J. Hart, Direct fabrication of graphene on SiO₂ enabled by thin film stress engineering, *Scientific reports*, 4 (2014) 1-9.
- [157] F.T. Johra, J.-W. Lee, W.-G. Jung, Facile and safe graphene preparation on solution based platform, *Journal of Industrial and Engineering Chemistry*, 20 (2014) 2883-2887.

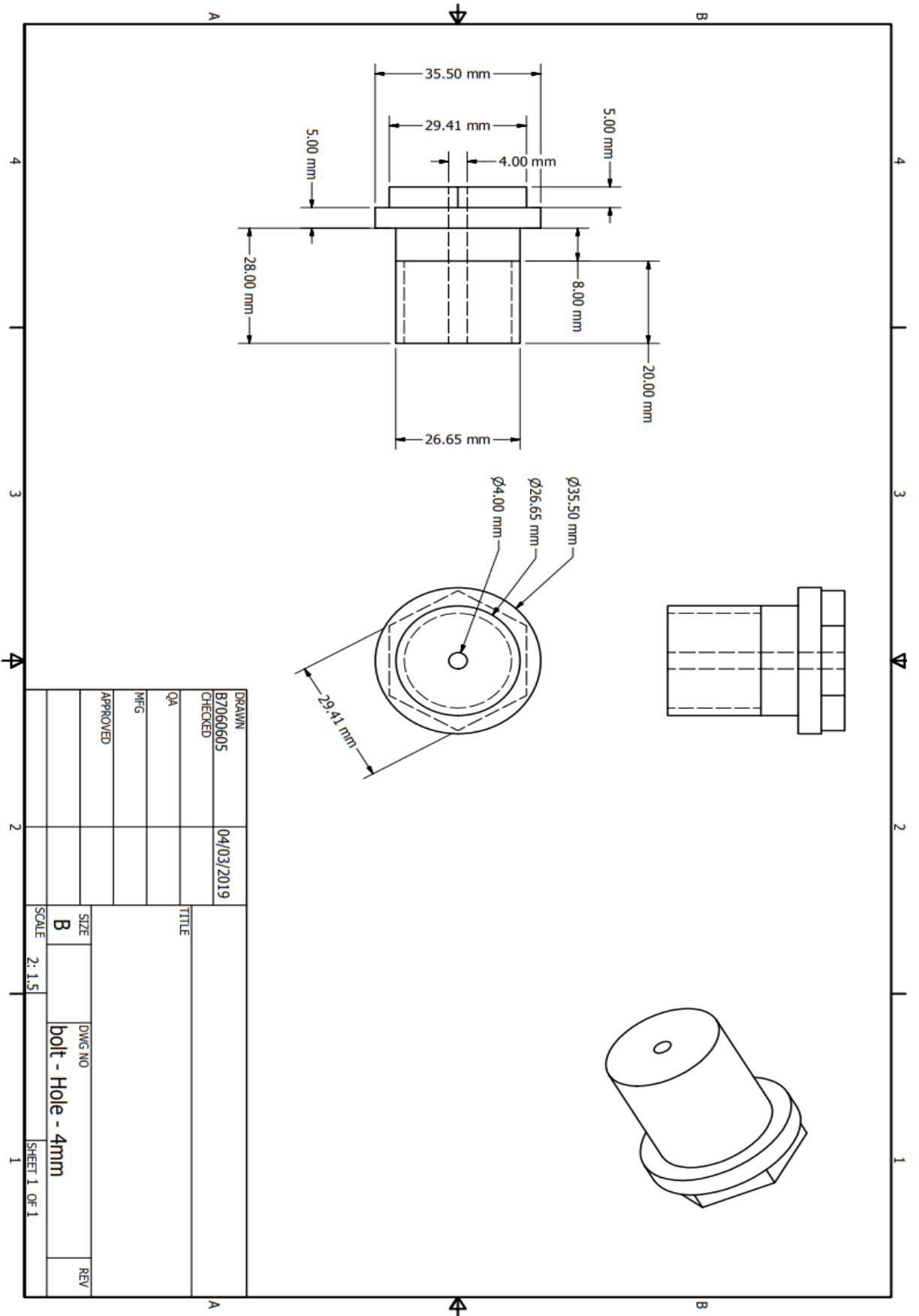
- [158] F. Priante, M. Salim, L. Ottaviano, F. Perrozzi, XPS study of graphene oxide reduction induced by (100) and (111)-oriented Si substrates, *Nanotechnology*, 29 (2018) 075704.
- [159] M.K. Rabchinskii, S.A. Ryzhkov, D.A. Kirilenko, N.V. Ulin, M.V. Baidakova, V.V. Shnitov, S.I. Pavlov, R.G. Chumakov, D.Y. Stolyarova, N.A. Besedina, From graphene oxide towards aminated graphene: Facile synthesis, its structure and electronic properties, *Scientific reports*, 10 (2020) 1-12.
- [160] W. Pang, J. Xue, H. Pang, A high energy density azobenzene/graphene oxide hybrid with weak nonbonding interactions for solar thermal storage, *Scientific reports*, 9 (2019) 1-12.
- [161] D.G. Stinson, M. Maguire, LightScribe direct disc labeling, *International Symposium on Optical Memory and Optical Data Storage*, Optica Publishing Group, 2005, pp. MA4.
- [162] K. Griffiths, C. Dale, J. Hedley, M.D. Kowal, R.B. Kaner, N. Keegan, Laser-scribed graphene presents an opportunity to print a new generation of disposable electrochemical sensors, *Nanoscale*, 6 (2014) 13613-13622.
- [163] M.F. El-Kady, V. Strong, S. Dubin, R.B. Kaner, Laser scribing of high-performance and flexible graphene-based electrochemical capacitors, *Science*, 335 (2012) 1326-1330.
- [164] D. Grieshaber, R. MacKenzie, J. Vörös, E. Reimhult, Electrochemical biosensors-sensor principles and architectures, *Sensors*, 8 (2008) 1400-1458.
- [165] O.e.m. science, Cyclic Voltammetry Basic Principles, Theory and Setup, <https://www.ossila.com/pages/cyclic-voltammetry>.
- [166] F. Liu, S. Song, D. Xue, H. Zhang, Folded structured graphene paper for high performance electrode materials, *Advanced Materials*, 24 (2012) 1089-1094.
- [167] S. Deng, V. Berry, Wrinkled, rippled and crumpled graphene: an overview of formation mechanism, electronic properties, and applications, *Materials Today*, 19 (2016) 197-212.
- [168] L. Cui, X. Du, G. Wei, Y. Feng, Thermal conductivity of graphene wrinkles: a molecular dynamics simulation, *The Journal of Physical Chemistry C*, 120 (2016) 23807-23812.
- [169] S. Thakur, N. Karak, Green reduction of graphene oxide by aqueous phytoextracts, *Carbon*, 50 (2012) 5331-5339.
- [170] E.F. Sheka, Y.A. Golubev, N.A. Popova, Graphene domain signature of Raman spectra of sp² amorphous carbons, *Nanomaterials*, 10 (2020) 2021.
- [171] M. Ali, Raman Characterization of Structural Properties of Thermally Modified Nanographite, 2015.
- [172] W. Lu, J.-B. Baek, L. Dai, Carbon nanomaterials for advanced energy systems: advances in materials synthesis and device applications, John Wiley & Sons, 2015.
- [173] A.A. Balandin, S. Ghosh, W. Bao, I. Calizo, D. Teweldebrhan, F. Miao, C.N. Lau, Superior thermal conductivity of single-layer graphene, *Nano letters*, 8 (2008) 902-907.
- [174] W. Wang, C. Shen, S. Li, J. Min, C. Yi, Mechanical properties of single layer graphene nanoribbons through bending experimental simulations, *AIP Advances*, 4 (2014) 031333.
- [175] X.-H. Lin, J.-G. Gai, Synthesis and applications of large-area single-layer graphene, *RSC advances*, 6 (2016) 17818-17844.
- [176] V. Kumar, A. Kumar, D.-J. Lee, S.-S. Park, Estimation of number of graphene layers using different methods: a focused review, *Materials*, 14 (2021) 4590.
- [177] D. Casimir, H. Alghamdi, I.Y. Ahmed, R. Garcia-Sanchez, P. Misra, Raman spectroscopy of graphene, graphite and graphene nanoplatelets, *IntechOpen London, UK*, 2019.
- [178] I. Childres, L.A. Jauregui, W. Park, H. Cao, Y.P. Chen, Raman spectroscopy of graphene and related materials, *New developments in photon and materials research*, 1 (2013) 1-20.
- [179] Z. Ni, Y. Wang, T. Yu, Z. Shen, Raman spectroscopy and imaging of graphene, *Nano Research*, 1 (2008) 273-291.
- [180] Q.A. Khan, A. Shaur, T.A. Khan, Y.F. Joya, M. Awan, Characterization of reduced graphene oxide produced through a modified Hoffman method, *Cogent Chemistry*, 3 (2017) 1298980.
- [181] G.T.S. How, A. Pandikumar, H.N. Ming, L.H. Ngee, Highly exposed {001} facets of titanium dioxide modified with reduced graphene oxide for dopamine sensing, *Scientific reports*, 4 (2014) 1-8.

- [182] P.T. Araujo, M. Terrones, M.S. Dresselhaus, Defects and impurities in graphene-like materials, *Materials Today*, 15 (2012) 98-109.
- [183] A. Niilisk, J. Kozlova, H. Alles, J. Aarik, V. Sammelselg, Raman characterization of stacking in multi-layer graphene grown on Ni, *Carbon*, 98 (2016) 658-665.
- [184] K. Tsirka, A. Katsiki, N. Chalmpes, D. Gournis, A.S. Paipetis, Mapping of graphene oxide and single layer graphene flakes—defects annealing and healing, *Frontiers in Materials*, 5 (2018) 37.
- [185] B. Tang, H. Guoxin, H. Gao, Raman spectroscopic characterization of graphene, *Applied Spectroscopy Reviews*, 45 (2010) 369-407.
- [186] G. Greczynski, L. Hultman, X-ray photoelectron spectroscopy: towards reliable binding energy referencing, *Progress in Materials Science*, 107 (2020) 100591.
- [187] F.A. Stevie, C.L. Donley, Introduction to x-ray photoelectron spectroscopy, *Journal of Vacuum Science & Technology A: Vacuum, Surfaces, and Films*, 38 (2020) 063204.
- [188] R.L. McCreery, M.T. McDermott, Comment on electrochemical kinetics at ordered graphite electrodes, *Analytical chemistry*, 84 (2012) 2602-2605.
- [189] K.J. Aoki, J. Chen, *Tips of voltammetry, Voltammetry*, IntechOpen London, UK, 2018.
- [190] M.H. Fahmy Taha, H. Ashraf, W. Caesarendra, A brief description of cyclic voltammetry transducer-based non-enzymatic glucose biosensor using synthesized graphene electrodes, *Applied System Innovation*, 3 (2020) 32.
- [191] D. Mampallil, K. Mathwig, S. Kang, S.G. Lemay, Reversible adsorption of outer-sphere redox molecules at Pt electrodes, *The Journal of Physical Chemistry Letters*, 5 (2014) 636-640.
- [192] J. Lin, Z. Peng, Y. Liu, F. Ruiz-Zepeda, R. Ye, E.L. Samuel, M.J. Yacaman, B.I. Yakobson, J.M. Tour, Laser-induced porous graphene films from commercial polymers, *Nature communications*, 5 (2014) 1-8.
- [193] R.S. Kelly, *Analytical electrochemistry: The basic concepts*, Analytical Sciences Digital Library, (2009).
- [194] E.O. Barnes, X. Chen, P. Li, R.G. Compton, Voltammetry at porous electrodes: A theoretical study, *Journal of Electroanalytical Chemistry*, 720 (2014) 92-100.
- [195] F. Yusoff, N.T. Khing, C.C. Hao, L.P. Sang, N.a.B. Muhamad, N.M. Saleh, The electrochemical behavior of zinc oxide/reduced graphene oxide composite electrode in dopamine, *Malaysian Journal of Analytical Sciences*, 22 (2018) 227-237.
- [196] J. Yang, S. Gunasekaran, Electrochemically reduced graphene oxide sheets for use in high performance supercapacitors, *Carbon*, 51 (2013) 36-44.
- [197] R. Vittal, K.-C. Ho, Cobalt oxide electrodes-problem and a solution through a novel approach using cetyltrimethylammonium bromide (CTAB), *Catalysis Reviews*, 57 (2015) 145-191.
- [198] J. Sethi, M. Van Bulck, A. Suhail, M. Safarzadeh, A. Perez-Castillo, G. Pan, A label-free biosensor based on graphene and reduced graphene oxide dual-layer for electrochemical determination of beta-amyloid biomarkers, *Microchimica Acta*, 187 (2020) 1-10.
- [199] D.A. Brownson, S.A. Varey, F. Hussain, S.J. Haigh, C.E. Banks, Electrochemical properties of CVD grown pristine graphene: monolayer-vs. quasi-graphene, *Nanoscale*, 6 (2014) 1607-1621.
- [200] D.A. Brownson, L.J. Munro, D.K. Kampouris, C.E. Banks, Electrochemistry of graphene: not such a beneficial electrode material?, *Rsc Advances*, 1 (2011) 978-988.

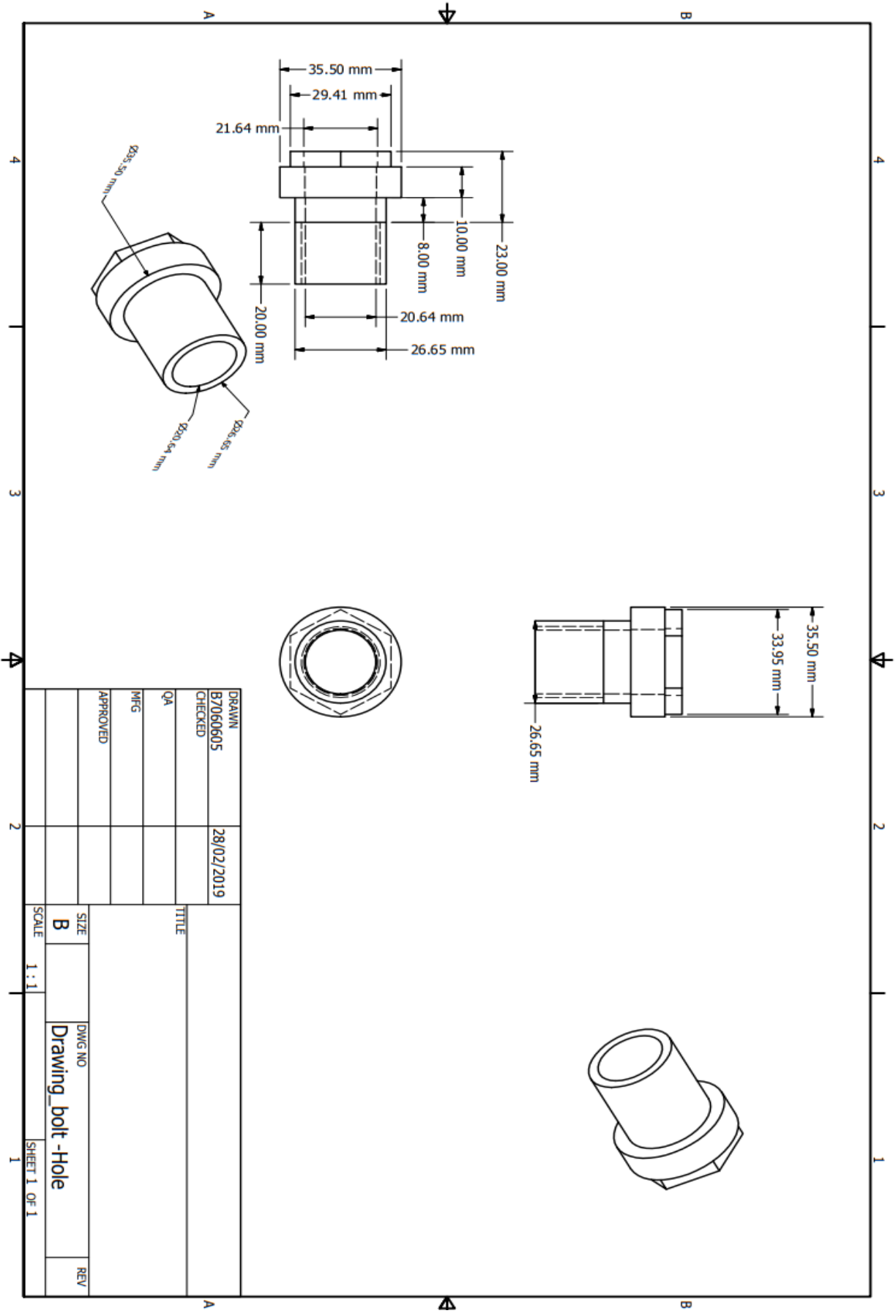
Appendix

- Set up of the components of the vacuum chamber are represented in the following diagrams.

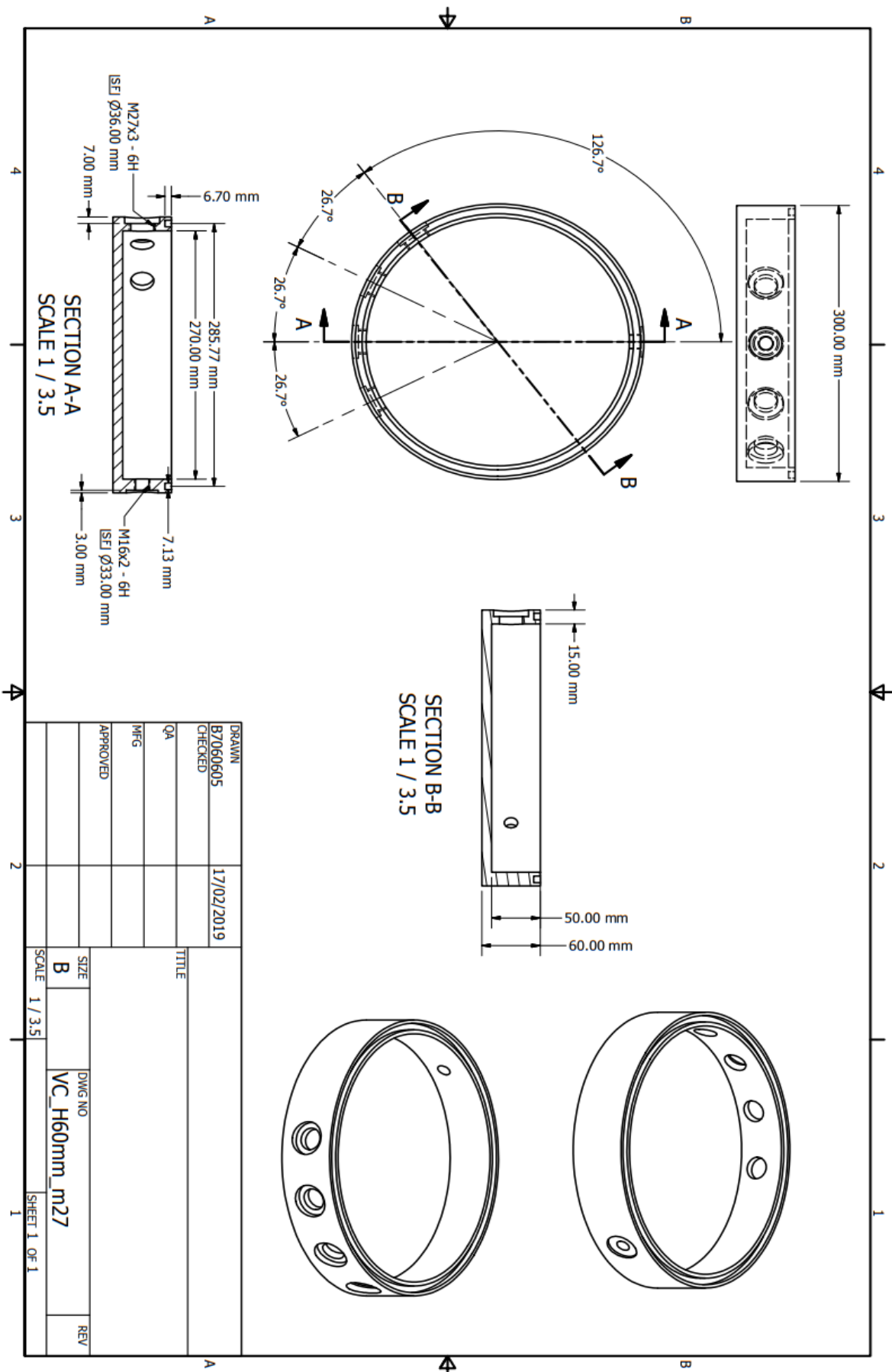




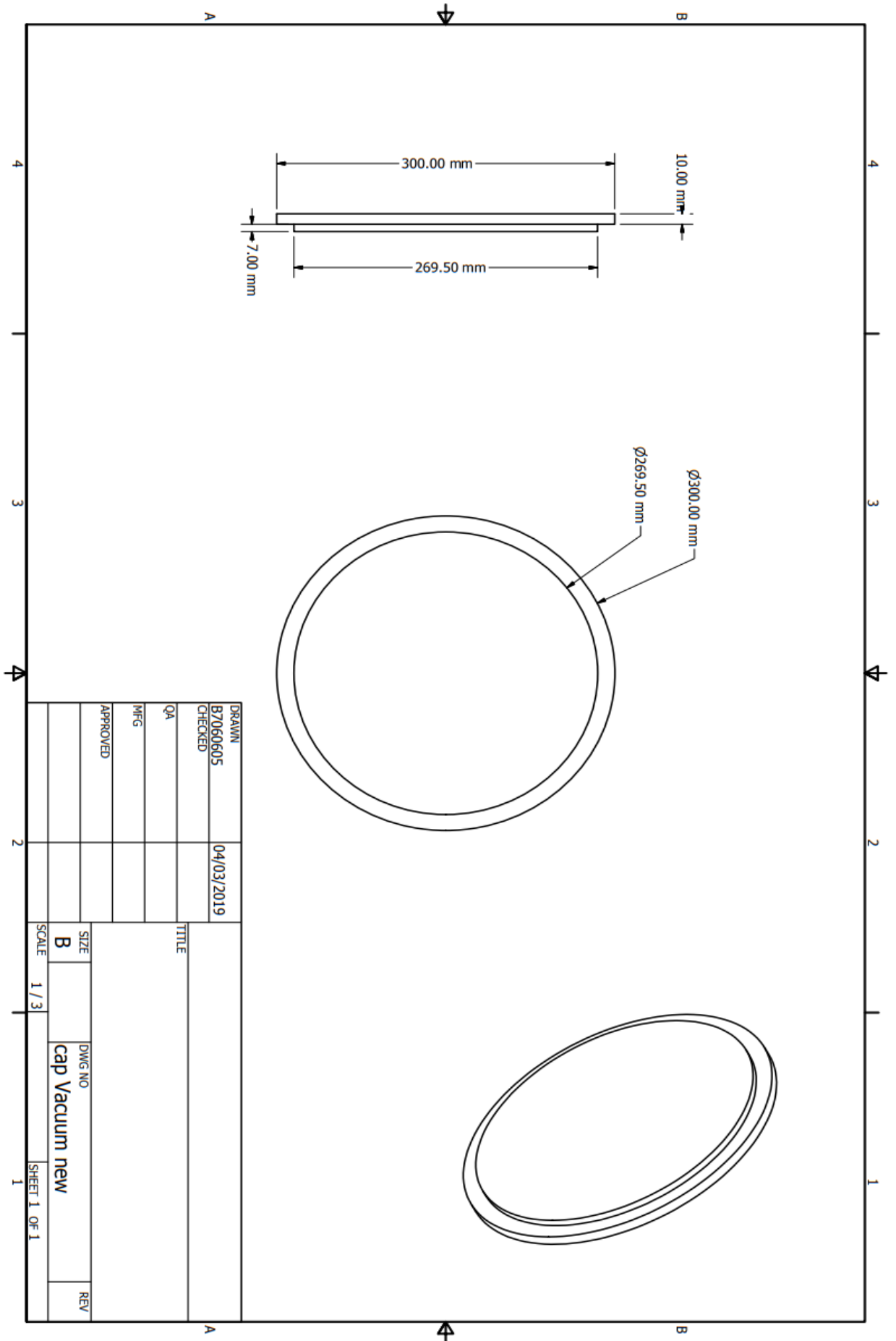
DRAWN	B7060605	04/03/2019	TITLE	SIZE	B	DWG NO	bolt - Hole - 4mm	REV
CHECKED				SCALE	2:1.5			
QA								
MFG								
APPROVED								



DRAWN	B7060605	28/02/2019	TITLE	
CHECKED			SIZE	B
QA			SCALE	1 : 1
MFG			DWG NO	Drawing_bolt - Hole
APPROVED			REV	
			SHEET 1 OF 1	



DRAWN	B7060605	17/02/2019	TITLE	SIZE	DWG NO	REV
CHECKED				B	VC_H60mm_m27	
QA				SCALE	1 / 3.5	SHEET 1 OF 1
MFG						
APPROVED						



DRAWN	B7060605	04/03/2019	TITLE	
CHECKED				
QA				
MFG				
APPROVED				
SIZE	B	DWG NO	cap Vacuum new	
SCALE	1 / 3	REV		
SHEET 1 OF 1				